Electronic Thesis and Dissertation Repository

11-5-2019 1:45 PM

High-throughput Fabrication of Drug-loaded Core-shell Tablets with Adjustable Release Profiles from Surface-erodible and Photocrosslinkable Polyanhydrides

Armin Geraili Nejadfomeshi
The University of Western Ontario

Supervisor
Mequanint, Kibret
The University of Western Ontario

Abstract

Controlled-release tablets enhance the effectiveness of therapies for various clinical conditions. Photocrosslinkable polyanhydrides that undergo surface erosion were recently introduced as suitable materials for manufacturing tablets with tunable release profiles. However, their erosion behavior has not been comprehensively studied. In this thesis, the erosion kinetics of photocrosslinkable polyanhydrides was studied by exploring the impact of different parameters (the polymer composition and geometry, as well as the temperature, pH, and shaking rate of the solution during the in vitro experiments) on their mass loss profiles, followed by a release kinetic model fitting. The results indicate that the temperature was the only parameter that could affect the induction period (the lag time) substantially. Moreover, polymers with the same surface area to volume ratios showed similar mass loss percentage despite their dissimilar volumes and surface areas. Although tablets with adjustable release profiles have been studied before, lack of a fast and large-scale production technique is a significant limitation that holds back their widespread application. A high-throughput fabrication platform was developed that was then utilized to manufacture controlled-release polyanhydride tablets. Tunable release profiles with the high-throughput fabricated tablets were achieved.

Keywords

Controlled-release drug delivery system, surface erosion, polyanhydrides, erosion kinetic, drug-loaded tablets, adjustable release profiles, high-throughput fabrication.

Summary for Lay Audience

Oral drug delivery is the preferred route for medication administration due to its lower cost and higher convenience for patients compared to other methods such as injection and implantation. The conventional form of oral tablets, however, requires multiple administrations to maintain the concentration of drugs in the bloodstream at an effective level. Controlled-release tablets have emerged as an alternative that can sustain the drug dosage at an effective level for a long period of time, aiming at enhancing the effectiveness of therapies in various clinical conditions. In addition, tablets with adjustable release profiles of the drug have been explored to improve the treatment efficacy for diseases that require different temporal profiles of the drug concentration. These tablets are typically made of a special class of polymers called biodegradable polymers, meaning that they are safely decomposed by the human body after they release the drug.

Polyanhydride is a biodegradable polymer that is considered as an appropriate option for being used in the fabrication of tablets with adjustable release profiles. Polyanhydrides are mostly eroded from their surfaces at predictable rates when they are exposed to the aqueous media. Understanding the erosion behavior (and hence the mass loss profile) of a newly introduced type of polyanhydride is an essential step before its utilization in fabricating tablets with adjustable release profiles. In this thesis, we first studied the erosion behavior of the new type of polyanhydride by exploring the impact of different parameters on their mass loss profiles. Moreover, we fitted the experimental mass loss data to different release kinetic models to gain a better understanding of the erosion behavior.

Although tablets with adjustable release profiles have been around for a while, lack of a fast and large-scale production technique has remained an important limitation that holds back their widespread application. We developed a high-throughput fabrication platform that we then utilized to manufacture polyanhydride tablets with controllable release profiles. We achieved tunable release profiles with the high-throughput fabricated tablets. Finally, we increased the capacity of the tablets for drug loading by implementing and fabricating modified tablet designs.

Acknowledgments

Table of Contents

List of Tables

List of Figures

List of Appendices

Chapter 1

1 Introduction

This chapter provides an overall introduction to the thesis work.

1.1 Overview

Oral drug delivery systems (DDSs) comprise more than 50% of the drug delivery market. Patients prefer the oral route for drug administration because it is economical, noninvasive, and does not require expertise for administration[1,2]. Conventional means of oral DDSs release the entire therapeutic substance immediately after administration. This leads to an instant increase, followed by a rapid decrease (to a sub-therapeutic level) in the drug concentration in the bloodstream. Therefore, to keep the drug concentration at therapeutic levels, multiple administrations at regular intervals are required.

Controlled release systems (CRSs) have emerged to enhance the patients' compliance and convenience by improving drugs' efficacy, reducing the chances of drug toxicity, and eliminating the need for multiple administrations[3]. Biodegradables polymers have been widely used in controlled DDSs because of their tunable mechanical properties. Synthetic biodegradable polymers, in particular, are of interest due to their unlimited availability[4].

A biodegradable polymer undergoes mass loss either by bulk erosion or by surface erosion. Most of the biodegradable polymers used in CRSs, e.g. polyesters, undergo bulk erosion. Bulk-erodible polymers erode from their interior and exterior simultaneously, resulting in low predictability of the drug release kinetics from these polymers. In contrast, surface-erodible polymers lose the polymer moieties from their surface, and therefore their initial geometry is preserved while the size of the polymer decreases. Besides, the mechanical properties of the surface-erodible polymers do not change during the erosion. The highly reproducible and predictable release kinetics of the surface eroding polymers make them desirable options in manufacturing the controlled DDSs[3].

Polyanhydrides predominantly undergo surface erosion because of their hydrophobic backbone and hydrolytically unstable anhydride bonds. Polyanhydrides have been shown

to maintain their surface eroding behavior at sizes as small as 100 μm, that is the smallest value reported for surface eroding polymers[5]. Unlike other surface-erodible polymers such as polyorthoesters (POEs) that undergo surface erosion only in acidic environments, polyanhydrides have shown surface erosion in acidic, alkaline, and neutral environments[6]. Despite their attractive properties for controlled DDSs[7], polyanhydrides have not been used as often compared to other biodegradable polymers such as polyesters. This can be attributed to the difficulties involved in their synthesis. In 2009, a new photocrosslinkable polyanhydride using thiol-ene polymerization was reporeted[8]. The polymerization process was straightforward and fast compared to other processes used for polyanhydrides synthesis.

Fully characterization of the new type of polyanhydrides, as well as investigating the impact of different parameters on its erosion behavior are essential before its utilization in controlled DDSs. There exist some parameters that may substantially affect the erosion of thiol-ene polyanhydrides, but have not yet been studied. For example, the polymer composition, temperature, pH of the media, the geometry of the polymers, and the media shaking rate (the convective force for the polymer erosion). The first objective of this study is to explore the erosion behavior of this type of polyanhydrides and gain a better understanding of their mass loss profiles. We then use these polymers for fabricating tablets with a new design proposed in this study (see below).

Controlling the temporal profile of drug release is vital for achieving the optimal therapeutic effect. Despite the substantial progress in developing controlled-release tablets, most of the existing designs only offer monotonic, or sustained release profiles. However, different types of clinical circumstances necessitate different types of release profiles for optimal treatment. The temporal patterns are mostly defined by the effect of the circadian rhythm on different clinical circumstances, giving rise to specific rhythms of medical conditions during the 24 hours of the day. Besides, various factors such as the patient's condition, age, and gender call for patient-specific treatments via personalized medicine. The increased awareness of individualized therapy and introduction of various biodegradable polymers with adjustable physicochemical properties encourage the

development of fabrication methods for manufacturing advanced controlled DDSs that enable releasing of drugs at controllable rates.

The traditional compression tableting that is used by pharmaceutical industries for manufacturing tablets and capsules[9] does not provide the flexibility required for fabricating controlled DDSs. Micro-fabrication has been used in some studies owing to its ability to manufacture tiny features while providing control over the shape or geometry of the delivery devices. The combination of micro-fabrication techniques such as standard photolithography, with repeated replica molding steps, has been reported that allows for easy, rapid, and precise manufacturing of drug delivery devices at relatively low costs[10,11]. This method has been used to fabricate microchips as CRSs that generate long-term pulsatile release[12]. Although the micro-fabrication methods provide a high resolution and have the potential for high-throughput manufacturing, the limitations associated with using implantable microchips have left the oral controlled DDSs the preferred option[13,1]. 3D printing is another technology that has been studied extensively by researchers for fabricating polymeric oral tablets with adjustable release profiles[14]. Most of the studies fabricated tablets with monotonic or constant release profiles of drugs, with some reporting more complicated (e.g. pulsatile) release profiles. The complicated release patterns were achieved by elaborate tablet designs and specific fabrication techniques, demonstrating the feasibility of creating tablets with various release patterns of drugs.

Although these studies show that the fabrication of personalized tablets is no longer an issue, there exist some limitations in the current fabrication methods used for modified-release tablets that can hinder their widespread application. Some of these limitations can be addressed by improving the tablet design and/or the appropriate choice of the fabrication method. As an example for the latter, the resolution of the fabrication method is an important parameter that can determine the precision of the release rate. The inexpensive and commercially available 3D printers have relatively low resolution, while higher resolution 3D printers are limited by their small range of resins (printable materials). On the other hand, micro-fabrication techniques such as photolithography are capable of creating miniaturized features with high resolution. Besides resolution,

scalability and high-throughput manufacturing is a critical characteristic of any potentially successful fabrication method. High-throughput manufacturing is currently a challenge for producing advanced controlled DDSs with adjustable release rates. Most of the studies reported the fabrication of a single tablet in each experiment, reducing the chances of their practical use in clinical settings. Manufacturing each tablet can take considerable amount of time, and the reproducibility level is low.

The second objective of this study is to use the thiol-ene polyanhydrides that we characterized during the first step for high-throughput fabrication of tablets with the new design proposed in this thesis. We aim at addressing the challenges in the fabrication of controlled-release tablets with adjustable release profiles of drugs by developing a high-throughput fabrication platform that manufactures tablets with high resolutions.

1.2   Thesis Outline

This thesis is divided into five chapters. A brief introduction and the motivation for this research are included in Chapter 1.

The relevant background information on the role of biodegradable polymers in controlled DDSs, the importance of polyanhydrides as surface eroding polymers, parameters affecting the erosion of polyanhydrides, the need for different release profiles of drugs, and the key concepts of advanced fabrication methods for manufacturing CRSs with adjustable release profiles is provided in Chapter 2. A broad literature review on the current research and challenges of obtaining erosion kinetics of thiol-ene polyanhydrides is also presented in Chapter 2. Lastly, the advances in controlled DDS fabrication methods are discussed focusing on micro-technology and 3D printing methods.

The main research findings are presented in chapters 3 and 4. Chapter 3 reports a comprehensive study on the mass loss profile of thiol-ene polyanhydrides. This chapter details the materials used in the mass loss experiments followed by the methodology of polymer preparation and characterization, experimental designs to explore the effect of different parameters on mass loss of the thiol-ene polyanhydrides, and the theoretical concepts for release kinetic model fitting. The results of the effects of parameters on mass

loss (erosion) profiles of polyanhydrides synthesized by thiol-ene photopolymerization are discussed. A comparative study on the release kinetic models and their fitting to the experimental data is carried out for a better understanding of polymers' erosion behavior.

Chapter 4 reports the high-throughput fabrication of tablets that are designed using a new approach, enabling adjustable drug release rates. The methodology of developing a high-throughput platform using a combination of micro-fabrication and 3D printing technology for rapid manufacturing of the erodible tablets is provided in this chapter. Several experiments were conducted with various tablet designs, and the results show the different release profiles obtained from these tablets.

Chapter 5 summarizes and concludes the results of chapters 3 and 4 and provides directions for future work.

References

1. Alhnan, M. A. *et al.* Emergence of 3D Printed Dosage Forms: Opportunities and Challenges. *Pharm. Res.* **33**, 1817–1832 (2016).

2. Deshpande, A. A., Rhodes, C. T., Shah, N. H. & Malick, A. W. Controlled-release drug delivery systems for prolonged gastric residence: An overview. *Drug Development and Industrial Pharmacy* (1996). doi:10.3109/03639049609108355

3. Uhrich, K. E., Cannizzaro, S. M., Langer, R. S. & Shakesheff, K. M. Polymeric Systems for Controlled Drug Release. *Chem. Rev.* **99**, 3181–3198 (1999).

4. Dhaliwal, K. Biodegradable Polymers and their Role in Drug Delivery Systems. *Biomed. J. Sci. Tech. Res.* (2018). doi:10.26717/bjstr.2018.11.002056

5. Burkersroda, F. Von, Schedl, L. & Göpferich, A. Why degradable polymers undergo surface erosion or bulk erosion. *Biomaterials* **23**, 4221–4231 (2002).

6. Göpferich, A. Mechanisms of polymer degradation and erosion. *Biomaterials* **17**, 103–114 (1996).

7. Domb, A., Jain, J. P. & Kumar, N. Polyanhydrides. in *Handbook of Biodegradable Polymers* 45–75 (Wiley-VCH Verlag GmbH & Co. KGaA, 2011). doi:10.1002/9783527635818.ch3

8. Shipp, D. A., McQuinn, C. W., Rutherglen, B. G. & McBath, R. A. Elastomeric and degradable polyanhydride network polymers by step-growth thiol-ene photopolymerization. *Chem. Commun.* (2009). doi:10.1039/b911557a

9. Davoodi, P. *et al.* Drug delivery systems for programmed and on-demand release. *Advanced Drug Delivery Reviews* (2018). doi:10.1016/j.addr.2018.07.002

10. Xia, Y., Rogers, J. A., Paul, K. E. & Whitesides, G. M. Unconventional Methods

for Fabricating and Patterning Nanostructures. *Chem. Rev.* (1999). doi:10.1021/cr980002q

11. Sant, S. *et al.* Microfabrication technologies for oral drug delivery. *Adv. Drug Deliv. Rev.* **64**, 496–507 (2012).

12. Santini Jr, J. T., Cima, M. J. & Langer, R. A controlled-release microchip. *Phys. Rev. B* **54**, 7128–7139 (1996).

13. Langer, R. *et al.* First-in-Human Testing of a Wirelessly Controlled Drug Delivery Microchip. *Sci. Transl. Med.* **4**, 122ra21-122ra21 (2012).

14. Hsiao, W. K., Lorber, B., Reitsamer, H. & Khinast, J. 3D printing of oral drugs: a new reality or hype? *Expert Opin. Drug Deliv.* **15**, 1–4 (2018).

Chapter 2

2   Background and Literature Review

This chapter provides the relevant background information on the emergence of controlled release technology, the role of biodegradable polymers in controlled release DDSs, and highlights the importance of polyanhydrides, as surface eroding polymers, in achieving desired release rates required in personalized medicine. Parameters affecting the erosion behavior of polyanhydrides and studies on these parameters is discussed. Lastly, this chapter discusses recent developments in fabrication methods of polymeric DDSs with controllable release profiles of drugs; focusing on using micro-technology and 3D printing for oral dosage forms.

2.1   Polymeric Controlled Drug Delivery Systems

This section describes the conventional DDSs and discusses the need for CRSs.

2.1.1   Conventional Drug Delivery Systems

The oral dosage is the most common route for the delivery of therapeutic agents, constituting about 40% of the drug administrations[1]. When administered orally, therapeutics are safely taken by patients without the assistance of a healthcare professional. In comparison to injection administration routes (e.g., subcutaneous, intramuscular, intravenous), oral delivery has minimal discomfort. These advantages of oral drug delivery over other drug administration routes, as well as the ease of the drug administration and the high level of patients' convenience, have resulted in the allocation of more than 50% of the drug delivery market to oral DDSs[2,3].

Conventional means of oral DDSs release therapeutic substances all at once (immediate-release) resulting in a sudden increase of drug concentration followed by a rapid decrease to a lower than effective level of drug in the bloodstream. In such settings, the duration in which the plasma concentration is effective without being tioxic is short, rendering the conventional release systems suboptimal. Figure 2-1 shows the importance of keeping the drug concentration level in the therapeutic window (below the toxic and above the sub-

therapeutic level). This figure also displays multiple administrations required for drugs to maintain their concentration within the therapeutic window. The multiple administrations reduce the patients' compliance and cause fluctuations in the drug dose level in the blood.
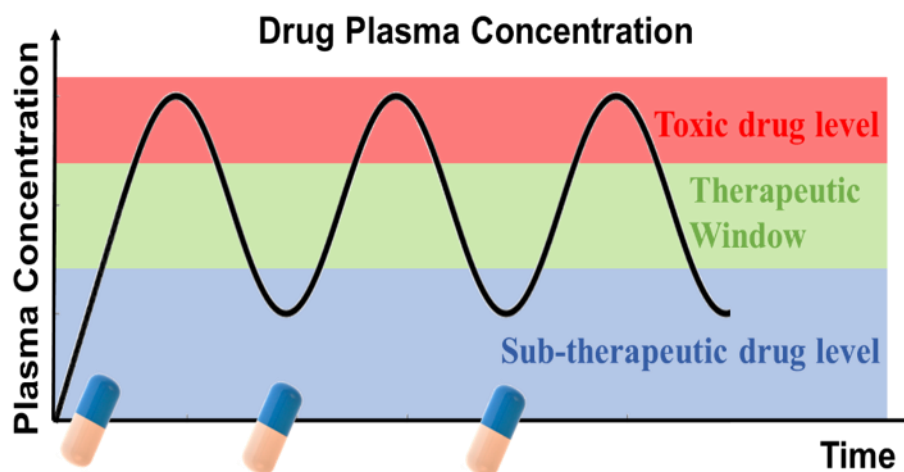
Figure 2-1: Drug plasma concentration in conventional DDSs that requires multiple drug administrations to keep the concentration of the drug in the therapeutic window.

2.1.2 Emergence of Controlled Release Technology

Controlled DDSs have emerged to improve patients' health by improving the drug efficacy, reducing the dose-dependent drug toxicity, and enhancing patient compliance and convenience. The tunable release of therapeutic substances in response to time or different stimuli (temperature, pH, enzymes, etc.), while maintaining the dose at the effective level, is called controlled release drug delivery[4]. Maintaining the level of the biologically active agents in the effective zone decreases the chances of drug toxicity, and hence the side effects. Controlled DDSs are designed to sustain the required plasma dosage for an extended period of time and consequently eliminate the need for frequent administrations. Figure 2-2 compares the burst release of a drug through the conventional means of delivery with drug release from a controlled DDS. Figure 2-2 also shows an example of a pulsatile release as an example of a physiologically required release profile that can be achieved by designing more complicated controlled DDSs[5].

Controlled DDSs often utilize synthetic biodegradable polymers to act as carriers for delivering their cargos. Several biodegradables polymers have been widely used to create the controlled DDSs. Based on the site of action and the desired temporal release profile, polymers with specific physicochemical properties can be utilized[6].
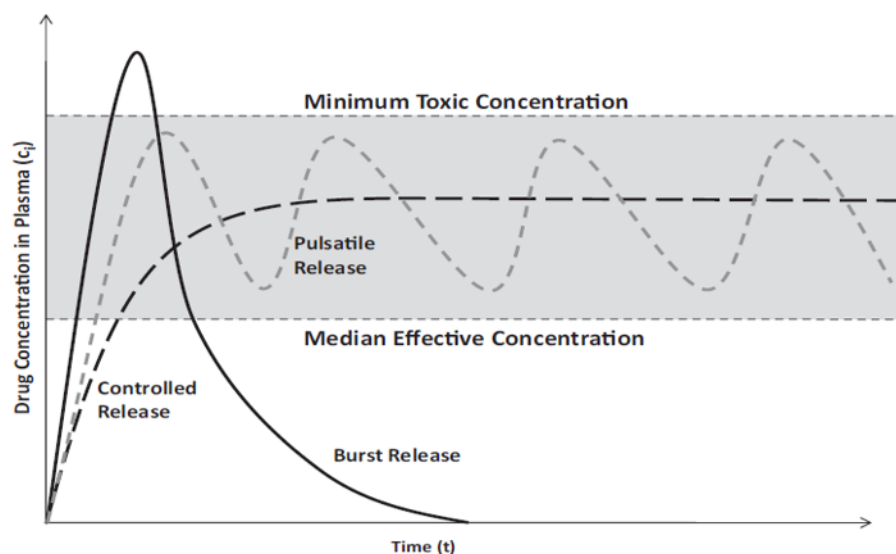
Figure 2-2: Comparison of the conventional DDSs' burst release with sustained-release obtained by a controlled DDS. The pulsatile release is one of the critical physiologically required release pattern, which is achievable using controlled DDSs. Reproduced from Ref [5] with permission.

2.1.2.1   Biodegradable Polymers in Controlled DDSs

Biodegradable polymers have been widely used in drug delivery applications because of their advantages over other materials, specifically their adjustable mechanical properties as an important factor for achieving more efficient DDSs. In the past 50 years, synthetic biodegradable polymers have been preferred over the naturally occurring ones for the use in advanced delivery systems due to their availability and their easily adjustable physicochemical properties[7]. In the 1960s, polyesters such as poly(D,L-lactic acid) (PLA), poly(glycolic acid) (PGA), and their copolymer poly(D,L-lactic-co-glycolic acid) (PLGA) were developed as synthetic biodegradable polymeric sutures[8]. Since then, synthetic biodegradable polymers have been extensively used as biocompatible delivery systems that are easily eliminated after the therapeutic is released in the human body.

Aliphatic polyesters such as PLA, PGA, and polycaprolactone (PCL), among biodegradable polymers, are the most frequently used materials in biomedical applications owing to their availability, biocompatibility, and flexible degradability[9]. These polyesters, as well as other synthetic biodegradable polymers, including polyphosphazenes, polyurethanes, polyanhydrides, and POEs, have been extensively studied over the past 20 years for advanced DDSs applications[9–11].

2.1.3   Controlled Drug Release Mechanisms

A variety of available drugs in the market for the treatment of different diseases increases the importance of using CRSs to elevate the efficacy of those drugs. The primary role of CRSs is releasing drugs for an extended period (days to weeks) at a controllable rate. A significant number of CRSs have been developed for various clinical conditions. Choosing the most suitable delivery system required for a specific clinical condition requires knowledge about different mechanisms of CRSs as well as their systems design factors[4].

CRSs utilizing polymers as carriers are divided into five main categories: diffusion and dissolution, solvent activated (swelling and osmotic-controlled), ion-exchange, stimuli-responsive, and chemically mediated (erosion and degradation controlled) systems[4,12]. These categories and the mechanisms by which they control the drug release will be briefly discussed in this chapter with the focus being on the chemically-controlled mechanisms, which are employed in this study.

2.1.3.1   Diffusion and Dissolution CRSs

Diffusion release is the most common mechanism of releasing drugs from polymers[12]. The migration of compounds from their initial point to the lower concentration area in the polymer is called a diffusion release mechanism. Diffusion CRSs are designed as reservoir systems or polymeric matrix systems. Reservoir systems typically consist of a water-insoluble polymeric membrane through which the drug diffuses out while in polymeric matrix systems, the drug is released by passing through the matrix itself.

As shown in Figure 2-3A, in both reservoir systems and polymeric matrices the drug can be dissolved in aqueous solution either above the saturation concentrations (constant drug source reservoir and monolithic dispersion matrices) or below the saturation level (non-constant drug source reservoir and monolithic solution matrices). In the former case, the concentration of the drug inside the polymer decreases over time by releasing the dissolved drug. Therefore, undissolved drug aggregates will be dissolved in order to replace the released drug, which leads to a controlled release rate (almost zero-order release). When the drug aggregates have fully dissolved, the concentration of the drug in the polymer goes under the saturation level. From this step onward, the constant drug source reservoir and monolithic dispersion matrices behave similarly to non-constant drug source reservoir and monolithic solution matrices, respectively, where the amount of the drug-releasing out of the polymer decreases over time until the completion of the drug release[4], as shown in Figure 2-3A.

Dissolution CRSs can also be designed as reservoirs or matrix systems (Figure 2-3B). Slowly dissolving polymers coat drugs in reservoir systems and the dissolution rate of the polymer defines the release rate of drugs. In dissolution-controlled matrix systems, drugs are encapsulated within a polymer and are released while the matrix is dissolving. Therefore, one of the essential factors for selecting the suitable polymer for a dissolution CRS is the solubility of the polymer that affects the release rate of the loaded drug[13].

Most of CRSs are a combination of the diffusion and dissolution systems in which drugs are trapped in polymeric membranes or matrices. Due to polymer dissolution, some pores will be created that allow water penetration to the polymer. As a result of the water flow inside the polymeric structure, the drug diffuses out of the polymeric matrices or membranes. Sometimes one of these mechanisms dominates the other that results in dissolution-limited or diffusion-limited CRSs[14].
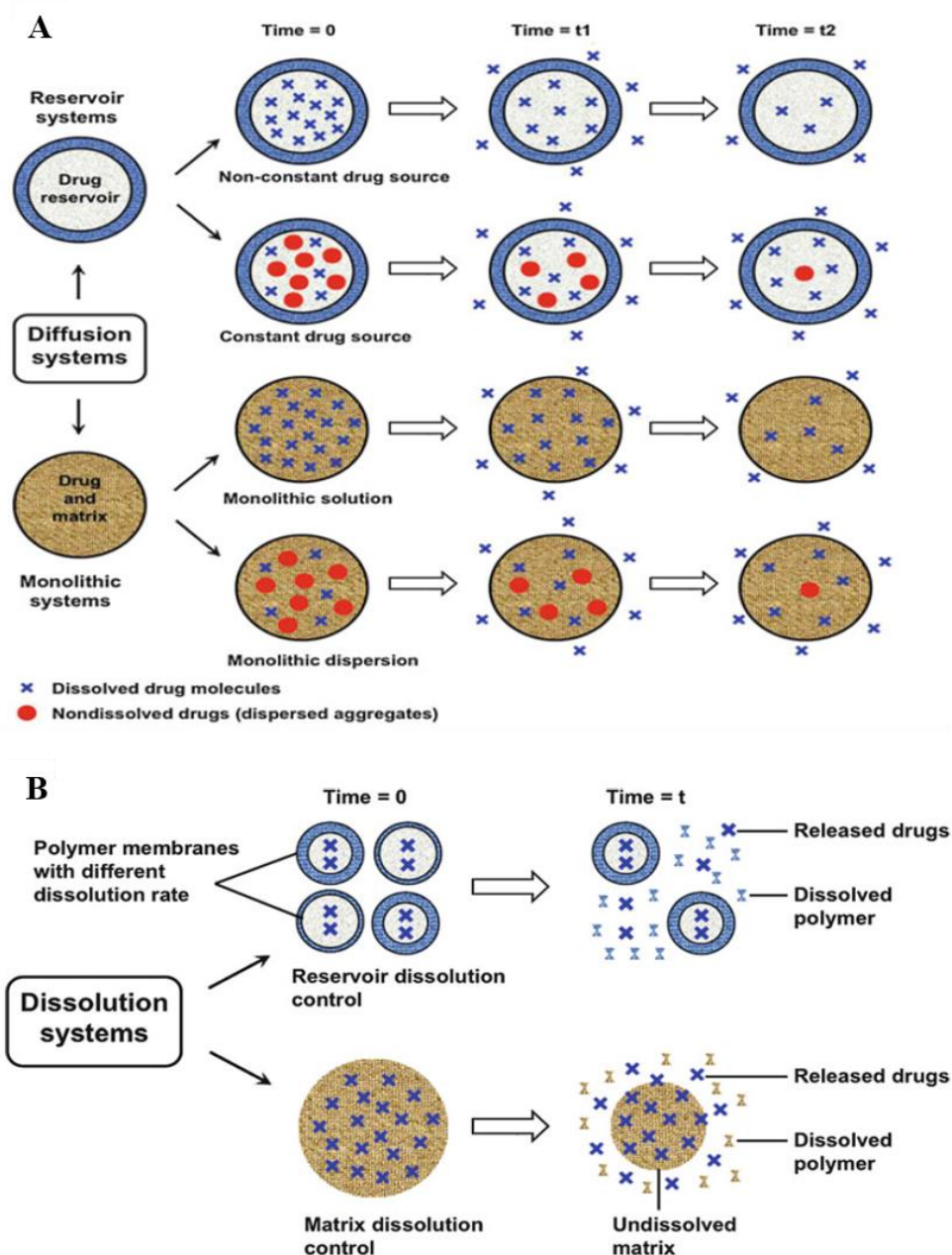
Figure 2-3: Schematic illustration of A) Diffusion CRSs. Drugs are trapped in systems at time t_0 and diffuse out through the reservoir systems or polymeric matrices at time t_1 and t_2. In non-constant drug source reservoirs or monolithic solution systems, the concentration of the drug reduces over time while the drug release can be controlled for a prolonged time in constant drug source reservoir or monolithic dispersion systems. B) Dissolution CRSs. In reservoir systems, the thickness of the membrane determines the drug release rate by controlling the dissolution rate of the polymer. In matrix systems, the dissolution of the boundary layer determines the release rate of the drug. Reproduced from Ref [4] with permission.

2.1.3.2   Solvent-activated CRSs

The penetration of water or body fluids into some polymeric systems causes the controlled release of drugs. Solvent-activated systems can be divided into swelling-controlled and osmotic pressure-controlled systems[12].

Semipermeable polymeric membranes which are permeable to water and impermeable to drugs produce osmotic pressure in osmotic pressure-controlled systems. There are small holes (orifices) on these membranes, acting as pathways for drugs to be released. Figure 2-4A shows two types of osmotic CRSs: 1) the drugs are loaded in the osmotic core (type A) or 2) the drugs are trapped in the reservoir surrounded by the osmotic core (type B). The osmotic pressure caused by the water permeation into the polymeric membrane through the orifices is the driving force of the drug release. Permeability of the polymeric membrane, the size of orifices, and the level of osmotic pressure control the release of the biologically activated agents[4,14,15].

In swelling-controlled systems, polymers such as natural or synthetic hydrogels are used that can absorb a considerable amount of water after being immersed in water. When these polymers swell in the presence of water or body fluids, their volume increases and the contents of the solvent come out from the polymer (Figure 2-4B). Diffusion of the drug through the polymer and the swelling characteristic of the polymer control the drug release rate[4,15].

2.1.3.3   Stimuli-responsive and Ion-exchange CRSs

Some of the polymeric carriers can be activated to release their cargo by external stimuli including physical, chemical, magnetic, electrical, or mechanical stimuli that create cues for polymers with specific properties to be activated. These structures can be used for both targeted drug delivery and temporal CRSs. Several studies have been conducted on thermo-responsive, light-responsive, redox-responsive, pH-responsive, and enzyme-responsive controlled release DDSs[9]. Figure 2-4C displays how physical stimuli can activate some responsive polymers to release their therapeutics.
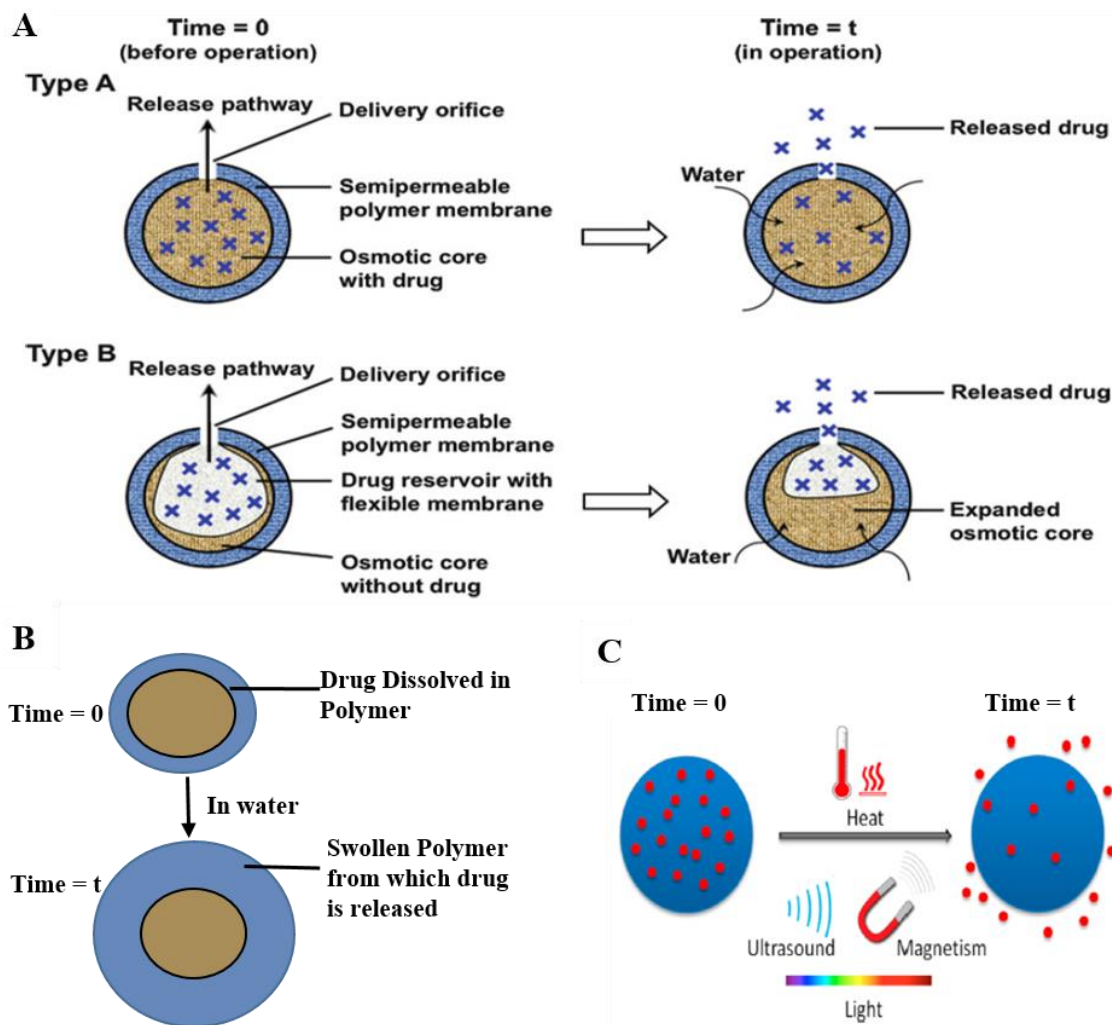
Figure 2-4: Schematic illustration of A) Osmotic-controlled systems. Reproduced from Ref [4] with permission. B) The swelling-controlled system. C) External physical stimuli to activate the responsive polymeric carriers to release their cargo in a controllable manner. Reproduced from Ref [9] with permission.

Ion-exchange CRSs typically consist of resins made of cross-linked polymers with a considerable number of anionic and cationic functional groups. Body fluids can flow into their structure because of the cross-linked backbone of the polymer, and at the same time, the ionic part of the structure enables the ionic groups to exchange their mobile ions with another cation or anion[16]. Therefore, there are two types of ionic exchange DDSs: the release of cationic drugs using anionic resins, or release of anionic drugs using cationic

resins. Ionic strength, pH of the human body environment, and cross-link density of the resin can control the drug release rate[4].

2.1.3.4   Chemically-mediated CRSs

Chemical reactions also play an integral role in controlling the release rate of drugs using polymeric systems. Chemically-controlled systems are generally divided into two groups: the pendant chain, and erosion-controlled systems. In pendant side chain systems, drugs are covalently linked to the polymer backbone with the polymers degrading once exposed to body fluids or water. The targeted site for delivering the drug has its own characteristics, which may lead to hydrolytic or enzymatic degradation of bonds between the drug and the polymer (Figure 2-5A). These systems can be used for targeted drug delivery. The rate of the hydrolysis and the enzymatic degradation rate of the drug-polymer conjugation determines the rate by which the drugs detach from the polymer backbone[4].

In erodible controlled release polymeric systems, drugs are dispersed in a matrix and will be released upon degradation of the erodible polymer (Figure 2-5B). If the drug diffusion rate from the polymer is much faster than the erosion rate of the polymeric matrix, the kinetics of the drug release is diffusion-controlled, which is described in previous sections. If the diffusion rate of the drug through the polymer is lower than the erosion rate of the polymeric matrix, it would be erosion-controlled system[17].

There are two types of erosion mechanisms, namely bulk and surface erosion. Bulk eroding polymers are those that degrade from their bulk in contact with water because the permeation rate of the water molecules into the bulk of the polymer is faster than the erosion rate of the polymer. Surface eroding polymers are eroded from their surface, because of their faster erosion rate than the water penetration rate to their polymer bulk. In surface erosion, polymer moieties are detached from the surface of the polymer such that the size of the polymer decreases while preserving the initial geometry of the polymer (Figure 2-5C)[6].
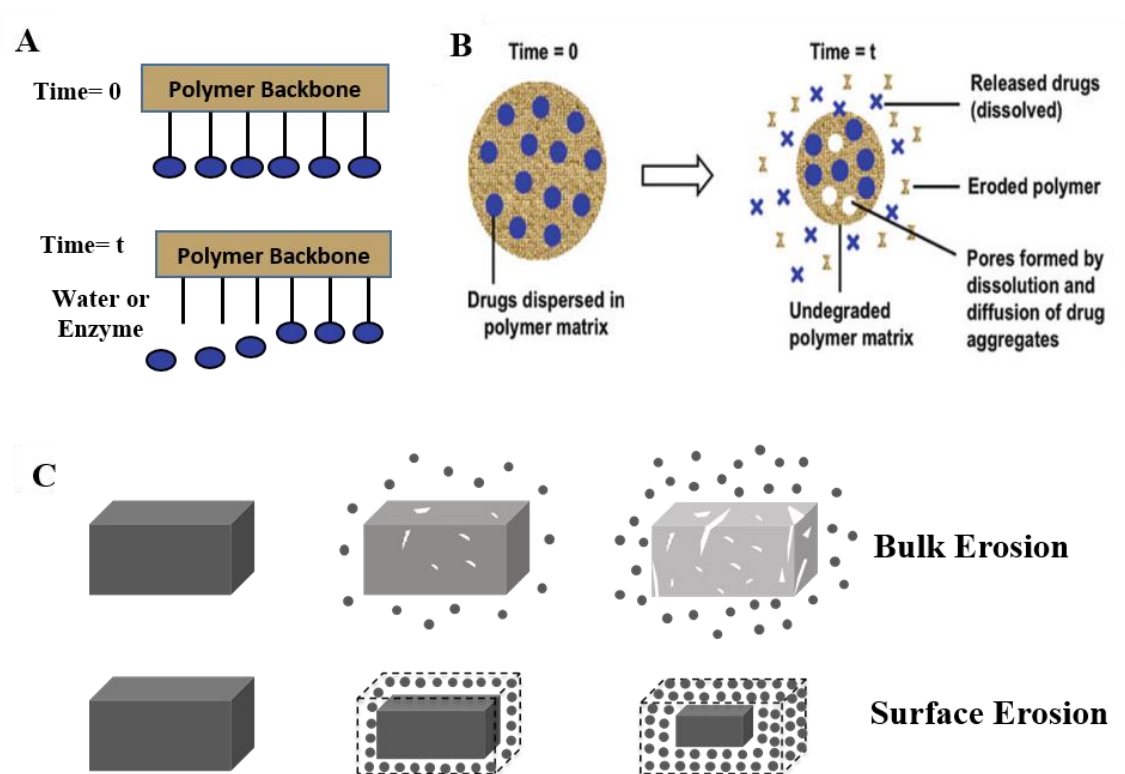
Figure 2-5: Schematic illustration of chemically-controlled release systems. A) Pendant side chain systems. B) Erosion controlled systems. Reproduced from Ref [4] with permission. C) Surface erosion versus bulk erosion mechanism.

Although for biodegradable polymers, a combination of both mechanisms occurs depending on the chemical structure of the polymer backbone, most of the biodegradable polymers used for CRSs (e.g. famous polyesters) undergo bulk erosion. Since water can penetrate to the bulk of these polymers, the drug is not sufficiently protected during the treatment, and the predictability of the drug release kinetics during the bulk erosion is low. In contrast, surface eroding systems protect the water labile drugs as water cannot rapidly permeate to the bulk of the polymer. Another exciting characteristic of surface eroding polymers is their mechanical properties which do not change during erosion. Besides, the highly reproducible and predictable release kinetics of the surface eroding systems make them desirable for controlled DDSs[6].

Two types of biodegradable polymers predominantly undergo surface erosion: POEs and polyanhydrides. They both have highly labile functional groups leading to fast hydrolysis

on the surface, and because of the hydrophobic backbone, water cannot quickly pass through the bulk of the polymer. The majority of water at the surface of the polymer is consumed before water can penetrate the polymer bulk. POEs showed surface erosion in lower PHs conditions (in an acidic environment) while Polyanhydrides showed surface erosion in acidic, alkaline, and neutral environment which makes the polyanhydrides a desirable option to be used as a CRS[18].

Recent considerable progress in the development of advanced micro- and nano-scale DDSs has encouraged the use of erodible systems in small scales. The critical device dimension ($L_{critical}$) is reported as a criterion for determining the type of erosion of a specific polymer. An erodible matrix with dimensions larger than $L_{critical}$ undergoes surface erosion; otherwise, it undergoes bulk erosion. The estimations of $L_{critical}$ for different polymers are available in the literature. The value of $L_{critical}$ for polyanhydrides was calculated to be 10^{-4} m, which is the smallest value reported for surface eroding polymers. It means that polyanhydrides undergo surface erosion down to almost 10^{-4} m, allowing for manufacturing erodible CRSs even in microscopic scales [19].

2.2   Polyanhydrides

Although Bucher and Slade had synthesized polyanhydrides for the first time in 1909, these polymers attracted more attention in the 1980s when Langer used them as controlled DDSs[20]. Polyanhydrides rapidly degrade in acidic, alkaline, and a neutral aqueous environment. In comparison to other hydrolytically degradable bonds such as amides and esters, anhydride bonds are more unstable and have the shortest average half-life. Furthermore, polyanhydrides predominantly undergo surface erosion because of the hydrophobic backbone and hydrolytically unstable anhydride bonds in their structure. Due to the surface erosion mechanism, the release rate of the dispersed drugs in these polymeric systems ideally follows the erosion rate of the polymer. Because of these capabilities, they have a high potential to be used as controlled DDSs[21].

Despite many interesting properties of polyanhydrides for drug delivery applications, these polymers have not been used as often compared to other biodegradable polymers such as polyesters. The only US Food and Drug Administration (FDA)-approved product

made of polyanhydrides is the Gliadel Wafer (a polyanhydride-based implant for locally delivering the anticancer agent to a brain tumor)[22]. Difficulties involved in the synthesis of polyanhydrides are the main reason for their less popularity compared to other biodegradable polymers.

2.2.1 Polyanhydrides' Synthesis Pathways towards Radical Polymerization

The high reactivity of anhydride functional groups in the vicinity of nucleophilic species, such as water causes difficulties in the synthesis of polyanhydrides. The most common pathway of synthesizing polyanhydrides is polycondensation. There are some limitations for polycondensation methods, including the very high temperature and the low pressure needed during the synthesis steps[23]. Domb et al. reported a method to synthesize polyanhydrides using coupling agents (phosgene and diphosgene) conducted at ambient temperature and eliminated the need for the purification steps required in polycondensation[24]. The limitation of this method is difficulties in removing the solvents such as toluene.

Photopolymerization of methacrylate anhydride monomers was investigated by Langer group to achieve more manageable synthesis steps in addition to the capability of in vivo synthesis. The use of the methacrylate group in this study paved the way for utilizing the radical polymerization for synthesizing polyanhydrides. The radical polymerization can be initiated by thermal-, redox- or photo-initiators. Among these radical polymerization methods, photopolymerization undergoes a faster reaction while having a spatiotemporal control over the polymer synthesis[23]. In 2009 Shipp et al. [25] have synthesized a new photocrosslinkable polyanhydrides using thiol-ene polymerization under more straightforward conditions. Facile synthesis of these polyanhydrides in quite rapid reactions (around 15 minutes) using commercially available monomers alleviated the challenges in the synthesis of polyanhydrides reported in previous approaches.

Thiol-ene polymerization, a type of click chemistry polymerization, is another radical polymerization process that has been used to synthesize polyanhydrides. The click chemistry is a method through which high yields of chemical species can be synthesized

in very rapid reactions while the reaction condition is simple[26]. It allows for the conversion of almost all monomers to higher molecular weight product in a simple way. Thiol-ene reactions can occur by the existence of radical initiators (thermal-, redox, or photo-initiators or a combination of these three). In thiol-ene reactions, the hydrogen atoms of the thiol moiety are abstracted and produce a thyl radical which is added to the alkene following an anti-Markonikov rule (Figure 2-6). Photo-crosslinking also allows for precise control over the polymer formation by directing the light source, and the reaction is quite rapid so that oxygen atoms do not have the chance to play a role in the reaction. This process generally takes from a few seconds to a few minutes[21].
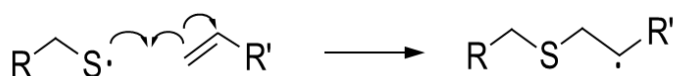
Figure 2-6: The thiol-ene reaction scheme.

2.2.2   Parameters affecting Polyanhydrides Erosion

A desired erosion-controlled DDS is the one that can complete the drug release at the same time when erosion is completed. Depending on the ultimate application, this time can vary from a few hours to weeks or even years. Polyanhydride was used for controlled DDSs in the early 1980s as an alternative to PLA, and PLGA which can only release drugs over a few weeks[20].

As described in previous sections, biodegradable polymers typically undergo two types of erosion: bulk and surface erosion. The essential characteristic of polyanhydrides is their highly unstable anhydride groups in addition to their hydrophobic structure, leading to almost complete surface erosion. The drug release rate from surface-erodible polymers such as polyanhydrides is proportional to the external surface area of polymers. Near zero-order drug release rate (following the polymer linear mass loss kinetic) which is a desired release rate for the controlled release DDSs is achievable using this class of polymers[27]. The most critical measure for polymer erosion is known to be the polymer mass loss. For example, for a matrix with slab geometry, surface erosion means a linear mass loss profile[28].

Different properties of polymers, including crystallinity, hydrophobicity, and water diffusivity, are dictated by polymer composition that affects the polymer erosion behavior[29]. By changing the monomers' initial mole ratios, the degradation rate can be adjusted while the surface erosion maintains the dominant mode of erosion. Monomers with different hydrophobicity form polymers with various crystallinity. More crystalline structures have shown a lower erosion rate than the amorphous domains. The retarded water penetration to the polymer structure in the crystalline domain, cause this slower rate of erosion[30]. Shakeshef et al.[31] prepared the poly (sebacic anhydride) (PSA) using melt polycondensation. They showed faster erosion rates for polyanhydrides with amorphous domains in comparison to more crystalline structures of the polymer with slower erosion rates. Adding drugs or model compounds to polyanhydrides may lower the cross-link density, leading to different erosion rates. For example, loading 2% bovine serum albumin to the poly (fumaric-co-sebacic anhydride) (p(FA-SA)) 20:80 polyanhydride has shown increased degradation rate of the system[32]. Several studies have shown various erosion rates using different mole ratios of monomers. The copolymer of the SA and 1,3-bis(p-carboxyphenoxy)propane or p(CPP-SA) was used to develop the Gliadel wafer[33]. The slower erosion velocity of the p(CPP-SA) when it has more CPP in its structure[28] is a good example of the effect of polymer composition on its erosion behavior. In another study, series of poly[bis(p-carboxyphenoxy)alkanes] made of six methylene units showed a very slower erosion rate in comparison to the polymer made of one methylene unit (three-fold decrease was observed in the release rate)[30].

Polyanhydrides erosion is also dependent on the pH and the temperature of the environment, the geometry of the polymeric DDS, and the flow rate of the media in contact with the polymer, besides the mentioned parameters.

The pH of the solution might change the erosion of polyanhydrides. The in vitro degradation of the copolymer derived from SA and FA were conducted in Phosphate Buffered Saline (PBS) with different pHs by Santos et al.[34]. Three different polymers (p(FA-SA) 70:30, p(FA-SA) 50:50, and p(FA-SA) 20:80) were degraded at three pHs equal to 8.8, 7.4, and 4.2. Results showed significantly higher erosion rates of all three polymers at pH=8.8 than the neutral and acidic conditions. Besides, the degradation of

p(CPP) matrices at pH ranging from 7.4 to 10 showed more stability of polyanhydrides at lower pHs[30].

As polyanhydrides predominantly undergo surface erosion, the geometry of delivery systems made of polyanhydrides is of high importance. The erosion of polyanhydrides as microparticles are faster than the rate of erosion from macro-scale delivery systems made of polyanhydrides[27]. Another study showed the dependency of the amount of the water uptake for p(CPP-SA) 40:60 to the geometry and the size of the polyanhydride delivery system which can change the erosion kinetics of the polymer[35].

To better simulating the in vivo situation, shaking the PBS solution could be applied during in vitro experiments. This agitation is the representative of the mass transfer affecting the erosion of the polymer. Sheh et al.[36] studied the effect of the mass transfer on Poly (fatty acid dimer: sebacic acid) (p(FAD:SA)) 50:50 by conducting the degradation test at three shaking rates (0, 60, and 120 rpm). No obvious differences were observed in this study for the erosion of this polymer with three different agitation speeds. Gopferich et al. and the Langer group have extensively studied the degradation and erosion of conventional polyanhydrides and parameters affecting their erosion behavior [27,37,38].

2.2.3 Parameters affecting the Erosion of Photopolymerized Thiol-ene Polyanhydrides

Full characterization of a new polyanhydride and investigation of the impact of essential parameters on its erosion is necessary for the newly introduced polymer in order to be utilized as a CRS. In 2009, a new type of linear and cross-linked polyanhydrides was synthesized using thiol-ene chemistry. The advantages of synthesizing these photocrosslinkable elastomeric polyanhydrides over conventional polyanhydrides are discussed in section 2.2.1. Recently, few studies have been conducted to explore the erosion mechanism of this type of polyanhydrides. For the first time, Shipp et al.[25] synthesized linear and cross-linked polymers using 4-pentenoic anhydride (PNA), 3,6-dioxa-1,8-dithiooctane (EGDT), and tetrakis(3-mercaptopropionate) (PETMP) monomers in the presence of a photo-initiator. They showed the surface erosion of this type of

polymer experimentally by measuring the mass loss of polymers in PBS at pH=7.4. Four different polymer compositions were synthesized to show different erosion times ranging from 30 to 70 hours. In another study, Rutherglen et al.[39] characterized the same polymers thermo-mechanically for better understanding of the polymers' properties.

The erosion and toxicity study for a specific cross-linked thiol-ene polyanhydride made of PNA and PETMP were conducted by Poetz et al.[40]. In this study, they determined the mass loss profile of this polymer, showing an almost 10 hours induction period and total erosion time of 25 hours for a polymer with slab geometry ($2 \times 10 \times 10$ mm). The erosion front (the thickness of water penetration during the induction period) for this polymer was measured to be almost 400 μm. The variation of the pH in the media caused by the degradation products during the polymer erosion was monitored to calculate the hydrolysis rate as a function of the pH. They also added 1wt% of a hydrophilic dye to the polymer and showed that the dye release profile qualitatively followed the mass loss profile of the polymer.

In 2015, the same group[41] synthesized a new semi-crystalline thiol-ene polyanhydrides with a broader range of erosion time starting from 24 hours to almost 10 days for polymers with cylindrical shape (10 mm diameter, 5 mm height). They showed the surface erosion of these polymers made of PNA, PETMP, and 1,6-hexanedithiol (HDT) with different initial mole ratios of monomers. In this study, the effect of the crystallinity of polymers on erosion time was investigated. Polymers with almost 60 % crystallinity showed ten times slower erosion rates than the polymer with the amorphous domain. Effect of adding various amounts of lidocaine (1, 2, and 3wt %) to polymers on the erosion of polymers showed slightly faster erosion for polymers loaded with drugs.

There are essential parameters that substantially affect the erosion of thiol-ene polyanhydrides that have not been explored yet. In this thesis, a comprehensive study on erosion (mass loss) of different thiol-ene photopolymerized polyanhydrides was conducted and the effect of various factors on polymers' mass loss and erosion rates is presented. The major part of chapter 3 of this thesis discusses the impact of parameters such as the temperature and pHs of media, the geometry of polymers, loading drugs or

model compounds to polymers, and media flow rate on erosion of cross-linked thiole-ene polyanhydrides.

2.3   Diseases and Release Profiles

Controlling the temporal profile of drug release is vital for achieving the optimal therapeutic effect. Despite significant advances in controlled release technologies, most of DDSs only offer monotonic, or constant (i.e., sustained) release profiles. However, different types of clinical circumstances require different types of timed-release. These temporal patterns are mostly defined by the effect of circadian rhythm on different clinical circumstances, giving rise to specific rhythms of medical conditions during the 24 hours of the day. Besides, various factors, such as the patients' condition, age, and gender necessitate patient-specific treatments via personalized medicine.

2.3.1   Circadian Time Structure

The study of the biological rhythm is called chronobiology, and the consequence of several biological rhythms is the temporal organization of human bodies. Suprachiasmatic nuclei (SCN) which are located in the hypothalamus control the human circadian rhythm[42]. Figure 2-7 illustrates the human circadian time structure. In this figure, sleep time is considered from 10:30 p.m. to 6:30 a.m. (the dark side) and the rest of the time during the 24 hours of the day is considered as activity time for a person with normal activity. The graph displays the peak of the basal gastric acid secretion and white blood cell count (WBC) at late night while the concentration of the hemoglobin and insulin is at the highest level at noon.

This circadian rhythm governs the cells- to organs-level activities of our body, and hence affect the occurrence and even severity of medical conditions. For example, peptic ulcer attack and gall bladder occur mostly at night while the myocardial infarction (MI) or heart attack occurs most frequently in the morning. These patterns of the symptom's severity show the necessity of precise treatments in which the exact amount of therapeutics are released in the body during exact times of the day, for specific durations. For example, Gonadotropin-releasing hormone (GnRH) necessitates pulsatile release for therapeutic effectiveness. Decreasing release profiles are beneficial for diseases that are

worse in the morning, including rheumatoid arthritis, asthma, and angina pectoris. Patients with osteoarthritis suffer from stronger pain in the afternoon and should benefit from an increasing release profile. Moreover, some agents or drugs require a particular administration profile during a specific period of time. For instance, patients who suffer from attention deficit hyperactivity disorder (ADHD) require a bimodal release profile of Ritalin-LA[43]. In addition to the temporal profile, for some drugs (e.g. anticoagulants, antihypertensives, and antiepileptics), achieving an accurate plasma concentration throughout the medication is very important due to the narrow therapeutic range and severe side effects.
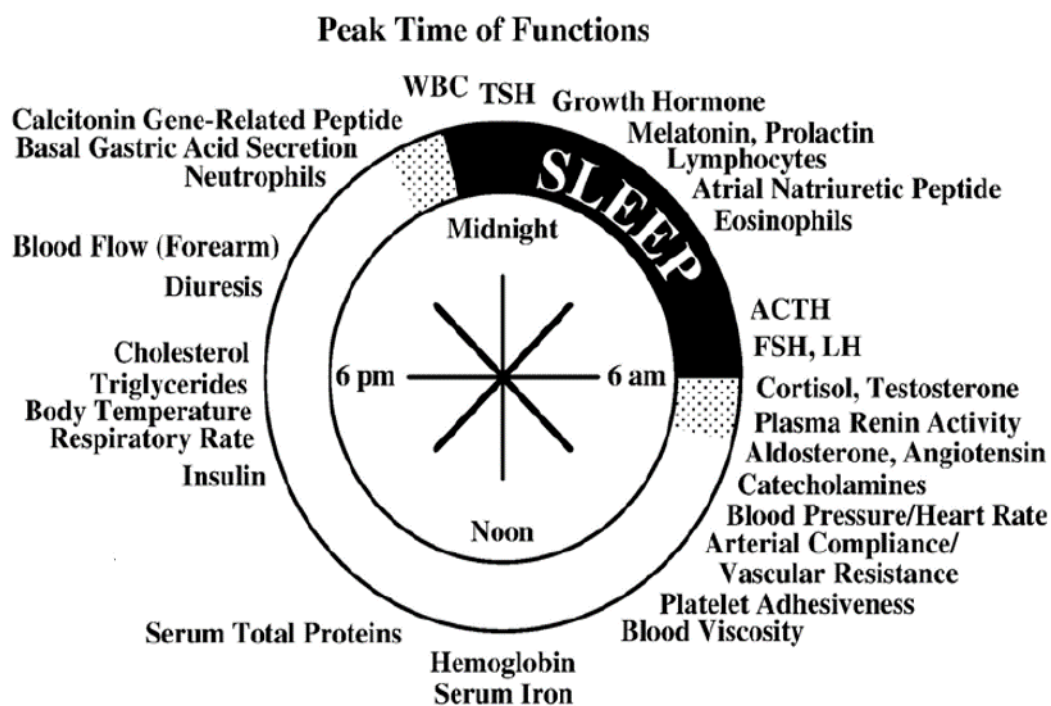
Figure 2-7: Human circadian time chart. Peaks of some biological features during 24 hours of the day in a person with normal daytime activity. The chart shows the Thyroid-stimulating hormone (TSH) as well as the growth hormone and melatonin peak in the bedtime while the concentration of the adrenocortical hormone (ACTH), follicle-stimulating hormone (FSH), and luteinizing hormone (LH) is at the highest level at the start of the daytime. Reproduced from Ref [43] with permission.

"Personalized medicine" in drug delivery systems has emerged as an approach to enhance the efficacy of treatments by designing customized therapy that follows the individual

patient's needs. For example, a release profile that mimics the circadian rhythm of the patient is considered advantageous for insulin dosing and enables innovative methods in cancer treatment, highlighting the importance of developing CRSs that can adjust and customize the release profile for different circumstances.

2.4 Recent Developments in Fabrication Methods of DDSs to Achieve Adjustable Release Profiles

Several fabrication methods exist for manufacturing different DDSs. Although traditional compression tableting is still being used by pharmaceutical industries for manufacturing tablets and capsules[44], increased awareness of individualized therapy and introduction of various biodegradable polymers with adjustable physicochemical properties, encourage the development of fabrication methods for manufacturing advanced controlled DDSs. In this section, recent developments in fabrication methods of advanced DDSs that enable releasing of drugs at controllable rates is reviewed. The focus of this section is on the micro-fabrication technique and the 3D printing technology that has attracted attention in recent years for the manufacturing of advanced controlled DDSs.

2.4.1 Micro-fabrication Technology

Micro-fabrication was originally adopted from the microelectronics industry and has been used for manufacturing advanced DDSs. Recently, micro-fabrication technology has been employed to manufacture high-throughput assays for drug discovery and tissue engineering applications[45]. Moreover, some issues of oral drug delivery can be addressed when micro-fabrication is used, owing to its ability to manufacture tiny features while providing control over the shape or geometry of delivery devices.

2.4.1.1 Micro-fabrication Methods: Photolithography Process

Micro-fabrication for creating delivery devices generally consist of repeated steps, including film deposition and photolithography. First, the desired two-dimensional (2D) features which are designed by a computer-aided design (CAD) software beforehand are printed as a photo-mask. Photolithography steps will in turn transfer the pattern to a substrate. In the first step, a photo-sensitive polymer coats the substrate to the desired

thickness. Then, the coated substrate is exposed to the Ultra Violet (UV) light while the photo-mask is located above the substrate and below the mask aligner (UV-light source). Finally, the cross-linked photo-resist encompasses embossed features, while the remaining uncross-linked polymer is washed away. Using the standard photolithography, it is possible to achieve features with fine resolution of 0.5 to 1 μm [46].

Based on the ultimate application of these micron-sized features, a hard substrate such as silicon can be used as a master mold for making the inverse replica of soft elastomers. This process is called soft-lithography (Figure 2-8 A-F) in which usually poly (dimethylsiloxane) (PDMS) is used as the soft elastomer material [46]. A combination of the micro-fabrication techniques such as standard photolithography with repeated replica molding steps allows for easy, rapid, and precise manufacturing of drug delivery devices at relatively low costs[47,48]. Fine features on a PDMS mold can be used to make channels through which minute amounts of fluid flow, creating a platform called microfluidics. Microfluidic devices have been extensively used for tissue engineering applications particularly for lab-on-a-chip studies, or as high-throughput platforms for drug screening. Microfluidics also has been used for fabrication of controlled release micro-particles as well as polymeric micro-containers in drug delivery devices [49].

Several characteristics of micro-fabrication technology can help simplify achieving CRSs. Various devices have been micro-fabricated that are capable of delivering drugs locally, on-demand, or through programmable devices. Several papers reviewed various micro-fabricated controlled DDSs developed over the past 20 years[50,51] covering both programed polymeric systems, on-demand or remotely programmable devices. Programmed polymeric systems are designed to deliver therapeutic contents in micro or nanoparticles at a pre-determined rate. The release of drugs from on-demand delivery devices is usually controlled remotely by operators. We review the advancement in the development of micro-fabricated programmable and on-demand devices designed for controlling the drug release profile.
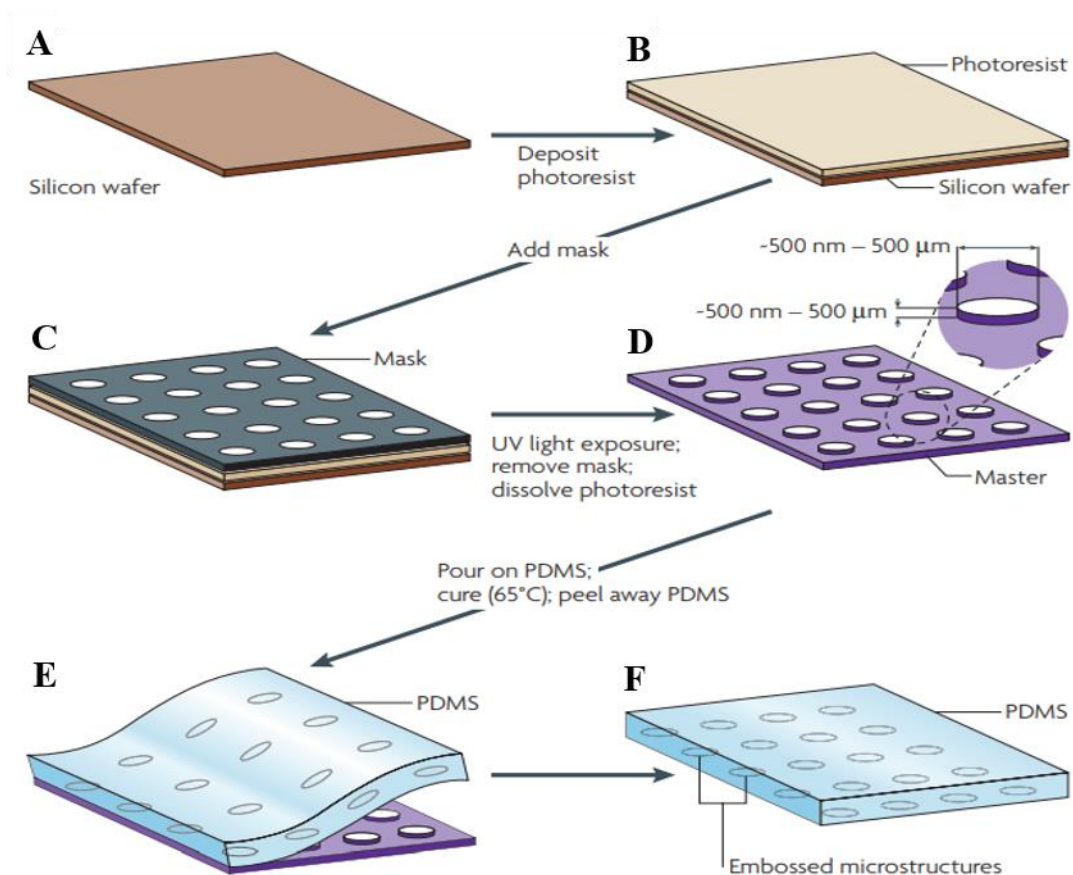
Figure 2-8: Schematic illustrations of the standard soft lithography process. A, B) The deposition of the photo-resist on a silicon wafer. C, D) the exposure of the coated substrate to the UV-light through the printed photo-mask. E) Pouring the PDMS on the embossed features of photoresist and peeling off the cured PDMS. F) Final PDMS molds containing designed features. Reproduced from Ref [46] with permission.

2.4.1.2   Microchip DDS

In oral dosage forms, many therapeutic molecules suffer from poor bioavailability and require other methods of delivery. Local DDSs that ensure the delivery of therapeutics to the proper site can enhance the effectiveness of treatment and potentially eliminate the harmful side effects to the liver that are often caused by oral means of delivery[52]. Implantable DDSs have attracted increasing attention for improving the local delivery and patient compliance.

Microchips as CRSs were originally introduced by Robert Langer and coworkers[53] and were designed to generate a long-term pulsatile release. Achieving pulsatile release is particularly important because the human body secretes molecules such as insulin3, growth hormone, and GnRH in a pulsatile manner. Accordingly, therapies targeting disorders related to these molecules need to be released in a pulsatile fashion to achieve an optimal therapeutic effect. In 1998, Robert Langer and his group conducted a proof-of-concept study with a solid-state silicon microchip that could provide on-demand controlled release of substances. In this microchip, single or multiple chemical substances were entrapped in ~25nl reservoirs covered with thin gold membranes acting as anodes (Figure 2-9A). The release mechanism was based on the electrochemical dissolution of individual anode membranes upon application of voltage. The fabrication of the microchip was a sequential process of photolithography and microelectronic processing techniques. The proof-of-concept study indicated the ability of this model microchip to generate pulsatile release profiles of chemical substances[53].

In 2003, the Langer group proposed a similar platform for achieving pulsatile release in a programmed manner without requiring external stimuli to initiate the release. Similar to the previous platform developed earlier, the device encapsulates single or multiple types of chemicals in 36 micro-sized reservoirs, covered with polymeric membranes on the one side (Figure 2-9B). The characteristics of this polymeric membrane that regulates its degradation rate (e.g., molecular weight, and compositions) determine the time of the release from the reservoir covered with this membrane. The reservoir-covering membranes are made of PLGA with various molecular weights, adjusting their rate of degradation and hence the time at which the chemicals (human growth hormone, dextran, and heparin) are released from each reservoir. The biodegradable polymeric device showed the ability to release four pulses of multiple chemicals over several months, and they successfully obtained a pulsatile release of bioactive heparin over 142 days (Figure 2-9C, D)[54].

The increasing interest in implantable DDSs was followed by the work of Santini and coworkers on developing advanced on-demand and programmed microchip platforms[55]. In 2006, they further enhanced the membrane-covered reservoir design to achieve

remotely controlled pulsatile release of Leuprorelin protein over 6 months in dogs[56]. The release of the therapeutic protein from 100 individual reservoirs was regulated electrothermally, and controlled by telemetry. This method of membrane removal (electrothermal) is preferable over electrochemistry, because it is independent of the chemical compounds of the surrounding environment, as well as being considerably faster. The results for the in vivo experiment of the remotely-controlled microchips indicate the feasibility of the delivery of therapeutic polypeptides using implantable DDSs[56].

The first clinical trial of implantable microchip devices for drug delivery was carried out in 2012. The therapeutic compound delivered in this trial was an osteoporosis treatment (Human parathyroid hormone fragment, hPTH) that generally requires repeated injections of daily dosage and hence has low patient compliance. The microchip device used in this clinical trial has dimensions of 13.0 mm × 5.4 mm × 0.5 mm with 20, 600-nL wirelessly controlled reservoirs containing lyophilized hPTH. The microchips were implanted in 8 women who were suffering from postmenopausal osteoporosis, in the subcutaneous space of the abdomen. The devices were implanted (Figure 2-9E) for four months and were controlled to deliver the once-daily dosage of the drug. The release of the reservoirs is controlled by a computer program that sends and receives information wirelessly to and from the implant, driving the precise timing of dose delivery. Microchip dosing proved capable of providing pharmacokinetic profiles similar to multiple subcutaneous injections, without the burden and pain of injections. This clinical trial demonstrated the potentials of this platform to improve current chronic delivery methods, e.g. repeated insulin injections for diabetic patients[57,58].
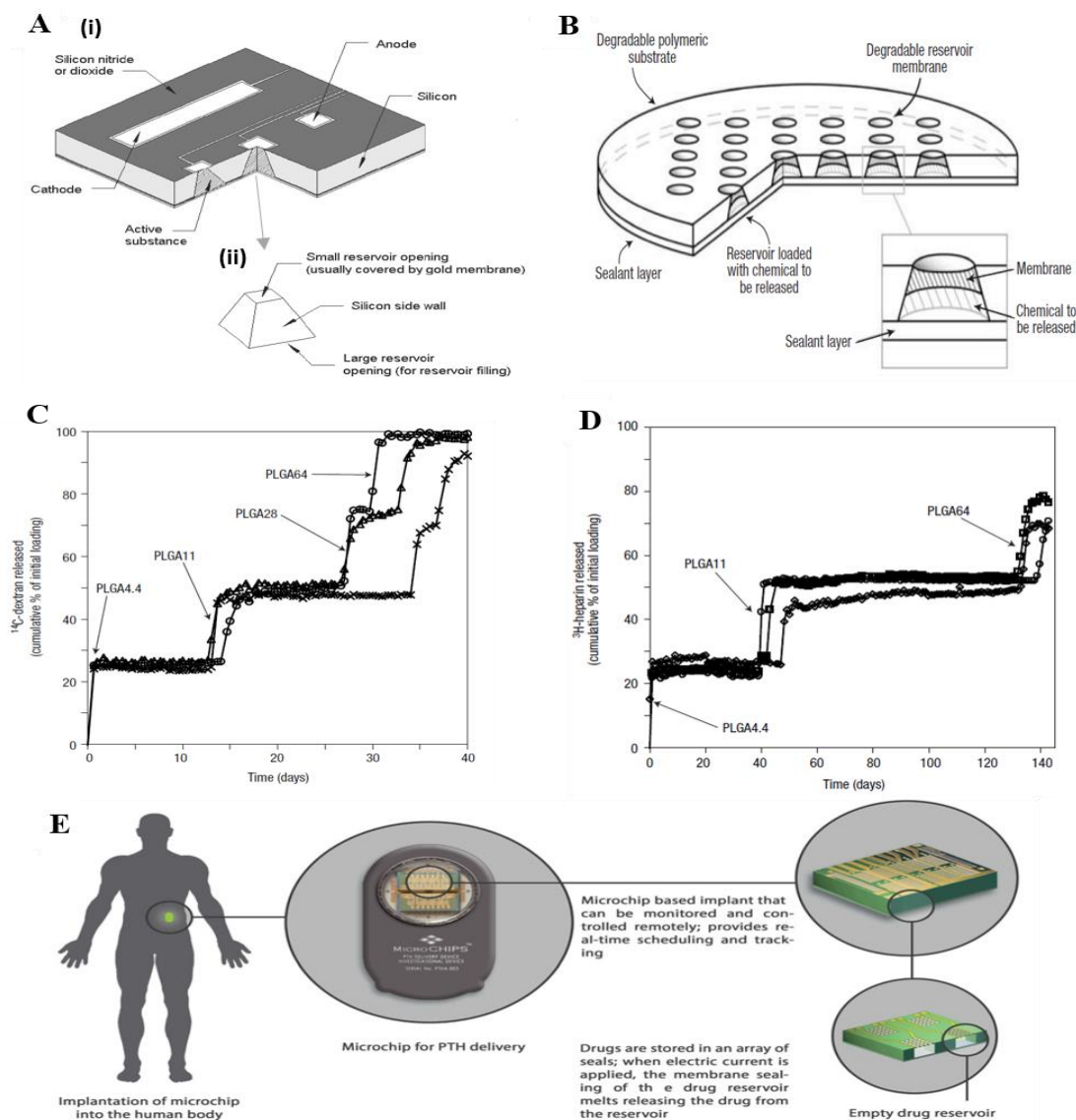
Figure 2-9: Microchip controlled DDSs. A) The implantable silicon microchip device for controlling the release profile of the drug using the electrochemical dissolution of anodes, (i) a view cut showing the reservoirs (ii) enlarged view of a single conical reservoir. Reproduced from Ref [53] with permission. B) The schematic of the microchip device, including the reservoir-containing substrate which is fabricated by a degradable polymer. C) Cumulative percentage of the initial loading of the C-dextran. Each symbol indicates the data from different devices in which the membranes are made of copolymers with different molecular weights. Increasing the molecular weight of the polymeric membranes caused the release times of the chemicals to increase. Arrows show the opening time for each membrane. D) Cumulative percentage of the initial loading of the H-heparin. Increasing the molecular weight of the polymeric membranes results in increased release times of the chemical. Reproduced from Ref [54] with permission. E) The final implantable microchip device and its location in the patients' body to release the hPTH (1-34). Reproduced from Ref [57,58] with permission.

Implantable microchips are attractive means of drug delivery and have proved advantageous in different applications. However, these devices come with their limitations. Implantable means of delivery are inherently invasive, requiring implant surgery to place the DDSs and an explant surgery to remove the device from the body after the dosage is completed. Patients may need to take painkillers and/or anti-inflammatory medications to alleviate the discomfort after surgeries. Current implantable DDSs have not incorporated measurements of the drug's concentration after or during the release; however, a closed-loop control on the release from the device is necessary to avoid under- or over-dosing of the drug. In addition, the methods used for the opening of the reservoirs in proposed microchip devices are not reversible, and accordingly, quality assurance on whether the membrane will be appropriately removed as programmed or upon external stimulation, before implantation, has not been reported. In the clinical trial, patients tolerated the size of the implant, with the microchip device enclosing only 20 reservoirs. An increased number of reservoirs is necessary for treatments requiring more frequent dosing and longer delivery periods, which may be associated with larger implant sizes. Despite attractive features implantable DDSs offer, their widespread development and use are constrained to these limitations, leaving oral dosage forms yet the most commonly used form of delivery[57,1].

2.4.2   3D Printing Technology for Manufacturing Oral Dosage Forms

The oral routes of the drug administration are preferred by patients since they are affordable, noninvasive, and convenient for the patients. Accordingly, oral controlled DDSs have been the focus of many research work in personalized medicine[1]. 3D printing technology has emerged as an attractive fabrication method in the food and pharmaceutical industry due to its ability to manufacture objects with fine features. Modified-release and/or personalized oral dosage forms have been fabricated using 3D printing technology. The oral dosage forms are either directly 3D printed, or indirectly fabricated where molds or containers are 3D printed. Among various types of 3D printing technologies, powder-bed inkjet, fused deposition modeling (FDM), and stereolithography (SLA) have been the most commonly used methods for fabricating

solid oral dosage forms[59]. In what follows, a review on the application of these three 3D printing technologies in the fabrication of solid oral dosage forms for achieving adjustable release rates is presented.

2.4.2.1   Powder-bed Inkjet 3D Printing

The first 3D printer to receive FDA approval for pharmaceutical applications was Aprecia and was based on inkjet printing a binder solution on a power bed. It was used for printing tablets for epilepsy. The inkjet powder-bed 3D printing process (Figure 2-10A) consists of spreading a powder layer onto a plate (bed) with a roller, and introduction of the binder solution to specific areas onto the powder to bind its particles in that area, based on the CAD design. This forms one layer of the structure of interest. The process is additive, meaning the same steps are repeated for each additional powder layer until the desired geometry is built. At last, the residual powder is brushed away. The structures fabricated by this 3D printing technology have high porosity which is beneficial for the production of immediate release tablets[60].

Cima and coworkers were one of the first groups that fabricated solid dosage forms using powder-bed 3D inkjet printing. They used standard pharmaceutical materials and varied the polymer contents to obtain delayed-release tablets. They fabricated tablets that underwent two different release mechanisms, namely erosion and diffusion. In erosion-based tablets, by adjusting the quantity of the polymer, they achieved lag times (the time before the drug starts releasing) varying from 25 to 50mins (Figure 2-10B). Increased polymer content resulted in longer lag times and hence slower release. In tablets with a diffusion-based release, an increase in polymer content resulted in a reduction in the maximum rate of release. The lag time was not affected by polymer content in diffusion-based tablets. The release profile characteristics were proved adjustable through modifying the quantity of polymer in inkjet 3D printers[60].

In a different study, they used the same powder-bed inkjet 3D printing system to develop four different solid dosage forms with distinct release behaviors[61]. The first tablet was designed for immediate/extended release pattern (Figure 2-10C-i). These tablets consisted of two sections, both loaded with chlorpheniramine maleate as the drug. The two sections

had different polymeric contents and hence had specific pH-sensitive release mechanisms. Experiments showed that the release of the drug from the first section happened with a 10min lag time, whereas the second section released the compound over an extended period of 7hrs (Figure 2-10D). The second dosage forms were breakaway tablets (Figure 2-10C-**ii)**. These tablets were programmed to split into two drug-loaded sections by the fast erosion of a part separating the two. The drug-loaded sections erode in gastric fluid over a 30-45 min period. The third type of tablet was designed to achieve enteric dual-pulse release (Figure 2-10C-iii). A total amount of 3.4 mg diclofenac sodium was printed as two separate compartments into the tablet. As for the fabrication, they printed 6 layers of powder with only the binder, followed by a drug-containing layer. The same procedure was repeated, followed by two final layers of powder without drug. The release mechanism is erosion and hence the two diclofenac compartments are released in turn, making two pulses at 1 and 8 hours, as indicated by the release experiments results. The dual pulse devices were designed such that a portion of the drug be released in response to the low pH in the stomach whereas the rest would be released at high pH conditions in the intestine. The tablet design is showed in Figure 2-10C-iv[61].

In 2009, Yu et al. [62] reported powder-bed inkjet 3D printing of a doughnut-shaped DDS with zero-order release kinetics. The tablet design consisted of a model drug in the middle, and release-retardant material containing ethyl cellulose (EC) as the barrier covering the top, bottom, and outer surface of the tablet. The results of the release experiments indicated linear profiles, irrespective of the diameter of the central aperture, the outer diameter, or the table height. The release rate was adjustable by modifying the thickness, and quantity of EC of the outer surface covering the core. This study demonstrated the application of powder-bed 3D inkjet printing for achieving zero-order release kinetics throughout the entire dissolution process.
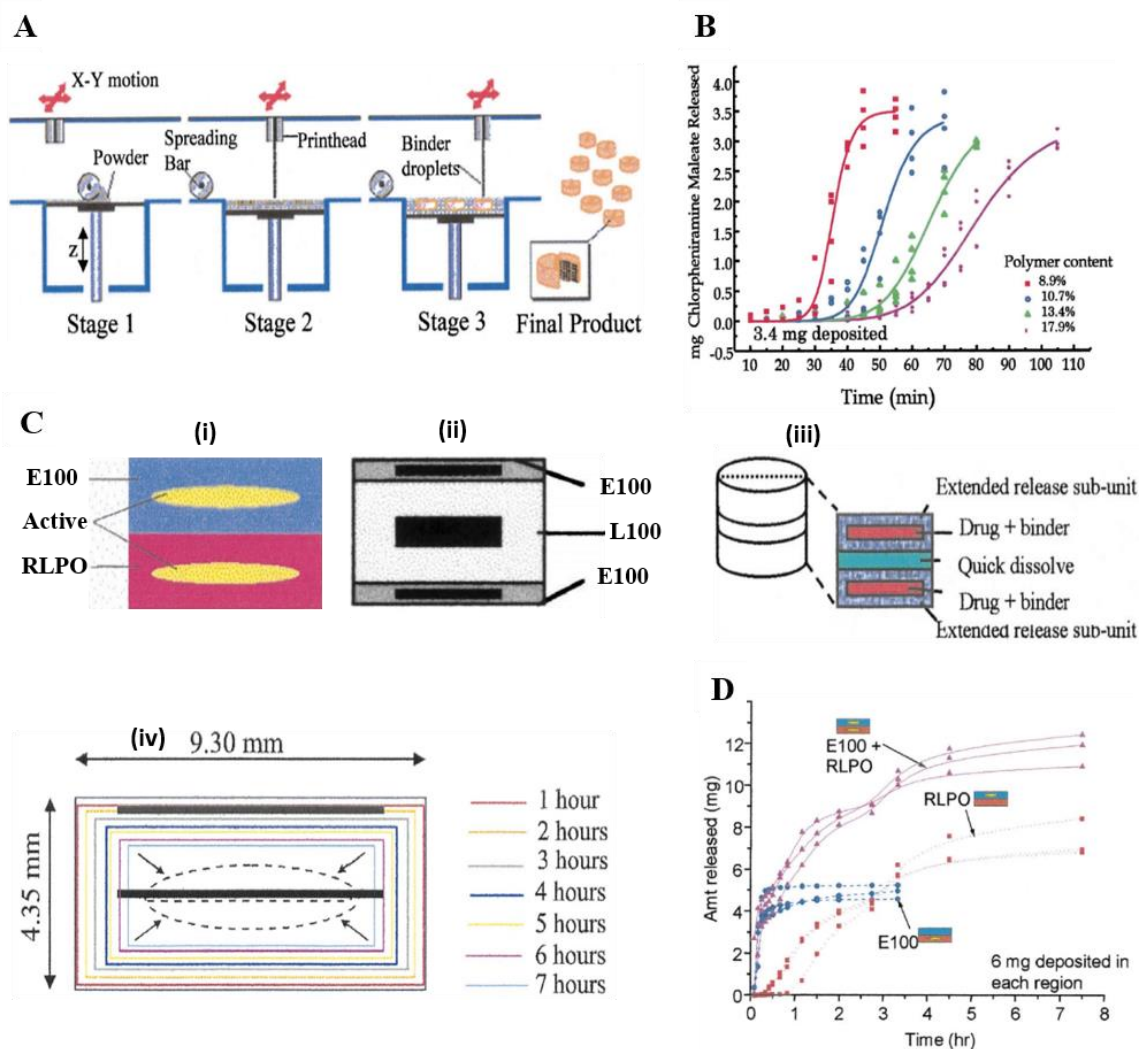
Figure 2-10: Directly printing the solid oral dosage forms using the powder-bed inkjet 3D printing process. A) The schematic illustration of the powder-bed inkjet 3D printing process. B) Variation of the lag times in releasing the chemicals by adjusting the content of the polymer. Reproduced from Ref [60] with permission. C) Four different tablets printed by the powder-bed inkjet 3D printer machine: schematics showing (i) immediate-extended release pattern tablet, (ii) the breakaway tablet, (iii) the enteric dual-pulse release tablet, and (iv) the dual-pulse release tablet. D) The release profile for the immediate-extended tablet. The first section made of E100 20% w/w started releasing after 10 minutes (lag time). The second section made of Eudragit RLPO and acetone released its content over an extended period of 7 hours. Reproduced from Ref [61] with permission.

In 2012, Genina et al. reported a novel method for fabricating solid dosage forms. It combines inkjet printing with flexographic printing to achieve controlled release patterns of therapeutics. They studied the impact of using three different paper substrates as porous carriers for DDSs on release characteristics. Release kinetic studies were conducted on tablets before and after coating various thickness of EC polymer film using flexographic printing. The release profile can be adjusted to decreasing or constant by changing the number of coating layers and/or the thickness of the coatings[63].

In 2017, Kyobula et al. reported a solvent-free 3D inkjet printing of solid dosage forms[64]. They fabricated matrix tablets containing a biocompatible and FDA approved wax as the carrier and a practically insoluble drug. In this study, they fabricated tablets with honeycomb geometries. They evaluated the ability to control the drug release profile by modifying the honeycomb characteristic, e.g. cell diameter and hence, the surface area. Larger than middle-sized honeycomb structures resulted in lower release rates due to a decrease in tablet surface area. This design allowed control over drug release rates by modifying the geometry[65].

2.4.2.2   Fused-deposition Modeling (FDM)

Another type of 3D printing is fused-deposition modeling (FDM). In FDM methods, thermoplastic polymer filaments are extruded. Once filaments are in a melted semi-liquid form, they pass through a nozzle with elevated temperature. Filaments exit the heated nozzle and are deposited on the build plate on specified locations where they will be hardened. FDM 3D printing poses some advantages that made this technology suitable for manufacturing oral dosage forms. It can produce tablets with higher resolution compared to inkjet 3D printing, allowing for more accurate drug release. FDM-based machines are also capable of printing relatively intricate designs to achieve modified release profiles. More importantly, FDM 3D printing is easily set up and is relatively cheap[59]. Studies in which FDM-based 3D printers have been used to fabricate oral tablets can be divided into two classes: direct printing of tablets and printing containers/molds, helping the preparation of controlled-release tablets indirectly. A brief review of some studies in both categories is presented below.

Goyanes et al. fabricated tablets using the combination of FDM and hot-melt extrusion (HME) processing. They showed the potential of FDM technique in manufacturing oral dosage forms by producing tablets with different geometries, which is not easily achievable using conventional methods of tablet fabrication, e.g. powder compaction. They successfully printed tablets with five different geometries (Figure 2-11A). The filament was made of a water-soluble polymer (polyvinyl alcohol, PVA) loaded with paracetamol. They investigated the impact of tablet geometries, including the tablet surface area, volume, and the surface area to volume ratio (SA/V ratio) on drug release profiles by conducting separate experiments. Results showed that the fractional drug release rates were dependent on the SA/V ratio of the dosage forms. When the SA/V ratios for all the tablets were identical, almost all of them released 90 percent of their loaded drugs in 10 hours regardless of the differences in surface areas and the volumes of the tablets (Figure 2-11B). This study indicated the potential of FDM 3D printing as a low-cost fabrication process for manufacturing tablets with relatively complex geometries, which allows for controlling the release rate of the drug by adjusting the geometry of dosage forms[66].

In another study, Tagami et al. fabricated composite tablets using the FDM 3D printing method to tune the release rate of a model drug (calcein) loaded in PVA. Filler components were either the water-soluble polymer (PVA) or a water-insoluble polymer (PLA) which did not contain any drug[67]. They used a dual nozzle 3D printer to print the drug component and the filler component separately. They produced different tablets with both PVA and PLA fillers (Figure 2-11C). By changing the thickness of the PLA, they could adjust the lag time. Results of in-vitro drug release tests indicated that an increased surface area increases the initial release rate of the model drug from the tablets. They designed two different shapes of the drug component with increasing and decreasing surface areas. Results indicated zero-order increasing and decreasing release rates, respectively. They also produced a cylindrical drug component with constant surface area and increased the thickness of the covering PVA to increase the lag time (Figure 2-11D). In addition, they showed the potential of the composite tablets to deliver drugs to certain locations through the GI tract by adjusting the release timing. Therefore, these tablets

with various wall thicknesses can be used as alternatives to pH-sensitive or other exogenously stimulated DDSs[67].
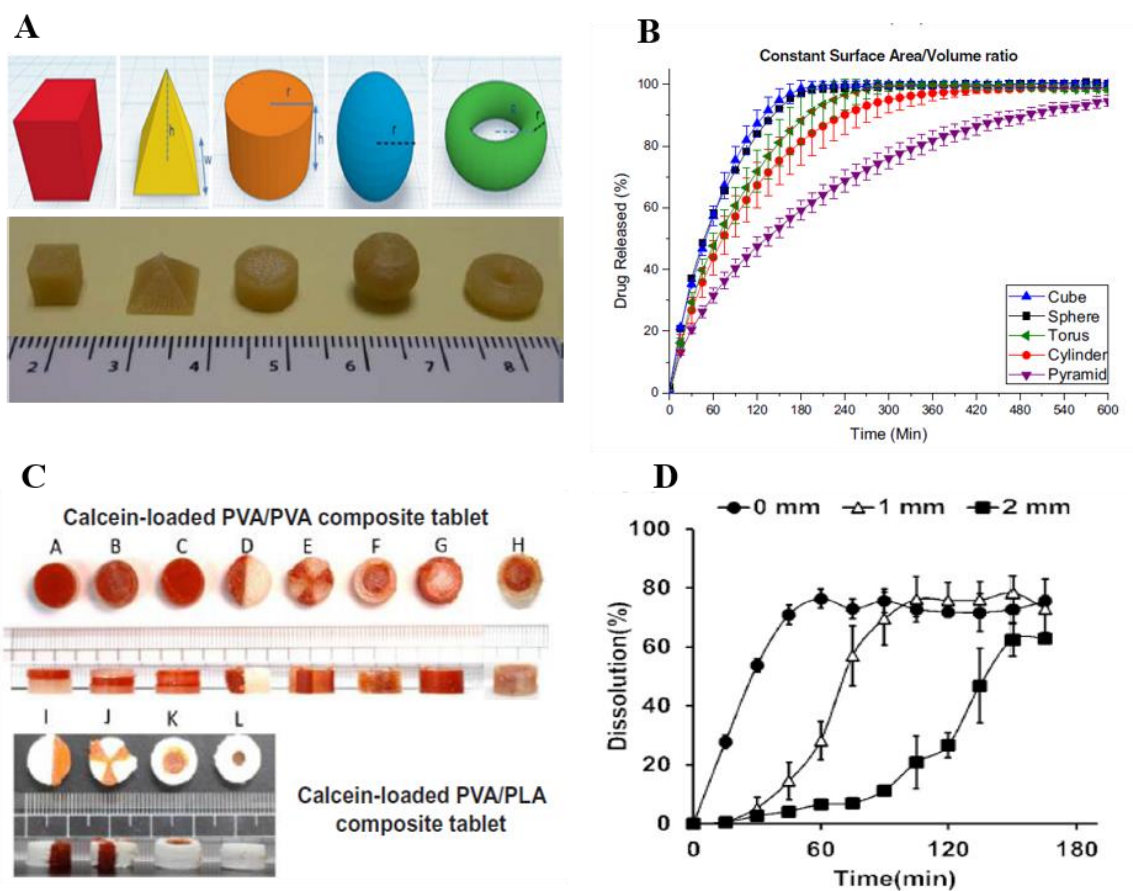
Figure 2-11: Direct FDM printing of oral tablets. A) Five different tablet geometries printed by FDM technique. B) Tablets released their contents in 2-3 hours when the SA/V ratio for all of them was the same. Reproduced from Ref [66] with permission. C) Eight calcein-loaded PVA/PVA composite tablets (top) and four calcein-loaded PVA/PLA composite tablets (bottom). D) By increasing the thickness of the covering layer, the lag time increased. Reproduced from Ref [67] with permission.

Despite the attractive properties of FDM for directly printing tablets and its potential for manufacturing the personalized treatments, it comes with certain limitations. FDM operation involves exposure of the polymer to high temperatures, which is only tolerated by thermoplastic polymers with a high glass transition temperature. These polymers have

relatively high molecular weights, and therefore the resultant structure exhibits extended-release patterns that are not always suitable for patient dosage needs[68].

FDM can be used indirectly for manufacturing controlled-release tablets. In 2015, Andrea Gazzaniga and his group used FDM technology to explore the possibility of using 3D printing for fabricating Hydroxypropyl cellulose (HPC)-based capsular controlled DDSs. The capsular DDSs design consisted of a cap and a body. They obtained the release characteristics and evaluated the possibility of obtaining a pulsatile release with this design. Lag time (in this study is defined to be the time passed before 10% of the chemical is released), and pulse time (the time duration between release of 10% and 90% of the drug), were measured 70min and 10min, respectively. The results indicated the potential of FDM for rapid prototyping of capsular DDSs, and hence avoiding the time-consuming process of mold development and enhancement[69].

Andrea Gazzaniga and his group improved the above design in an attempt to provide more flexibility with the capsular devices[70]. They modified the capsule design and composition to encapsulate different therapeutic compounds. The capsule was partitioned into two hollow halves, with the timing of release from each half independently during the capsule design by changing the thickness and/or composition of the compartment. Using combinations of compartment wall thickness and polymer characteristics, they could achieve immediate, enteric, and pulsatile releases. They obtained the release profile of the capsules, with compartments fabricated from PVA filaments with different thicknesses (Figure 2-12A). Release profiles of capsules with the same compartment thickness and different compartment compositions were also obtained (Figure 2-12B). This design can be particularly advantageous for improving patient compliance by ensuring the dosing schedule of prescribed with therapies that are not compatible or interact in gastrointestinal tract[71].

In another study, Sun et al.[72] fabricated tablets using a commercially available FDM printer to achieve pre-determined release rates of drugs. They fabricated polymeric tablets within molds and containers created by extruded polymeric filaments. The impermeable container made of PLA was utilized to seal all surfaces of the drug-

containing polymer. Drugs were released from the one side that was not covered by the container. Different release patterns were obtained from tablets due to the near zero-order erosion of polyanhydrides from the surface exposed to PBS. This design was also capable of incorporating two model drugs into one tablet and releasing them with different patterns. (Figure 2-12C, D). This study shows the potential of FDM 3D printing technology for creating containers and molds for achieving different tablet designs.
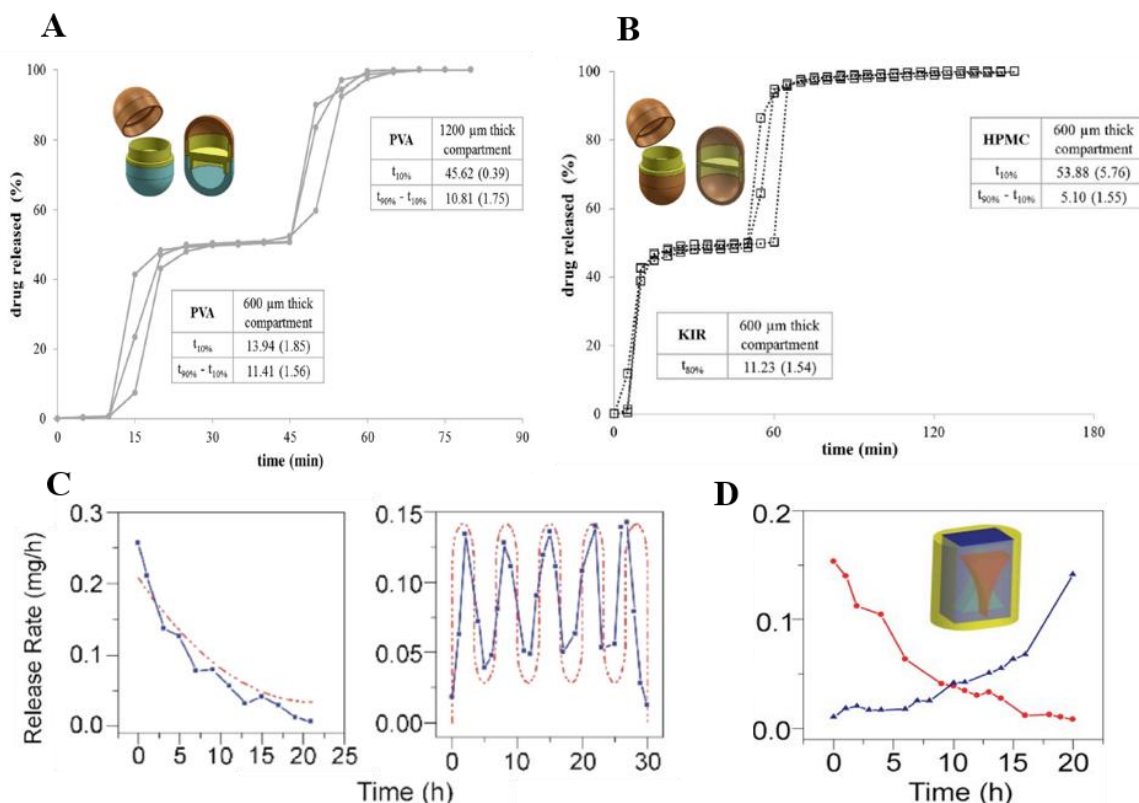
Figure 2-12: FDM printing of containers and molds to create controlled-release tablets. A) The capsular DDS with different thicknesses, producing a two-pulse release profile. B) Two pulse release profile of the capsular DDS achieved by having two different materials for each compartment, with consistent thicknesses. Reproduced from Ref[70] with permission. C) Customizable release rates of drugs (e.g., decreasing and pulsatile) from erodible tablets fabricated by containers and molds printed by FDM 3D printers. D) Tablets for releasing two drugs with different release rates at the same time. Reproduced from Ref [72] with permission.

FDM is an interesting substitute for conventional fabrication methods of tablets due to its potential in manufacturing desired geometries to achieve a more accurate dosage. Unlike

conventional additive manufacturing methods, FDM can be used to create rounded corners which enhances patient compliance. However, there are limitations to this method which reduces its flexibility and wide-spread use. The high temperature required during FDM steps can damage thermally labile drugs. Besides, only a few biodegradable thermoplastic polymers can tolerate such high-temperature conditions. Although FDM has been used in fabrication of various geometries, the resolution of these printers may not be high enough to achieve the desired surface quality, as well as acute angles required in some dosage forms.

2.4.2.3 Lithography-based 3D Printing

Research on Stereolithography (SLA) 3D printing has been around since 1970s; however, Chuck Hull introduced the term in 1984 and was granted the patent for SLA in 1986. SLA technology is based on photopolymerization, that is, polymerization and hence solidification of the liquid resin upon exposure to laser. Photopolymerization is conducted in an additive manner (similar to other 3D printing technologies) where for each layer a CAD design guides the depth of the laser focus, obtaining localized photopolymerization, and eventually producing the 3D object of interest. SLA offers several advantages over other 3D printing technologies previously reviewed. In contrast to FDM methods, SLA does not expose the materials to high temperatures, and therefore it is suitable for fabricating DDSs with thermally labile therapeutics. SLA's resolution is superior to other 3D printing technologies and is only restrained by the laser width[73]. Digital light processing (DLP) 3D printing is also a lithography-based method with higher resolution and printing speed in comparison to SLA 3D printing. Typically, a UV-curable resin that can be printed by SLA would also be used in DLP. SLA utilizes lasers to cure the photo-curable solution point by point, while DLP uses a digital projector to cast and cure an entire slice of objects. Fast manufacturing times for the fabrication of complex structures with high resolution can be achieved by both methods, especially by DLP 3D printers. Recently, there has been increased attention to use DLP for manufacturing oral dosage forms[74].

The use of SLA technology for printing oral dosage forms was introduced by Simon Gaisford and Abdul W. Basit, and coworkers[73]. In this study, Polyethylene glycol

diacrylate (PEGDA) and polyethylene glycol 300 (PEG 300) were used as monomers in different ratios, aiming at obtaining different release kinetics at each ratio. The SLA 3D printed tablets with two different drugs (paracetamol and 4-ASA) are shown in Figure 2-13A. Tablets were printed in torus shapes, which are complicated structures to achieve by other manufacturing methods. An increase in the PEGDA portion resulted in slower release rates. The release kinetics proved independent from changes in the pH, as shown in the release profile graphs (Figure 2-13B, C)[73]. This study proved the potential of SLA 3D printing in the fabrication of high-resolution solid oral dosage forms from thermally labile drugs, with adjustable release rates to achieve immediate or extended profile.
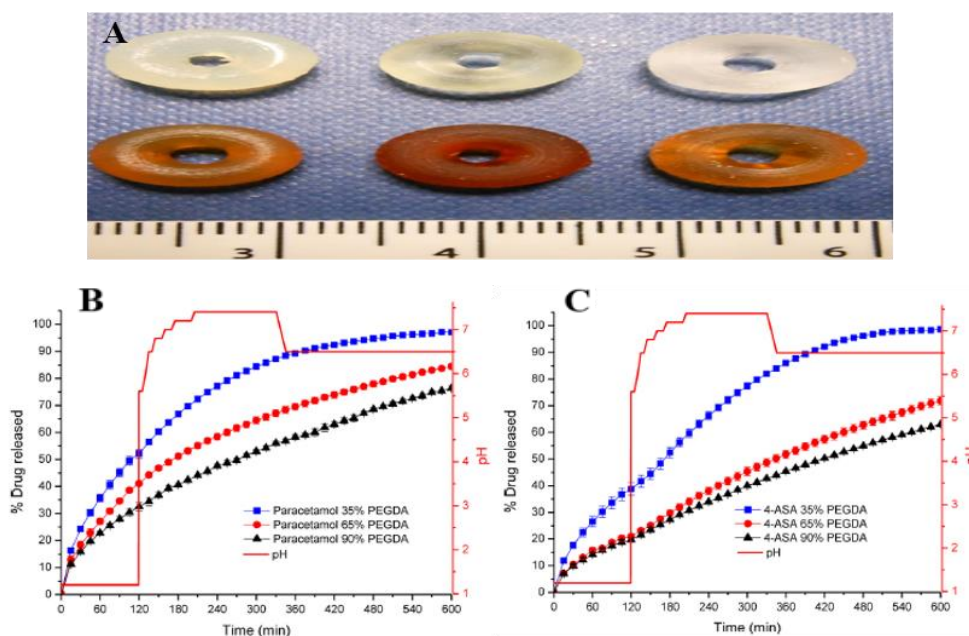
Figure 2-13: SLA printed tablet structure and release behavior. A) SLA printed tablets with paracetamol (top row) and 4-ASA (bottom row) as model drugs. Each row from left to right show tablets with PEGDA to PEG 300 ratios of 3.5:6.5, 6.5:3.5, and 9:1. B) The release profiles of the paracetamol from tablets with different polymer ratios. The release is slower for higher PEGDA percentages and is insensitive to changes in the pH. C) The release profiles of the 4-ASA. Slower release from higher PEGDS tablets was observed. The release showed independent from pH. Reproduced from Ref [73] with permission.

SLA 3D printing technology has offered benefits over conventional 3D printing methods that are promising for further advances in fabricating personalized oral dosage forms. The

main limitation associated with SLA 3D printing, however, is the limited number of photocrosslinkable resins that are at the same time non-toxic, safe, and biocompatible.

In this section, recent developments in the fabrication of advanced controlled DDSs for achieving various release profiles of drugs are reviewed. Micro-fabrication has been used to create microchip devices that are implanted in the body to release drugs with pre-determined rates of release. Despite the high resolution of micro-fabrication methods and their ability to produce high-throughput platforms, several limitations of using implantable microchips (discussed in section 2.4.1.2), make the oral controlled DDSs the most desired option. Numerous studies such as studies reviewed in section 2.4.2 show substantial progress in the fabrication of polymeric oral tablets with adjustable release profiles using 3D printing technology. Most of the studies reported monotonic or constant release profiles of drugs, while some others achieved more complicated release profiles such as pulsatile release rates. The more complicated release patterns were achieved by more elaborate tablet designs and specific fabrication techniques, demonstrating the feasibility of creating tablets with various release patterns of drugs. Although these studies show that personalized medicine is no longer a dream, there exist some limitations in fabrication of modified release tablets that can hinder their widespread application. Some of these limitations can be addressed by improving the tablet designs and using appropriate fabrication methods. For example, the resolution of the fabrication method can determine the precision of the release rates. Micro-fabrication techniques such as photolithography are capable of creating miniaturized fine features with high resolution, whereas the resolution of the inexpensive and commercially available 3D printers such as FDM-based printers are not sufficient for printing tablets with complex geometries. SLA or DLP 3D printers have higher resolution for producing tablets; however, the limited number of printable materials that are compatible with these types of machines reduces their widespread application in producing controlled-release tablets. In addition, scalability and high-throughput manufacturing is a critical characteristic of any potentially successful fabrication method. High-throughput manufacturing is currently a significant challenge in production of advanced controlled DDSs with adjustable release rates. Most of the studies described in section 2.4.2, reported fabrication of a single tablet in each experiment, reducing the chances of their practical

use in clinical settings. Manufacturing each tablet can take considerable amount of time, and the reproducibility level is low.

2.5   Objectives

The objectives of this study are to:

(i) prepare and characterize surface eroding polymers used in the fabrication of drug-loaded tablets, and to study the mass loss profile of the polymers comprehensively.

(ii) develop a high-throughput fabrication platform for manufacturing the tablets that can provide adjustable drug release patterns.

References

1.   Alhnan, M. A. *et al.* Emergence of 3D Printed Dosage Forms: Opportunities and Challenges. *Pharm. Res.* **33**, 1817–1832 (2016).

2.   Deshpande, A. A., Rhodes, C. T., Shah, N. H. & Malick, A. W. Controlled-release drug delivery systems for prolonged gastric residence: An overview. *Drug Development and Industrial Pharmacy* (1996). doi:10.3109/03639049609108355

3.   Verma, R. K., & Garg, S. Drug delivery technologies and future directions. *Pharmaceutical Technology* (2001), 25(2), 1-14.

4.   Huynh, C. T. & Lee, D. S. Controlled Release. in *Encyclopedia of Polymeric Nanomaterials* 439–449 (Springer Berlin Heidelberg, 2015). doi:10.1007/978-3-642-29648-2_314

5.   Liechty, W. B., Kryscio, D. R., Slaughter, B. V. & Peppas, N. A. Polymers for Drug Delivery Systems. *Annu. Rev. Chem. Biomol. Eng.* (2010). doi:10.1146/annurev-chembioeng-073009-100847

6.   Uhrich, K. E., Cannizzaro, S. M., Langer, R. S. & Shakesheff, K. M. Polymeric Systems for Controlled Drug Release. *Chem. Rev.* **99**, 3181–3198 (1999).

7.   Dhaliwal, K. Biodegradable Polymers and their Role in Drug Delivery Systems. *Biomed. J. Sci. Tech. Res.* (2018). doi:10.26717/bjstr.2018.11.002056

8.   Kulkarni, R. K., Moore, E. G., Hegyeli, A. F. & Leonard, F. Biodegradable poly(lactic acid) polymers. *J. Biomed. Mater. Res.* **5**, 169–81 (1971).

9.   Kamaly, N., Yameen, B., Wu, J. & Farokhzad, O. C. Degradable Controlled-Release Polymers and Polymeric Nanoparticles: Mechanisms of Controlling Drug Release. *Chem. Rev.* **116**, 2602–63 (2016).

10.   Heller, J. Biodegradable polymers in controlled drug delivery. *Crit. Rev. Ther. Drug Carrier Syst.* **1**, 39–90 (1984).

11. Ulery, B. D., Nair, L. S. & Laurencin, C. T. Biomedical applications of biodegradable polymers. *Journal of Polymer Science, Part B: Polymer Physics* (2011). doi:10.1002/polb.22259

12. Langer, R. New methods of drug delivery. *Science (80-.).* (1990). doi:10.1126/science.2218494

13. Siegel, R. A. & Rathbone, M. J. Overview of controlled release mechanisms. in *Fundamentals and Applications of Controlled Release Drug Delivery* (2012). doi:10.1007/978-1-4614-0881-9_2

14. Robinson, J. & Jantzen, G. Sustained-and Controlled-Release Drug-Delivery Systems. in (2002). doi:10.1201/9780824744694.ch15

15. Stamatialis, D., Sanopoulou, M. & Papadokostaki, K. G. Controlled Drug Release Systems: Mechanisms and Kinetics. in *Biomedical Membranes and (Bio)Artificial Organs* (2018). doi:10.1142/9789813223974_0001

16. Omidian, H. & Park, K. Hydrogels. in *Fundamentals and Applications of Controlled Release Drug Delivery* 75–105 (Springer US, 2012). doi:10.1007/978-1-4614-0881-9_4

17. Peppas, N. A. & Narasimhan, B. Mathematical models in drug delivery: how modeling has shaped the way we design new drug delivery systems. *J. Control. Release* **190**, 75–81 (2014).

18. Göpferich, A. Mechanisms of polymer degradation and erosion. *Biomaterials* **17**, 103–114 (1996).

19. Burkersroda, F. Von, Schedl, L. & Göpferich, A. Why degradable polymers undergo surface erosion or bulk erosion. *Biomaterials* (2002). doi:10.1016/S0142-9612(02)00170-9

20. Rosen, H. B., Chang, J., Wnek, G. E., Linhardt, R. J. & Langer, R. Bioerodible polyanhydrides for controlled drug delivery. *Biomaterials* **4**, 131–3 (1983).

21. Domb, A., Jain, J. P. & Kumar, N. Polyanhydrides. in *Handbook of Biodegradable Polymers* 45–75 (Wiley-VCH Verlag GmbH & Co. KGaA, 2011). doi:10.1002/9783527635818.ch3

22. Lesniak, M. S. & Brem, H. Targeted therapy for brain tumours. *Nature Reviews Drug Discovery* (2004). doi:10.1038/nrd1414

23. Poetz, K. L. & Shipp, D. A. Polyanhydrides: Synthesis, Properties, and Applications. *Australian Journal of Chemistry* (2016). doi:10.1071/CH16144

24. Domb, A. J., Ron, E. & Langer, R. Poly (anhydrides). 2. One-Step Polymerization Using Phosgene or Diphosgene as Coupling Agents. *Macromolecules* (1988). doi:10.1021/ma00185a008

25. Shipp, D. A., McQuinn, C. W., Rutherglen, B. G. & McBath, R. A. Elastomeric and degradable polyanhydride network polymers by step-growth thiol-ene photopolymerization. *Chem. Commun.* (2009). doi:10.1039/b911557a

26. Kolb, H. C., Finn, M. G. & Sharpless, K. B. Click Chemistry: Diverse Chemical

Function from a Few Good Reactions. *Angewandte Chemie - International Edition* (2001).

27. Göpferich, A. & Tessmar, J. Polyanhydride degradation and erosion. *Adv. Drug Deliv. Rev.* (2002). doi:10.1016/S0169-409X(02)00051-0

28. Göpferich, A. & Langer, R. The influence of microstructure and monomer properties on the erosion mechanism of a class of polyanhydrides. *J. Polym. Sci. Part A Polym. Chem.* **31**, 2445–2458 (1993).

29. Gopferich, A. & Langer, R. *Modeling of Polymer Erosiont. Macromolecules* **26**, (1993).

30. Leong, K. W., Brott, B. C. & Langer, R. Bioerodible polyanhydrides as drug-carrier matrices. I: Characterization, degradation, and release characteristics. *J. Biomed. Mater. Res.* **19**, 941–55 (1985).

31. Shakesheff, K. M. *et al. In Situ Atomic Force Microscopy Imaging of Polymer Degradation in an Aqueous Environment. Langmuir* **10**, (1994).

32. Sandor, M., Bailey, N. A. & Mathiowitz, E. Characterization of polyanhydride microsphere degradation by DSC. *Polymer (Guildf).* **43**, 279–288 (2002).

33. Brem, H. Polymers to treat brain tumours. *Biomaterials* **11**, 699–701 (1990).

34. Santos, C. A. *et al.* Poly(fumaric-co-sebacic anhydride). A degradation study as evaluated by FTIR, DSC, GPC and X-ray diffraction. *J. Control. Release* **60**, 11–22 (1999).

35. Akbari, H., D'Emanuele, A. & Attwood, D. Effect of geometry on the erosion characteristics of polyanhydride devices. 965–966 (1997).

36. Shieh, L. *et al.* Erosion of a new family of biodegradable polyanhydrides. *J. Biomed. Mater. Res.* **28**, 1465–1475 (1994).

37. Tamada, J. A. & Langer, R. Erosion kinetics of hydrolytically degradable polymers. *Proc. Natl. Acad. Sci. U. S. A.* **90**, 552–556 (1993).

38. Langer, R. Biomaterials in drug delivery and tissue engineering: One laboratory's experience. *Acc. Chem. Res.* **33**, 94–101 (2000).

39. Rutherglen, B. G., McBath, R. A., Huang, Y. L. & Shipp, D. A. Polyanhydride networks from thiol-ene polymerizations. *Macromolecules* **43**, 10297–10303 (2010).

40. Poetz, K. L. *et al.* Photopolymerized cross-linked thiol-ene polyanhydrides: Erosion, release, and toxicity studies. *Biomacromolecules* **15**, 2573–2582 (2014).

41. Poetz, K. L., Mohammed, H. S. & Shipp, D. A. Surface eroding, semicrystalline polyanhydrides via thiol-ene 'click' photopolymerization. *Biomacromolecules* **16**, 1650–1659 (2015).

42. Kalsbeek, A. *et al.* SCN outputs and the hypothalamic balance of life. *J. Biol. Rhythms* **21**, 458–69 (2006).

43. Smolensky, M. H. & Peppas, N. A. Chronobiology, drug delivery, and

chronotherapeutics. *Adv. Drug Deliv. Rev.* **59**, 828–51 (2007).

44. Davoodi, P. *et al.* Drug delivery systems for programmed and on-demand release. *Advanced Drug Delivery Reviews* (2018). doi:10.1016/j.addr.2018.07.002

45. Chung, B. G., Kang, L. & Khademhosseini, A. Micro- and nanoscale technologies for tissue engineering and drug discovery applications. *Expert Opin. Drug Discov.* **2**, 1653–68 (2007).

46. Weibel, D. B., Diluzio, W. R. & Whitesides, G. M. Microfabrication meets microbiology. *Nat. Rev. Microbiol.* **5**, 209–18 (2007).

47. Xia, Y., Rogers, J. A., Paul, K. E. & Whitesides, G. M. Unconventional Methods for Fabricating and Patterning Nanostructures. *Chem. Rev.* (1999). doi:10.1021/cr980002q

48. Sant, S. *et al.* Microfabrication technologies for oral drug delivery. *Adv. Drug Deliv. Rev.* **64**, 496–507 (2012).

49. Mcdonald, J. C. & Whitesides, G. M. Poly(dimethylsiloxane) as a Material for Fabricating Microfluidic Devices. (2002). doi:10.1021/ar010110q

50. Tao, S. L. & Desai, T. A. Microfabricated drug delivery systems: From particles to pores. *Advanced Drug Delivery Reviews* (2003). doi:10.1016/S0169-409X(02)00227-2

51. Hilt, J. Z. & Peppas, N. A. Microfabricated drug delivery devices. *International Journal of Pharmaceutics* (2005). doi:10.1016/j.ijpharm.2005.09.022

52. Brem, H. & Langer, R. Polymer-Based Drug Delivery to the Brain. **3**, 52–61

53. Santini Jr, J. T., Cima, M. J. & Langer, R. Acontrolled-releasemicrochip. *Phys. Rev. B* **54**, 7128–7139 (1996).

54. Richards Grayson, A. C. *et al.* Multi-pulse drug delivery from a resorbable polymeric microchip device. *Nat. Mater.* (2003). doi:10.1038/nmat998

55. Maloney, J. M. *et al.* Electrothermally activated microchips for implantable drug delivery and biosensing. *J. Control. Release* **109**, 244–255 (2005).

56. Prescott, J. H. *et al.* Chronic, programmed polypeptide delivery from an implanted, multireservoir microchip device. *Nat. Biotechnol.* **24**, 437–438 (2006).

57. Langer, R. *et al.* First-in-Human Testing of a Wirelessly Controlled Drug Delivery Microchip. *Sci. Transl. Med.* **4**, 122ra21-122ra21 (2012).

58. Sutradhar, K. B. & Sumi, C. D. Implantable microchip: The futuristic controlled drug delivery system. *Drug Deliv.* **23**, 1–11 (2016).

59. Hsiao, W. K., Lorber, B., Reitsamer, H. & Khinast, J. 3D printing of oral drugs: a new reality or hype? *Expert Opin. Drug Deliv.* **15**, 1–4 (2018).

60. Katstra, W. E. *et al.* Oral dosage forms fabricated by Three Dimensional Printing(TM). *J. Control. Release* (2000). doi:10.1016/S0168-3659(99)00225-4

61. Rowe, C. . *et al.* Multimechanism oral dosage forms fabricated by three dimensional printing[TM]. *J. Control. Release* **66**, 11–17 (2000).

62.   Yu, D. G. *et al.* Novel drug delivery devices for providing linear release profiles fabricated by 3DP. *Int. J. Pharm.* **370**, 160–166 (2009).

63.   Genina, N. *et al.* European Journal of Pharmaceutical Sciences Tailoring controlled-release oral dosage forms by combining inkjet and flexographic printing techniques. *Eur. J. Pharm. Sci.* **47**, 615–623 (2012).

64.   Kyobula, M. *et al.* 3D inkjet printing of tablets exploiting bespoke complex geometries for controlled and tuneable drug release. *J. Control. Release* **261**, 207–215 (2017).

65.   Grodowska, K. & Parczewski, A. Organic solvents in the pharmaceutical industry. *Acta Pol. Pharm. - Drug Res.* **67**, 3–12 (2010).

66.   Goyanes, A., Robles Martinez, P., Buanz, A., Basit, A. W. & Gaisford, S. Effect of geometry on drug release from 3D printed tablets. *Int. J. Pharm.* **494**, 657–663 (2015).

67.   Tagami, T. *et al.* Defined drug release from 3D-printed composite tablets consisting of drug-loaded polyvinylalcohol and a water-soluble or water-insoluble polymer filler. *Int. J. Pharm.* **543**, 361–367 (2018).

68.   Arafat, B. *et al.* Tablet fragmentation without a disintegrant: A novel design approach for accelerating disintegration and drug release from 3D printed cellulosic tablets. *Eur. J. Pharm. Sci.* **118**, 191–199 (2018).

69.   Melocchi, A. *et al.* 3D printing by fused deposition modeling (FDM) of a swellable/erodible capsular device for oral pulsatile release of drugs. *J. Drug Deliv. Sci. Technol.* **30**, 360–367 (2015).

70.   Maroni, A. *et al.* 3D printed multi-compartment capsular devices for two-pulse oral drug delivery. *J. Control. Release* **268**, 10–18 (2017).

71.   Maroni, A., Zema, L., Curto, M. D. Del, Loreti, G. & Gazzaniga, A. Oral pulsatile delivery: Rationale and chronopharmaceutical formulations. *Int. J. Pharm.* **398**, 1–8 (2010).

72.   Sun, Y. & Soh, S. Printing Tablets with Fully Customizable Release Profiles for Personalized Medicine. *Adv. Mater.* **27**, 7847–53 (2015).

73.   Wang, J., Goyanes, A., Gaisford, S. & Basit, A. W. Stereolithographic (SLA) 3D printing of oral modified-release dosage forms. *Int. J. Pharm.* **503**, 207–212 (2016).

74.   Awad, A., Trenfield, S. J., Goyanes, A., Gaisford, S. & Basit, A. W. Reshaping drug development using 3D printing. *Drug Discovery Today* **23**, 1547–1555 (2018).

Chapter 3

3   A Comprehensive Study on Mass Loss Profile of Thiol-ene Polyanhydrides

In this chapter, we explore the effect of different parameters on mass loss (erosion) profiles of polyanhydrides synthesized by thiol-ene photopolymerization. A comparative study on release kinetic models fitting for better understanding of the polymers' erosion behavior is also described.

3.1   Materials and Methods

3.1.1   Materials

4-pentenoic anhydride (PNA), 2, 2-(Ethylenedioxy)diethanethiol (3,6-Dioxa-1,8-octane-dithiol, EGDT), Pentaerythritol tetrakis(3-mercaptopropionate) (PETMP), 1-Hydroxycyclohexyl phenyl ketone, and acid orange 10 (orange G) were purchased from Sigma Aldrich Chemical Co. and were used as received. 3D printer acrylate-based resin (Clear 2005T) was purchased from MiiCraft. Sylgard 184 Silicone Elastomer pre-polymer and curing agent were purchased from Ellsworth Adhesive Chemical Co., for making PDMS.

3.1.2   Polymer Synthesis Procedure

1-Hydroxycyclohexyl phenyl ketone (photo-initiator, 0.1wt %) was weighed and placed into a 15 ml Falcon tube. Then, PNA was transferred into the tube, followed by the mixture of EGDT and PETMP. The solution was mixed to obtain a homogenous mixture. The initial mole ratio of PNA to the total amount of monomers containing thiol groups (EGDT and PETMP) was 100:100. In this study, four different initial mole ratios of PNA to PETMP and EGDT were prepared and used including PNA: PETMP: EGDT = 100:100:0, 100:75:25, 100:50:50, and 100:25:75. The homogenous mixture was then purged under the inert gas (nitrogen or argon) for 3 minutes and was transferred to PDMS molds. The pre-polymer solution in molds was exposed to UV-light (CL-1000 UVP Cross-linker) equipped with 365 nm UV lamps (intensity=~5 mW/cm^2) for 5 minutes.

For some of the experiments, we added a model compound for which acid orange 10 (1-3wt %) was weighted and added to the purged solution and mixed using sonication for 25 minutes. Similar to the pre-polymer without the model compound, the dye-loaded solution was transferred to PDMS molds and was synthesized under the same UV-light for 5 to 15 minutes. The reaction scheme is presented in Appendix A-1.

3.1.3   Polymer Characterization

Four polymers with initial mole ratios of PNA to PETMP and EGDT were synthesized. The attenuated total reflectance Fourier-Transform Infrared Spectroscopy (ATR-FTIR) spectra were collected on a Bruker Vector 22 Infrared instrument. Differential Scanning Calorimetry (DSC) was performed using a DSC Q20 TA instrument. Samples of approximately 8 mg were placed in an aluminum Tzero pan where they underwent a heat/cool/heat profile at 10 °C min^{-1} under nitrogen (N2) atmosphere (50 mL min^{-1}). Data was obtained from the final heat cycle of the heat/cool/heat profile. Before conducting the DSC experiments, the variation of the mass of samples was measured using the thermal gravimetric analysis (TGA) by a TA instrument Q50 TGA instrument under an atmosphere of N2 while the temperature was changing over time. Samples were put in a platinum pan and were heated at a rate of 10 °C min–1 under a flow of N2 (60 mL min–1). Water contact angles (WCAs) were measured by a Kruss DSA100 Drop Shape Analyzer. The WCAs were measured three times for bottom and three times for the top surface of each polymer, and the mean of these six measurements was calculated. Synthesized polyanhydrides were evaluated using the powder x-ray diffraction (PXRD) technique at room temperature. Rigaku-MiniFlex powder diffractometer (made in Japan) was used to collect PXRD data using Cu Ka (k = 1.54059 Å) over the range of $0^o < 2\theta < 60^o$ with a step width of 0.02^o. The NIH ImageJ software (version 1.8.0) was used to measure polymer dimensions from photos taken by a Canon SX201 IS digital camera. The concentration of acid orange 10 in the solution was calculated using the absorbance measured by either a UV-visible spectrophotometry device (UV-VIS-NIR Spectrophotometer Shimadzu) or a micro-plate reader (Asys UVM 340) instrument.

3.1.4   Fabrication of 3D Printed Master Molds

Polymers with different initial mole ratios of PNA to the PETMP and EGDT were synthesized in PDMS molds in order to be used for mass loss study. PDMS molds were fabricated using master molds printed by commercial DLP 3D printer (PICO2, ASIGA). Desired 3D models were designed by AutoCAD software and printed layer by layer from an UV-curable resin (Clear 2500T). The layer thickness was set as 250 μm, and the irradiation time for each layer was 5s. The 3D printed objects were treated using sonication in ethanol for 10 min and washed by Deionized (DI) water to remove any uncured polymer.

3.1.5   Polymer Mass Loss

The main focus of this chapter is on studying the mass loss profile of polyanhydrides synthesized by thiol-ene photopolymerization. Understanding of the mass loss profile is crucial for determining the erosion rate of the polymer, which is ideally proportional to the release rate of loaded drugs. The typical mass loss profile of this class of polyanhydrides is shown in Figure 3-1. This profile can be divided into two parts: the induction period and the erosion period. When polymers are immersed in the aqueous media, for a few hours they uptake some water (induction period), then start eroding until the completion of the polymer mass loss (erosion period).

The mass loss profiles of polymers with different initial mole ratios of PNA to PETMP and EGDT were studied. Herein, the typical mass loss measurement method used during this study is described (unless otherwise specified). To obtain the mass loss profile, polymers were immersed in 5 ml PBS (pH=7.4) in glass vials, before being placed on a shaker (VWR micro-plate shaker). The shaker was set up at 37 °C with specific shaking rates (120 rpm). At certain time points (mostly every hour), the polymers were extracted from the solution, the water on the surface of the polymer was carefully wiped off using the disposable wipes (Kimwipes), and the dry polymer was weighted using the weight balance.
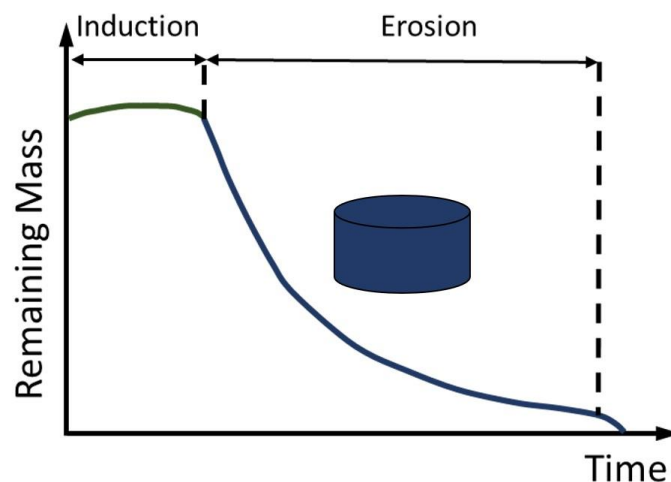
Figure 3-1: Mass loss profile of thiol-ene polyanhydrides for a cylindrical polymeric tablet. The mass loss profile consists of two main parts: the induction period, and subsequent erosion part.

3.1.5.1 The Effect of Parameters on Mass Loss Profile of Thiol-ene Polyanhydrides

As discussed in section 2.2.2, there are several parameters affecting the erosion of polyanhydrides. Various studies have been performed to examine the effect of different parameters on the erosion behavior of polyanhydrides (see section 2.2.2). Recently, a new type of polyanhydrides was synthesized using thiol-ene photopolymerization which is used in this thesis study. To our knowledge, the erosion behavior of this type of polyanhydrides under different parameters has not yet been studied. An extensive study on the effect of different parameters on mass loss (erosion) profile of this type of polymer was performed.

In most of the experiments, the typical mass loss measurement described in section 3.1.5 was used (unless otherwise specified). Briefly, the synthesized cylindrical polymers were placed into PBS at pH=7.4. For most of the experiments, the dimensions of cylindrical polymers were 8.7 mm × 8.7 mm (diameter × height). The shaker was set on 120 rpm and 37 °C to mimic the human gastrointestinal (GI) tract environment. The polymers were extracted from PBS and weighted at once every hour until the completion of the polymer mass loss. All experiments were conducted in triplicate. After measuring the mass of polymers over time, the remaining mass percentage and the fractional mass loss

percentage were calculated using Equation 3-1 and 3-2 where M_0 is the initial mass of the polymer, and M_t is the polymer mass at time, t.

$$Remaining\ mass\ percentage = \frac{M_t}{M_0} \times 100, \qquad (3\text{-}1)$$

$$Fractional\ mass\ loss\ percentage = \frac{M_0 - M_t}{M_0} \times 100, \qquad (3\text{-}2)$$

The parameters that were evaluated in this study for their effect on the polymer's mass loss profile included: the temperature, agitation rate, and pH of the media, as well as the geometry and the composition of polymers.

To explore the effect of polymer compositions on the mass loss profile, four different initial mole ratios of PETMP over EGDT (PETMP: EGDT = 100:0, 75:25, 50:50, and 25:75) were used. After synthesizing polymers in cylindrical PDMS molds, experiment parameters were the same as explained in the previous paragraph, except for the temperature. This set of experiments was performed at room temperature. The previously described typical mass loss measurement was conducted for all of the polymers in this set until the vanishing of the polymers' mass. In a similar set of experiments, the same procedures of mass loss measurements were conducted for the three polymers with initial mole ratios of PETMP: EGDT = 100:0, 75:25, and 50:50, this time at 37°C. By comparing the mass loss data obtained from these two sets of experiments, the effect of temperature on mass loss profiles of polymers was examined.

The emergence of advanced fabrication techniques such as micro-fabrication technology and 3D printing made the fabrication of tablets with complex geometries easier. The importance of the tablet geometry on the polymer erosion and drug release can be studied by designing and fabricating of polymers with complicated geometries. The impact of the polymer geometry on the mass loss profile was investigated by fabricating several cylindrical polymers with different diameters and heights. Firstly, polymers made of two initial mole ratios of PETMP to EGDT of 100:0, and 75:25 were fabricated with diameter and height both equal to 3.3 mm. After measuring the polymers' mass loss, the pattern of the mass loss profiles of the smaller polymers was compared to that of the bigger

polymers (diameter and height = 8.7 mm). This experiment also answers the question of whether the induction period and/or the mass-loss rates are affected by the substantial reduction in the volume of the cylindrical polymers from $\pi(4.35^2 \times 8.7)$ to $\pi\,(1.65^2 \times 3.3)$ with the same compositions.

Three separate experiments were designed to examine the effect of the polymer surface area, volume, and surface area to volume (SA/V) ratio on the mass loss profile of the polymer containing PNA and PETMP monomers (EGDT was not used in this set of experiments). In the first experiment, two cylindrical polymers with the same surface area were fabricated, with the volume of one 36% higher than the other. In the second experiment, the volumes of the two cylinders were kept constant and the surface areas had a 44 % difference. Finally, two polymers with different surface areas and volumes, but equal SA/V ratios were fabricated.

Oral tablets experience different pHs through the GI tract, and therefore investigating the impact of different pHs on erosion behavior of polymers that have potential applications in oral tablets is of high importance. Five PBS solutions with five different pH values (2.55, 4.27, 6.09, 7.41, and 7.98) were prepared to mimic the pH of different parts of GI tract. The mass loss measurement was conducted for polymer cubes (8.7×8.7×8.7mm) consists of PNA and PETMP monomers at room temperature.

To investigate the effect of the mass transfer (mixing) on polymer mass loss profile, the polymers synthesized from PNA and PETM monomers were placed at different shaking rates (0, 60, and 120 rpm). These experiments help us understand the impact of the velocity of the solution on mass loss of the polymer.

Adding drugs or model compounds changes the composition of the polymer, which can result in changes in the mass loss profile of polymers. Polymers made of PNA and PETMP were synthesized with and without the model compound. In the latter case, acid orange 10, 1wt % was loaded in the polymer which was then synthesized under the UV-light for 15 minutes. The mass loss measurements were conducted for both polymers.

3.1.5.2　Fitting Mass Loss Data

Several studies have shown that polyanhydrides predominantly undergo surface erosion[1,2]. Researchers have shown that the linear mass loss profile of polyanhydrides results in a near zero-order drug release from these polymers[3,4]. Most of these studies used polyanhydrides in the form of a slab (a thin layer of polymer). Using the new type of polyanhydrides synthesized by thiol-ene photopolymerization, a rectangular slab ($2 \times 10 \times 10$ mm) made of PNA and PETMP showed a linear mass loss profile. More complicated mass loss profiles were observed for a cube made of the same polymer [5]. In this section, the behavior of the mass loss over time was examined. The data collected for polymeric cylinders and cubes made with mole ratios of PNA: PETMP: EGDT = 100:100:0, 1:0.9:0.1, 1:0.75:0.25, 1:0.5:0.5, and 1:0.25:0.75 were fitted to linear, quadratic, and cubic equations and the r-squared values were compared to find the best-fitted curve.

3.1.5.3　Release Kinetic Models Fitting

Mathematical modeling is a helpful tool to accelerate the development of pharmaceutical products. Mathematical models play an important role in understanding the physicochemical mechanisms governing the advanced CRSs and help with predicting the drug release rates. Prediction of the profile of drug release from polymers not only reduces the cost and time associated with experiments but also helps with providing effective therapies through using a more precise release rate of drugs[6].

There are numerous mathematical release kinetic models available for polymeric DDSs including the mechanistic or phenomenological, empirical, and semi-empirical models.

Mechanistic release models for polymers that are predominantly controlled by diffusion mechanisms are extensively reviewed by Siepman et al[7]. Mechanistic models based on diffusion, dissolution, degradation and erosion mechanisms of polymeric DDSs that have used for the past 30 years have been reviewed by Fu and Kao et al.[8]. Various mechanisms affect the release of drugs from a solid oral dosage form, rendering mechanistic release modeling very complicated[9]. In advanced DDSs, various biomaterials with different

characteristics and complex geometries are employed and therefore current mechanistic models cannot adequately describe their drug release profiles.

Empirical models are the equation-based mathematical models which are not dependent on physical or chemical laws. Semi-empirical models are based on empirical models; however, they can be explained by physical and/or chemical laws under certain conditions[9]. Empirical models have been frequently used because of the complexity of the mechanisms involved in drug release from DDSs. The drug release profile can be obtained by selecting the suitable model equation and estimating the model parameters based on experimental data.

There are several release kinetic models available, among which zero-order, first-order, Higuchi, Korsmeyer-Peppas, Hixson-Crowell, Hofenberg, and Weibull, are the most commonly used for describing the release profile from polymeric systems[10,11]. As drug release rate from surface eroding polyanhydrides follows the polymer mass loss profile (i.e. it is proportional to the erosion rate of the polymer), release kinetic models fitting on the mass loss data for thiol-ene polyanhydrides were examined. Zero-order, first-order, Higuchi, Korsmeyer-Peppas, Hixon-Crowell, Hopfenberg, and Weibull kinetic models were studied. The mass loss measurements were conducted for polymeric cylinders and cubes with mole ratios of PNA: PETMP: EGDT = 1:1:0, 1:0.75:0.25, 1:0.5:0.5, and 1:0.25:0.75. Mass loss data were fitted to these seven mathematical models using MATLAB MathWorks software. The coefficient of correlation R^2 and the root mean squared error (RMSE) were used for verifying the fitting accuracy in order to find the best-fitted model. Below are brief explanations of each model and how each model is used to fit the mass loss data.

The zero-order kinetic model describes a release system where the drug is released at a constant rate regardless of its concentration. Equation 3-3 shows the zero-order release kinetic model where C_0 is the initial amount of the drug in the solution, C_t is the total released drug until time t, and K_0 is the zero-order rate constant. Most of the transdermal systems and some tablet matrix systems containing drugs with low solubility are the

examples of zero-order release kinetics applications[12]. Here, the zero-order model described in Equation 3-3 to the measured cumulative mass released over time is used.

$$C_t = C_0 - K_0 t \tag{3-3}$$

The first-order model describes concentration-dependent release behavior. Equation 3-4 shows the first-order kinetics model where C_t is the total released drug until time t, and K is the first-order rate constant. Equation 3-4 can be reorganized to another form of first-order release kinetics model which is shown in Equation 3-5 where C_0 is the initial concentration of drug in the solution. The main application of this model is for water-soluble drug-loaded dosage forms in porous structures[13]. The log of the remaining mass percentage (calculated by Equation 3-1) versus time to the first-order model (Equation 3-4) gives a straight line with a slope of $\frac{-Kt}{2.303}$.

$$\frac{dC_t}{dt} = -KC \tag{3-4}$$

$$log C_t = log C_0 - \frac{Kt}{2.303} \tag{3-5}$$

The first and most commonly used mathematical model for describing the drug release rate from matrices have been developed by Higuchi[14] in 1961. At first, the model was only developed for planar systems which was later modified to a more complicated equation that considers porous polymers in different geometries[15]. The basic Higuchi model is shown in Equation 3-6 where C is the amount of the drug release per unit area of the matrix, D is the diffusion coefficient for the drug in the matrix, qt is the total amount of drug in a unit volume of matrix, C_S is the dimensional solubility of drug in the polymer matrix, and t is the time. Higuchi model can be simplified to Equation 3-7, which relates the cumulative drug release (the total released drug until time t) to the square root of time by Higuchi constant (K_H). The measured cumulative amount of mass released verses square root of time was fitted to Equation 3-7.

$$C = [D(2qt - C_S)C_S t]^{\frac{1}{2}} \tag{3-6}$$

$$\frac{C_t}{C_\infty} = K_H t^{\frac{1}{2}}$$

(3-7)

The power law is a semi-empirical model that relates drug release with time exponentially, as described by Equation 3-8. Korsmeyer-Peppas equation[16] was developed in 1983 for drug release from hydrophilic polymers as shown in Equation 3-9 where $\frac{C_t}{C_\infty}$ is the drug release fraction at time $= t$, K is the rate constant, and n is the release exponent. By deriving the release exponent n (ranging from 0 to 1), the release mechanism of the polymeric system with certain geometry can be interpreted [17]. To find the release mechanism, the first 60% of mass loss data calculated from Equation 3-2 were fitted to the Korsmeyer-Peppas model (Equation 3-8).

$$\frac{C_t}{C_\infty} = K t^n$$

(3-8)

The above equation can also be written as:

$$log \frac{C_t}{C_\infty} = log K + n \, log \, t$$

(3-9)

In 1931, Hixson-Crowell model was developed[18] with the argument that the surface area of a group of particles is proportional to the cubic root of their volume. Equation 3-10 describes their model. C_0 is the initial amount of the drug, C_t is the total amount of the drug released by time t, and K_{HC} is the Hixson-Crowell rate constant. This model describes the systems in which the surface area and diameter of particles or tablets change over time. In this study, the measured remaining mass percentage versus cubic root of time was fitted to the Hixson-Crowell model.

$$C_0^{\frac{1}{3}} - C_t^{\frac{1}{3}} = K_{HC} t$$

(3-10)

Hopfenberg model describes drug release from erodible systems with different geometries. In Hopfenberg model, the release rate is proportional to the surface area of the system. Equation 3-11 shows the Hopfenberg empirical equation where C_∞ is the

initial amount of drug-loaded in the system, C_t is the amount of drug released at time t, K_0 is the rate constant of surface erosion process, a is the half-thickness (half-thickness in case of slab or radius in case of cylinders or spheres), C_l is the initial drug concentration in the system, and n is the release exponent ($n = 1$ for slab, $n = 2$ for cylindrical, and $n = 3$ for spherical geometries) [19]. In this study, the fractional mass release (mass loss) versus time was fitted to Hopfenberg model with $n = 1$ for cubic and $n = 2$ for cylindrical tablets.

$$\frac{C_t}{C_\infty} = 1 - \left[1 - \frac{K_0 t}{C_l a}\right]^n \tag{3-11}$$

The Weibull kinetic model is another empirical model which can be used for dissolution and releasing drugs from oral dosage forms[20]. Weibull model is shown in Equation 3-12 where C_0 is the total amount of drug released, C is the amount of the drug dissolved at time t, T is the lag time, a is the scale parameter, and b is the release curve shape. The fractional mass release (mass loss) verses time were fitted to Weibull model (Equation 3-12).

$$C = C_0 \left[1 - e^{\frac{-(t-T)^b}{a}}\right] \tag{3-12}$$

Table 3-1 summarizes all the above-mentioned release kinetic models' equations with a brief description of their release mechanisms.

Table 3-1: Release kinetic mathematical models [12,21–23].

Model	Mathematical Equation	Release Mechanism
Zero order	$C = C_0 - K_0 t$	Diffusion mechanism
First Order	$log C = log C_0 - \dfrac{Kt}{2.303}$	Diffusion mechanism Fick's first law
Higuchi	$C = [D(2qt - C_S)C_S t]^{\frac{1}{2}}$ or $\dfrac{C_t}{C_\infty} = K_H t^{\frac{1}{2}}$	Diffusion-based mechanism Fick's first law
Korsmeyer-Peppas Power Law	$log \dfrac{C_t}{C_\infty} = log K + n\, log t$ $\dfrac{C_t}{C_\infty} = Kt^n$	Semi empirical model Diffusion mechanism
Hixson-Crowell	$C_0^{\frac{1}{3}} - C_t^{\frac{1}{3}} = K_{HC} t$	Erosion mechanism Mechanistic model
Hopfenberg	$\dfrac{C_t}{C_\infty} = 1 - \left[1 - \dfrac{K_0 t}{C_l a}\right]^n$	Erosion mechanism Empirical and mechanistic model
Weibull	$C = C_0 \left[1 - e^{\frac{-(t-T)^b}{a}}\right]$	Empirical model Life-time distribution function

3.2   Results and Discussion

This section presents and discusses the results of the experiments conducted for studying the mass loss profile of the polyanhydrides synthesized using thiol-ene photopolymerization as well as the results for kinetic models fitting study.

3.2.1   Polymer Preparation and Characterization

Cross-linked polyanhydrides were synthesized using thiol-ene photopolymerization reaction. ATR-FTIR results showed the absence of thiol and vinyl peaks at 2565 cm^{-1} and 1640-1650 cm^{-1}, respectively. It also specified the dual peaks of anhydride functional groups at 1730-1740 cm^{-1}. These peaks indicate that almost all the thiol and vinyl functional groups were reacted. The FTIR spectra, which is shown in Appendix A-2 is in agreement with the FTIR data obtained by Rutherglen et al.[24] for the same polymers.

PXRD was used to show the crystallinity of polymers. PXRD data (Figure 3-2) for all synthesized polymers demonstrated the amorphous domains of the polymers' structure. Amorphous polymers do not contain the periodically arranged atoms, unlike the crystalline polymers. In amorphous structures with atoms distributed randomly, the X-ray scatters in different directions, resulting in a large bump in the FTIR spectrum in a wide range (2θ). In contrast, in crystalline structures, there are sharp peaks with high intensity which are narrow at some points (periodically arranged atoms result in scattered X-ray in certain directions)[25]. Semi-crystalline structures have both the large bump and narrow peaks in their PXRD pattern such as the semi-crystalline polyanhydrides synthesized by Poetz et al.[26]. The XRD results indicate the same large bumps without any sharp peaks with high intensity for all polymers, showing their amorphous domains.

TGA studies demonstrated that synthesized polyanhydrides (PNA: PETMP: EGDT = 100:100:0, 100:75:25, 100:50:50, 100:25:75), had thermal stability with the onset of decomposition observed at 329 °C, 328 °C, 324 °C, and 317 °C respectively (Appendix A-3). High stability of the samples allowed conducting DSC experiments. DSC was conducted to obtain the glass transition temperature (Tg) of each polymer. Tg values were specified from the second cycle of heat/cool steps to be -25.1°C, -36.6°C, -48.9°C, and -55.8°C respectively which are similar to Tg values previously reported using dynamic mechanical analysis (DMA)[24]. Besides, DSC results did not display any crystalline melt temperature (T$_m$), which confirmed the results of PXRD regarding the amorphousness of the polymers' domains (Appendix A-4).
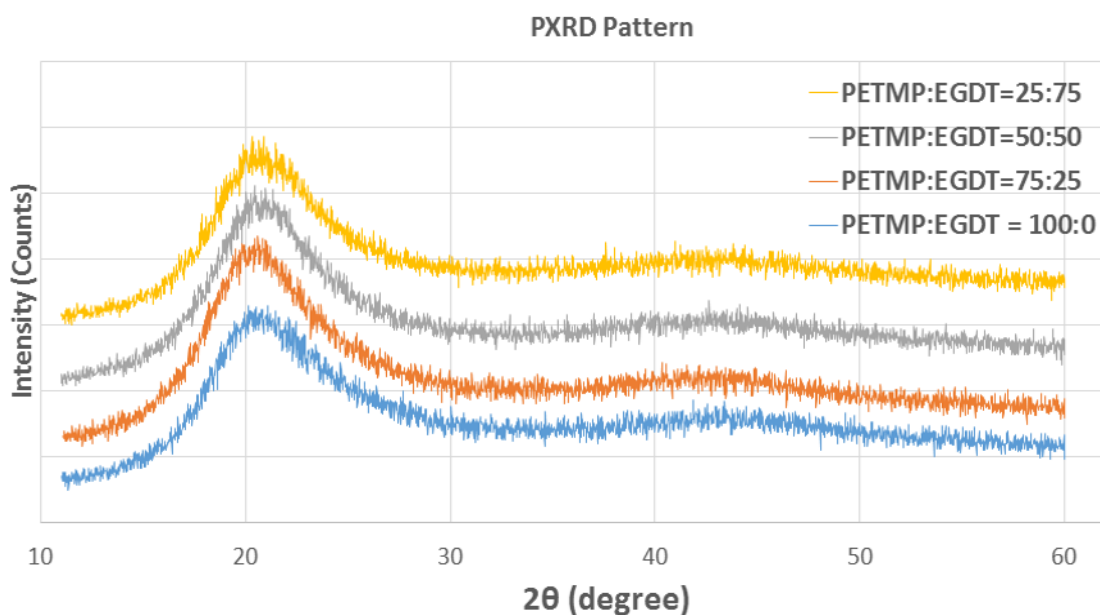
Figure 3-2: PXRD patterns of four thiol-ene polyanhydrides.

Hydrophobicity of four polymers (PNA: PETMP: EGDT = 100:100:0, 100:75:25, 100:50:50, 100:25:75) was also evaluated using the water contact angle measurement. The angle between the water droplet and the top and bottom surfaces of the synthesized polymers were measured three times for each side of the surface. The mean of the six measurements for each polymer was calculated to be $81.8° ± 4.8$, $72.0° ± 7.0$, $68.5°± 8.5$, and $63.5° ± 7.3$, respectively. A water contact angle smaller than $90°$ shows a relative hydrophilic solid surface whereas angles higher than $90°$ show a hydrophobic surface. A decrease in the water contact angle values is observed with increased EGDT to PETMP initial mole ratios. The reason is known to be the higher cross-link density of polymers with higher initial mole ratios of PETMP [24]. The range of the measured water contact angles (from $64°$ to $82°$) is in agreement with other surface-erodible polymers[27] and polyanhydrides in particular[28].

3.2.2   Polymer Mass Loss Profile

In this section, the impact of various parameters on the mass loss profile of thiol-ene polyanhydrides is investigated.

3.2.2.1   The Impact of Polymer Composition

The remaining mass percentage (Figure 3-3A), as well as the fractional mass loss percentage (Figure 3-3B) were plotted for all four polymers. Mass loss profiles showed approximately 10 hours of induction period, which is in close agreement with the results obtained by Ship et al.[29] for the same polymers. Total erosion times ranged from 20h to 50h. Figure 3A indicates that an increased initial mole ratio of EGDT results in a shorter total erosion time. Figure 3B also indicates faster erosion rates for polymers with higher mole ratios of EGDT against PETMP in their networks. However, induction periods did not change by changing the polymer composition using different mole ratios of monomers.

The primary reason for differences in erosion rates is known to be the cross-linking density of polymers. The cross-linking density decreases with an increased ratio of EGDT[26]. Another reason could be the crystallinity of the polymers since, as discussed in section 2.2.3, polyanhydrides with higher crystallinity show lower erosion rates than polyanhydrides with amorphous domains[26,30]. PXRD and DSC were used to evaluate the level of the crystallinity of four polymers. As explained in section 3.2.1, PXRD data displayed the amorphous domains for these polymers, and DSC data did not show any T_m, that confirms the lack of the crystallinity in their structures. Water contact angles were also measured to obtain the relative hydrophobicity of polymers as another potential reason for different erosion rates observed in mass loss profiles of our four different polymers. Results for water contact angles measurements are discussed in detail in section 3.2.2.1. Table 3-2 summarizes the results of experiments performed to explore the reasons behind different erosion rates of different polymer compositions as well as the cross-link density of polymers obtained from Ref[26].
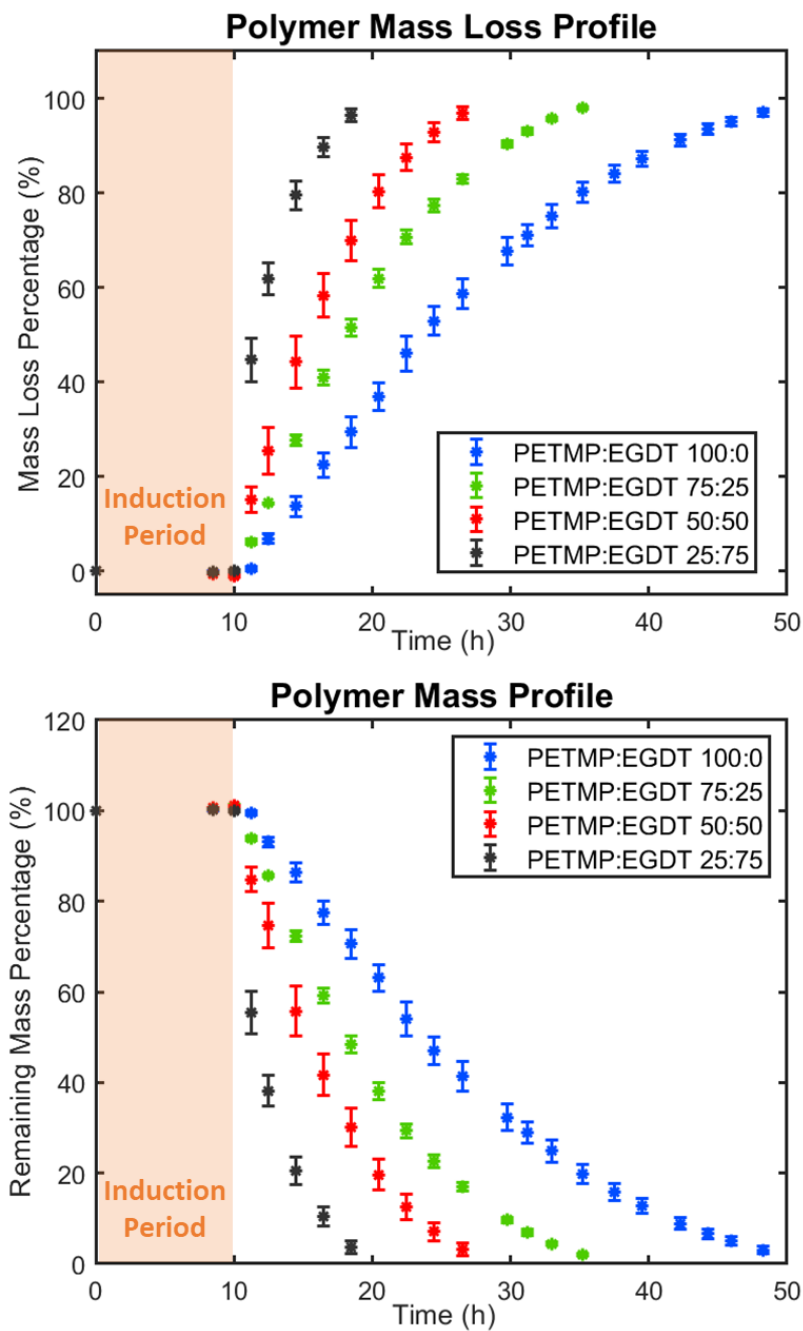
Figure 3-3: The impact of polymer compositions on mass loss profiles. A) Remaining mass percentage and B) Fractional mass loss percentage of thiol-ene based polyanhydrides. Increasing the EGDT in polymer networks leads to faster erosion rates. However, changing the mole ratios of EGDT over PETMP did not change the induction periods.

Table 3-2: Properties of polymers obtained from experiments for exploring reasons for the change in erosion rates of different compositions of polymers.

PETMP:EGDT (mol ratio)	Cross-link Density	Water contact Angle (°)	Tg (°C)
100 : 0	0.91	81.8 ± 4.8	-25.1
75 : 25	0.66	72.0 ± 7.0	-36.6
50 : 50	0.61	68.5 ± 8.5	-48.9
25 : 75	0.55	63.5 ± 7.3	-55.8

3.2.2.2   The Effect of Temperature

The reactions occurring between polymer bonds in contact with the aqueous media drive degradation of biodegradable polymers. Temperature can change the reaction rates and consequently change the erosion rate of polymers. The impact of temperature on polymers' mass loss profiles was investigated by measuring the mass loss of polymers in PBS set at two different temperatures (the ambient temperature (25°C) and the physiological temperature (37°C)). Figure 3-4 compares the results by showing the mass loss data for polymers at the two temperatures. The induction period was reduced from approximately 10 hours to 5 hours at a higher temperature for all polymers. Erosion rates were considerably higher at PBS with 37°C in comparison to the room temperature environment. The acceleration of degradation rates by elevation of the temperature for biodegradable polymers such as PLA and PLGA have reported in several studies [31–33].
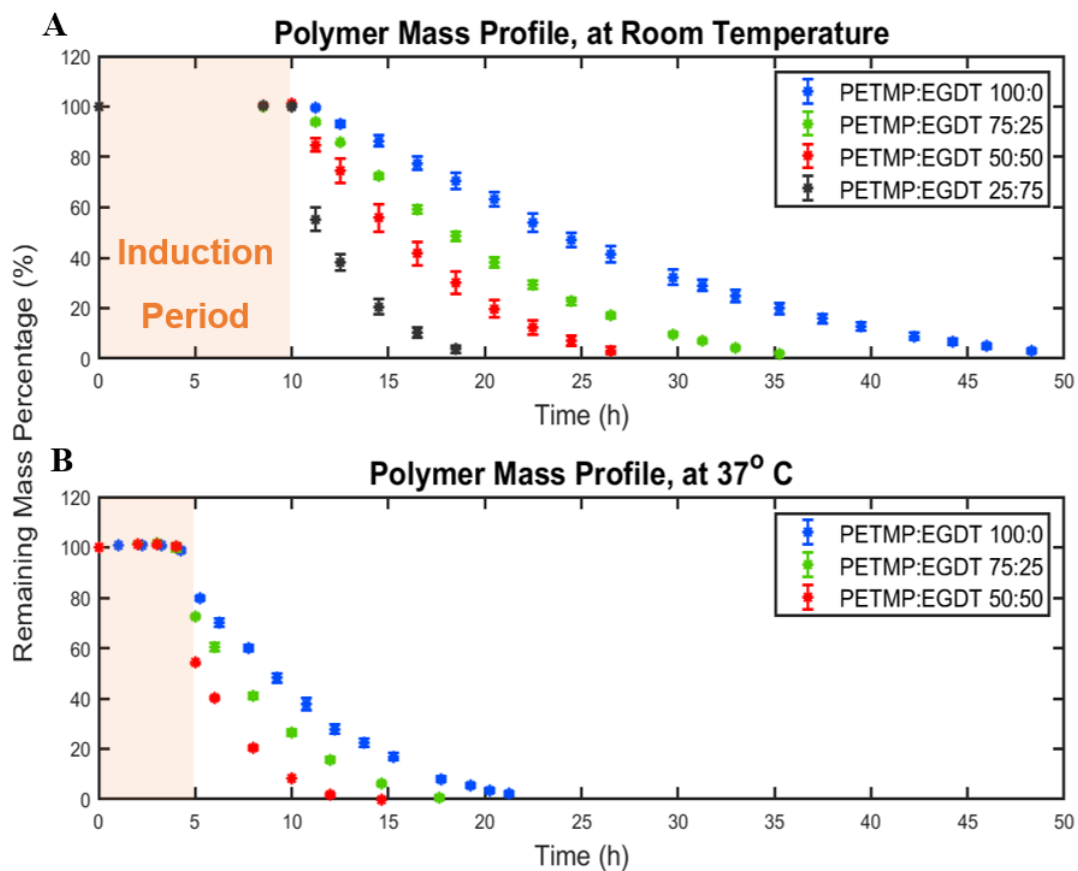
Figure 3-4: The impact of temperature on polymer mass loss profile. The remaining mass percentage of A) Four polymer compositions at room temperature. B) Three polymer compositions at 37°C. Higher temperature leads to shorter induction periods and shorter erosion times.

3.2.2.3   The Effect of Tablet Geometry

First, the mass loss data for two small cylindrical polymers were compared to the mass loss of the larger polymers with the same compositions. Results show a similar induction period (∼5hours) for smaller polymers compared to the larger ones (Figure 3-4). The total erosion times for the smaller and larger polymers reduced from 17h to 13h and 9h to 6.5h when PETMP: EGDT = 100:0 was changed to PETMP: EGDT = 75:25, respectively. The reason for shorter total erosion times for the smaller tablets is their reduced mass, which erodes entirely in a shorter time. Results of a study conducted by

Akbari et al. show similar changes to the induction periods and mass loss rates when the effect of different geometries of p(CPP:SA) on mass loss profiles was examined[34].

Similar patterns of the mass loss profile observed for both tablet geometries in our study confirms that thiol-ene polyanhydrides' maintain their surface erosion behavior even at very small sizes. This observation agrees with previous findings regarding the very small critical device dimension value for polyanhydrides (discussed in section 2.1.3.4)[4]. Results indicate the high potential of this type of polyanhydrides to be used for various applications that require small size DDSs such as mini-tablets to benefit pediatric patients[35].
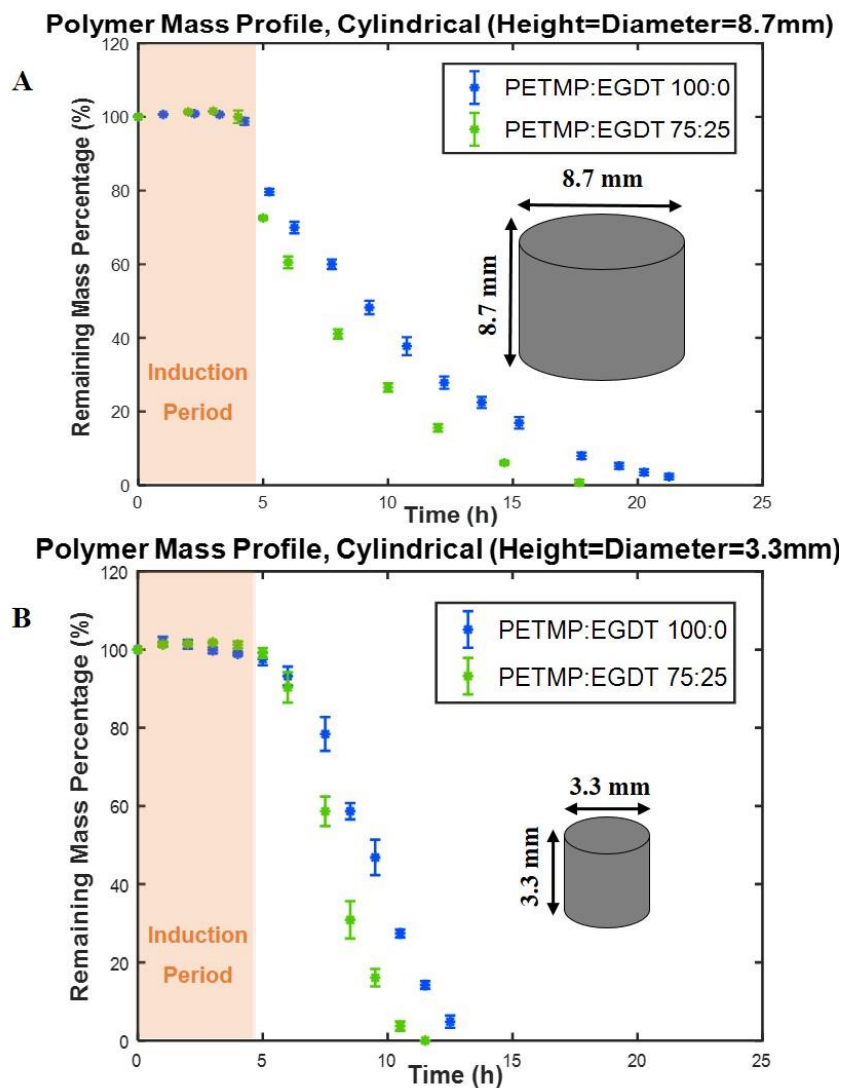
Figure 3-5: Impact of tablet geometry. The remaining mass percentage for bigger cylindrical tablets (diameter and height equal to 8.7mm) (A) and smaller cylindrical tablets (diameter and height equal to 3.3mm) (B).

The effect of the tablet surface area, volume, and SA/V ratio on the mass loss rates and induction periods of two cylindrical tablets with the same polymer compositions was also studied. The induction periods for the tablets with the same surface areas and different volumes were similar ($\sim$5hours), while the total erosion time for the tablet with lower volume was shorter. The reason is that the mass of the smaller volume tablet is less than the other tablet. Although both tablets had similar induction periods, the cylindrical

polymer with higher volume has taken longer to erode, with a slower remaining mass loss percentage rate as shown in Figure 3-6.
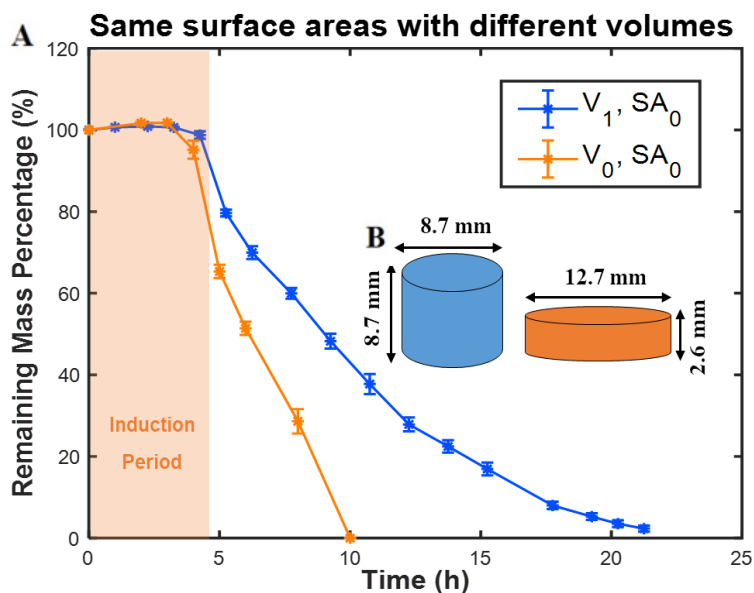
Figure 3-6: Impact of geometry on the mass loss profile of polymers. A) Remaining mass percentage of two tablets with the same surface areas and different volumes ($V_1 = 1.36\ V_2$). B) Schematics of tablet designs and dimensions.

To explore the effect of the surface area on mass loss profiles, two cylindrical tablets were designed and fabricated with same volumes but different surface areas. The mass loss data for both tablets show similar induction periods; however, the mass-loss rate for the tablet with 44% higher surface area is faster. Although in this case the total mass of both tablets was initially the same, the tablet with a higher surface area exposed to PBS, showed faster mass loss rate and consequently higher erosion rate (Figure 3-7). Results show that the same total amount of drugs can be delivered at different rates by changing the surface areas of the tablet and keeping the volumes constant.

Figure 3-7: Impact of geometry on the mass loss profile of polymers. A) Remaining mass percentage of two tablets with the same volumes and different surface areas. B) Schematics of tablet designs and dimensions.

Finally, two tablets with different surface areas and volumes were fabricated. For both tablets, the SA/V ratio was equal to 0.69. Although one of the tablets (the orange tablet in Figure 3-7 B) had a higher surface area and higher total volume, the mass loss data of both tablets closely follow each other as shown in Figure 3-8A with similar mass loss percentage rates. In addition, no change is observed in induction periods of the two tablets.

Results show the importance of the SA/V ratio of the tablet for determining the mass loss percentage rates of polymers. The induction period was not affected by the tablet geometries, while the mass-loss rate for a polymer with higher surface area and lower volume was shown to be faster. Polymers with the same SA/V ratios showed similar mass loss percentage rates despite the higher volume and larger surface area of one tablet against the other. Recently, the importance of the SA/V ratio of tablets has been studied by researchers, and their results agree with our findings. For example, Goyans et al. showed that the fractional drug release from an erosion mediated controlled-release tablet, made of PVA filaments, is only dependent on the SA/V ratio rather than the surface area or the volume separately[36]. Martinez et al. performed a dissolution test on

various tablet geometries with the same SA/V ratios. Tablets with similar SA/V ratios resulted in a similar fractional drug release rate, while tablets with same surface areas showed different fractional release rates. They also showed an increase in dissolution rates of tablets by increasing the SA/V ratio of tablets, which were made of polyethylene glycol diacrylate (PEGda) [37]. The similar results have been obtained for a controlled-release tablet made of hydroxypropylmethylcellulose (HPMC)[38].
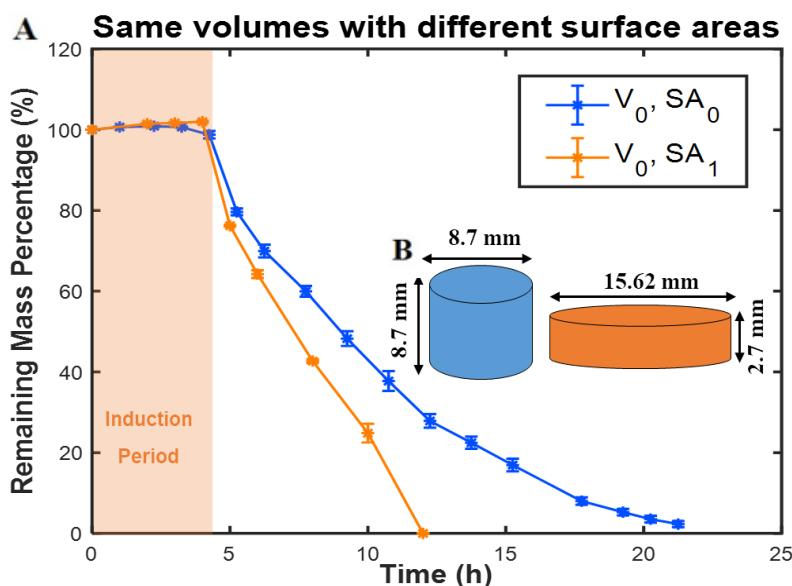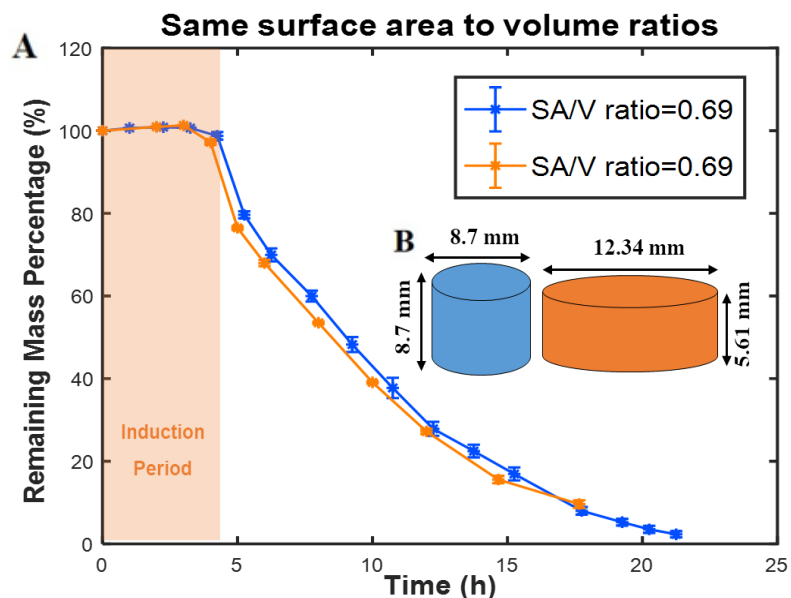

Figure 3-8: Impact of geometry on the mass loss profile of polymer. A) Remaining mass percentage of two tablets with the same SA/V ratio while both surface areas and volumes are different. B) Schematics of tablet designs and dimensions.

3.2.2.4 The Effect of pH

Oral tablets reside in different parts of the GI tract for specific time intervals at various pHs ranging from 1-2.5 at the stomach to 7.88 at the distal small intestine (Figure 3-9A). Therefore, the effect of pH on mass loss profile of a thiol-ene polyanhydride made of PNA and PETMP was studied. The induction periods and mass loss rates were similar for all samples except for the one in pH=7.89, which showed shorter induction period and faster mass loss rate. The faster mass loss rate of the polymer in alkaline solution is in close agreement with studies that showed acceleration in degradation of biodegradable polymers in more alkaline environment[39,40]. Considering the induction period that lasts a

few hours and based on the mass loss data obtained from different pHs, it can be assumed that a tablet made of this polymer will pass the parts of the GI tract with acidic environment, and will reside in pHs around 7 while eroding.
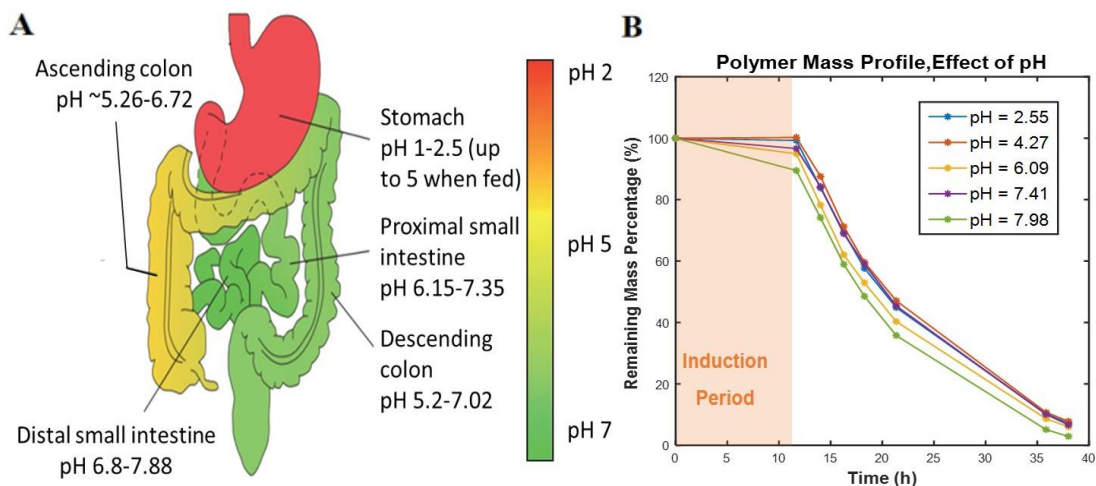
Figure 3-9: Impact of pHs on mass loss profile of polymers. A) Schematic representation of GI tract pathway with various pHs. Reproduced from Ref [41] with permission. B) Remaining mass percentage of polymers in provided solutions with different pHs.

3.2.2.5   The Effect of Mass Transfer

To explore the effect of mass transfer on the polymer mass loss profile, various shaking rates were used. Different shaking rates create different convective forces in PBS that can change the reaction rates by carrying the detached monomers away from the polymeric tablets. The induction periods and erosion rates stayed similar, with a slightly slower erosion rate at 0 rpm shaking rate (Figure 3-10). These findings indicate the non-significant effect of shaking rates on polymer mass loss profile. Shieh et al.[42] found a similar trend in their study on p(FDA:SA) polyanhydrides.
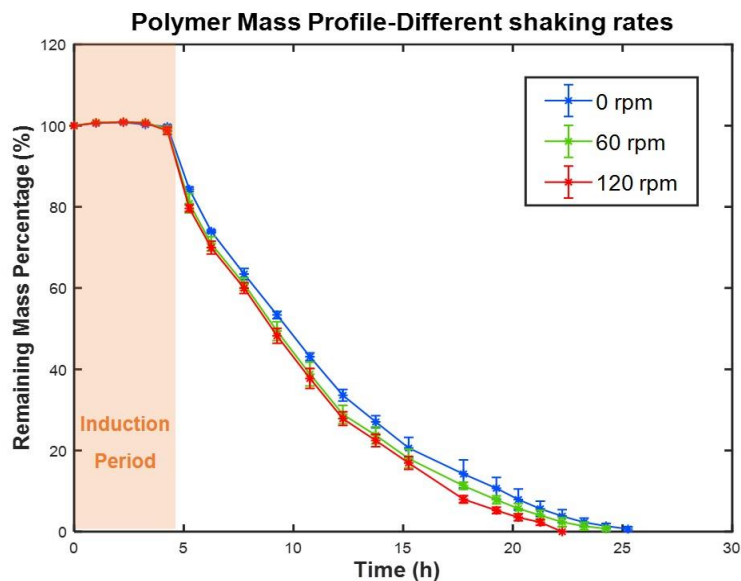
Figure 3-10: Mass transfer effect on the polymer mass loss profile. Different shaking rates (0, 60, 120 rpm) were used.

3.2.2.6   The Effect of adding a Model Compound

Adding drugs to the polymer change some physicochemical properties of polymers that may cause changes in polymer degradation. The polymer and the dye-loaded polymer are shown in Figure 3-11. Results of the mass loss for the two tablets indicate no considerable differences in the induction periods and the mass loss rates (Figure 3-11). During the final five hours of the erosion period, the polymer containing the model compound eroded very fast (see the orange line in Figure 3-11). This is potentially due to the presence of uncross-linked monomers in the center of the dye-loaded polymer that indicates a reduction in the penetration depth of the UV-light in the dye-loaded polymer. To obtain the same behavior for the dye-loaded polymer as the other polymer, the polymer loaded with dye should be put under the UV-light for longer times, or at higher intensities.
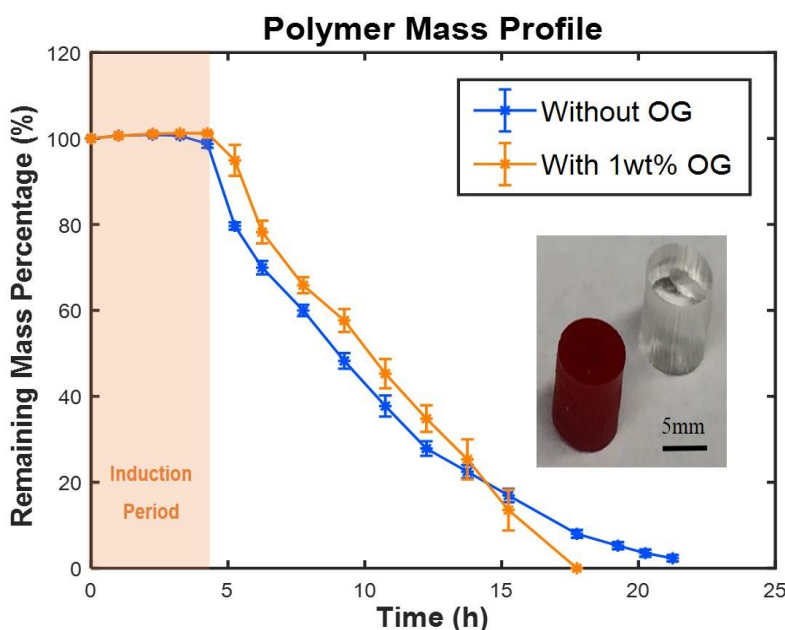
Figure 3-11: Effect of adding the model compound to the polymer on mass loss profile.

3.2.2.7   Pre-Erosion for Eliminating the Induction Period

The induction period (or lag time) during which polymer only absorbs some water lowers the predictability of the polymer mass loss and therefore is undesired. In addition, for treating some diseases, the drug needs to start releasing as soon as the patient swallows the tablet. For eliminating the induction period, a pre-erosion experiment was performed. The cylindrical polymers made of initial mole ratios of PNA: PETMP: EGDT = 100:75:25 were immersed in PBS for 8 hours. The polymers were extracted from the solution after the induction period and when the erosion had been started and were put under the vacuum for 10 hours. After 10 hours, the polymers were again placed in PBS and the mass loss measurements were carried out. Figure 3-12 indicates how the mass loss of the samples after pre-erosion follows the mass loss profile of the samples that were not pre-eroded. This finding shows that the induction period can be removed for this polymer by means of the pre-erosion process. Langer group studied the elimination of the lag time for Poly[bis(p-carboxyphenoxy)methane (PCPM) polyanhydride by pre-eroding it for 50 hours at 60 °C [43].

Results for pre-erosion experiments showed that when the polymer is placed in PBS again, after pre-erosion and vacuuming, the polymer continues the erosion from where it left off, instead of undergoing a second induction period. This can be attributed to a decrease in the hydrophobicity of the polymer surface due to hydrolysis when it is in contact with PBS in the pre-erosion period. This experiment was a proof of concept for the feasibility of eliminating the induction period for thiol-ene polyanhydrides. Further experiments should be designed and performed to further investigate the elimination of the induction period using the mentioned pre-erosion process.
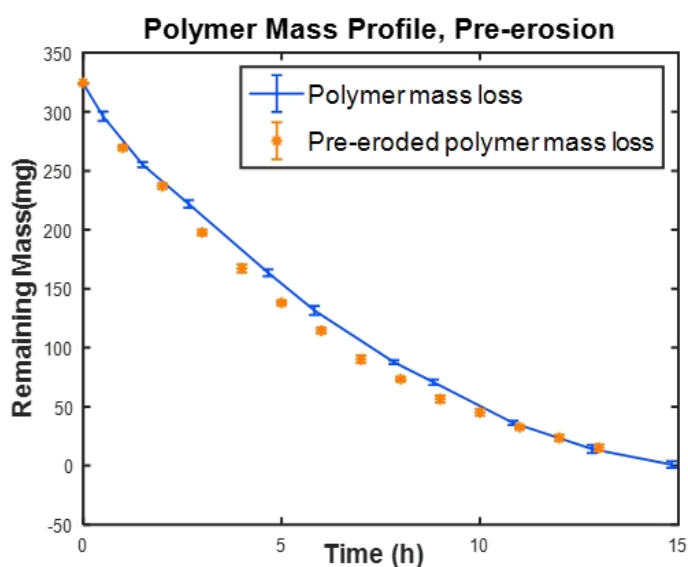
Figure 3-12: The pre-erosion process to eliminate the induction period.

3.2.2.8   Fitting Mass Loss Data

The mass loss data collected for cuboid and cylindrical polymers were used for fitting with the linear, quadratic, and cubic polynomials. The collected data during the erosion period were used since there are no considerable changes during the induction period to be evaluated. Mass loss data were fitted to the functions using Microsoft Excel and the R^2 for each fit was calculated for two of the polymers (Figure 3-13). The results of curve fitting for other cuboid and cylindrical polymers are shown in Appendix B-1 and B-2. Table 3-3 summarizes the mathematical equations and the R^2 values of each fit to the mass loss data for a cuboid and a cylindrical polymer. Although polyanhydrides are well

known for their near-linear mass loss, the linear equation does not describe the mass loss data very well, as also indicated by lower R^2. The best fit for both the cylindrical and cuboid polymers mass loss data is the cubic equation because of the slightly higher R^2 values in comparison to quadratic functions.
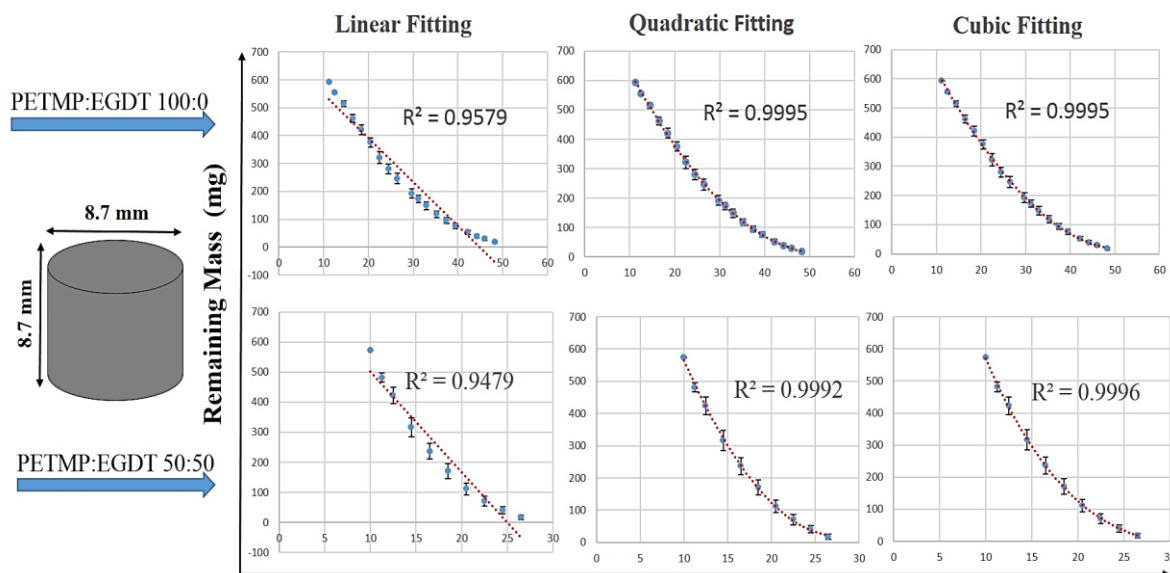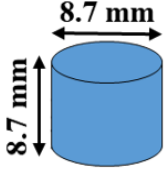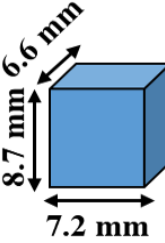
Figure 3-13: Fitting mass loss data for two cylindrical polymers with initial mole ratios of PETMP: EGDT = 100:0 and 50:50. The linear, quadratic, and cubic fits and their R^2 show that the best fit is the cubic function.

Table 3-3: Mass loss data fitting. Linear, quadratic, and cubic polynomials were fitted to the mass loss data of four polymers with different compositions of monomers in two different shapes.

Geometry	Mole ratio PNA:PETMP:EGDT	Fitting Curve	(R²)
	100:100:0	Linear	0.9579
		Quadratic	0.9995
		Cubic	0.9995
	100:75:25	Linear	0.9448
		Quadratic	0.9995
		Cubic	0.9995
	100:50:50	Linear	0.9479
		Quadratic	0.9992
		Cubic	0.9996
	100:25:75	Linear	0.8318
		Quadratic	0.9673
		Cubic	0.994
	100:100:0	Linear	0.9647
		Quadratic	0.9983
		Cubic	0.9988
	100:75:25	Linear	0.9656
		Quadratic	0.9978
		Cubic	0.9993
	100:50:50	Linear	0.929
		Quadratic	0.993
		Cubic	0.9982
	100:25:75	Linear	0.8569
		Quadratic	0.8689
		Cubic	0.9998

3.2.3 Release Kinetic Models Fitting

The curve fitting toolbox of MATLAB R2016 was used to fit the mass loss data to the above-mentioned equations mentioned in Table 3-1. A model with the highest R^2 (correlation coefficient closest to 1) and the minimum RMSE (equal to highest concentrated data around the line of fit) were considered as the best fitted model. The

regression coefficient, R^2, and the best-fit model parameters are reported. Figure 3-14 shows the selected models and their corresponding R^2 values. According to Table 3-4 that summarizes results for cylindrical systems, the best fit was obtained using the Hopfenberg and Hixson-Crowell models for the polymer compositions used in our tablet fabrication (PETMP: EGDT = 100:0, 75:25). The same study was conducted for the data collected for the cuboid polymers. Figure 3-15 shows some of the experimental data and their fitted curves. Table 3-5 summarizes the results for the polymer cubes. The Hixson-Crowell and Weibull models yield the best fit for the cuboid polymeric system mass loss data points.

Based on the best-fitted models, both cylindrical and cubic systems obeyed the Hixson-Crowell and Hopfenberg models, which describe polymers with erosion mechanisms rather than diffusion-controlled systems. This study, mathematically proved that the fabricated polymeric systems undergo surface erosion, which has been shown before experimentally[29]. While finding the best fit models, the parameters of each release kinetic models were derived and summarized in Table 3-4 and 3-5. Using these parameters, the release of the drug through these polymers can be predicted. The results of curve fitting to other models can be found in Appendix C1-5 for both cylindrical and cuboid polymers.
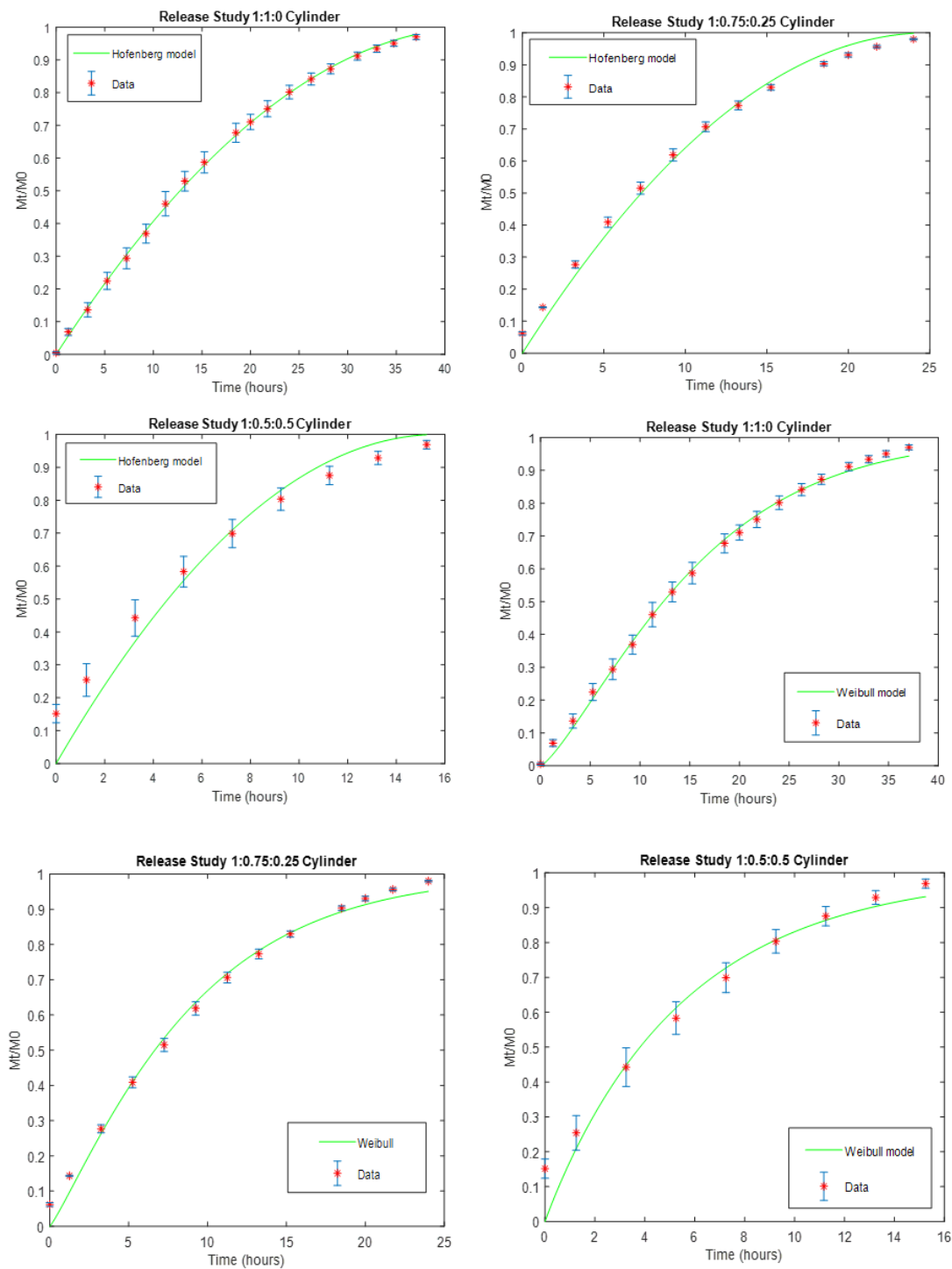
Figure 3-14: Selected some of the best fitted kinetic models for cylindrical tablets.

Table 3-4: Release kinetic models fitting for a cylindrical system. The models with their equations, mole ratios of monomers, R^2, and derived parameters are shown in this table.

| Model	Mathematical Equation	PNA:PETMP: EGDT	(R^2)	Estimated Parameters
Zero-order	$C = C_0 - K_0 t$	1:1:0	0.9217	$k_0 = -18.34\ (-19.55, -17.14)$
		1:0.75:0.25	0.8953	$k_0 = -26.5\ (-29.1, -23.89)$
		1:05:0.5	0.9226	$k_0 = -35.23\ (-39.29, -31.18)$
		1:0.25:0.75	0.9001	$k_0 = -45.09\ (-55.85, -34.33)$
First-order	$logC = logC_0 - \dfrac{Kt}{2.303}$	1:1:0	0.9370	$k = 0.07648\ (0.07046, 0.0824)$
		1:0.75:0.25	0.9451	$k = 0.1346\ (0.1222, 0.1471)$
		1:05:0.5	0.9624	$k = 0.1992\ (0.1804, 0.218)$
		1:0.25:0.75	0.8867	$k = 0.458\ (0.3527, 0.5633)$
Higuchi	$\dfrac{C_t}{C_\infty} = K_H t^{\frac{1}{2}}$ $(n = \frac{1}{2})$	1:1:0	0.9494	$K_H = 15.54\ (14.72, 16.36)$
		1:0.75:0.25	0.9770	$K_H = 20.36\ (19.51, 21.22)$
		1:05:0.5	0.9628	$K_H = 25.52\ (23.89, 27.15)$
		1:0.25:0.75	0.2902	$K_H = 39.84\ (30.07, 49.6)$
Korsmeyer-Peppas (Power Law)	$\dfrac{C_t}{C_\infty} = Kt^n$ $log\dfrac{C_t}{C_\infty} = logK + n\,logt$	1:1:0	0.8318	$logk = 0.2571\ (-0.1998, 0.714)$ $n = 1.367\ (0.8176, 1.916)$
		1:0.75:0.25	0.9514	$logk = 0.938\ (0.7709, 1.105)$ $n = 0.9001\ (0.6661, 1.134)$
		1:05:0.5	0.9555	$logk = 1.259\ (1.104, 1.414)$ $n = 0.7061\ (0.4262, 0.986)$
		1:0.25:0.75	0.8341	$logk = 1.695\ (0.976, 2.414)$ $n = 0.4218\ (-1.968, 2.812)$
Hixson-Crowell	$C_0^{\frac{1}{3}} - C_t^{\frac{1}{3}} = K_{HC} t$	1:1:0	0.9954	$k = 0.01771\ (0.01738, 0.0180)$
		1:0.75:0.25	0.9983	$k = 0.02973\ (0.02931, 0.0301)$
		1:05:0.5	0.9856	$k = 0.04508\ (0.0428, 0.04736)$
		1:0.25:0.75	0.5750	$k = 0.1009\ (0.06404, 0.1377)$
Hofenberg	$\dfrac{C_t}{C_\infty} = 1 - \left[1 - \dfrac{K_0 t}{C_l a}\right]^n$ $(n = 2)$	1:1:0	0.9994	$k = 3.146\ (3.113, 3.179)$
		1:0.75:0.25	0.9901	$k = 5.366\ (5.073, 5.659)$
		1:05:0.5	0.9364	$k = 8.295\ (6.895, 9.695)$
		1:0.25:0.75	0.9508	$k = 18.21\ (14, 22.42)$
Weibull	$C = C_0 \left[1 - e^{\frac{-(t-T)^b}{a}}\right]$	1:1:0	0.9976	$b = 1.294\ (1.233, 1.354)$ $a = 37.26\ (30.76, 43.76)$
		1:0.75:0.25	0.9926	$b = 1.146\ (1.023, 1.268)$ $a = 12.66\ (8.982, 16.33)$
		1:05:0.5	0.9591	$b = 0.974\ (0.6625, 1.286)$ $a = 5.301\ (2.068, 8.534)$
		1:0.25:0.75	0.1248	$b = 0.6196\ (-1.627, 2.866)$ $a = 1.221\ (-1.886, 4.328)$
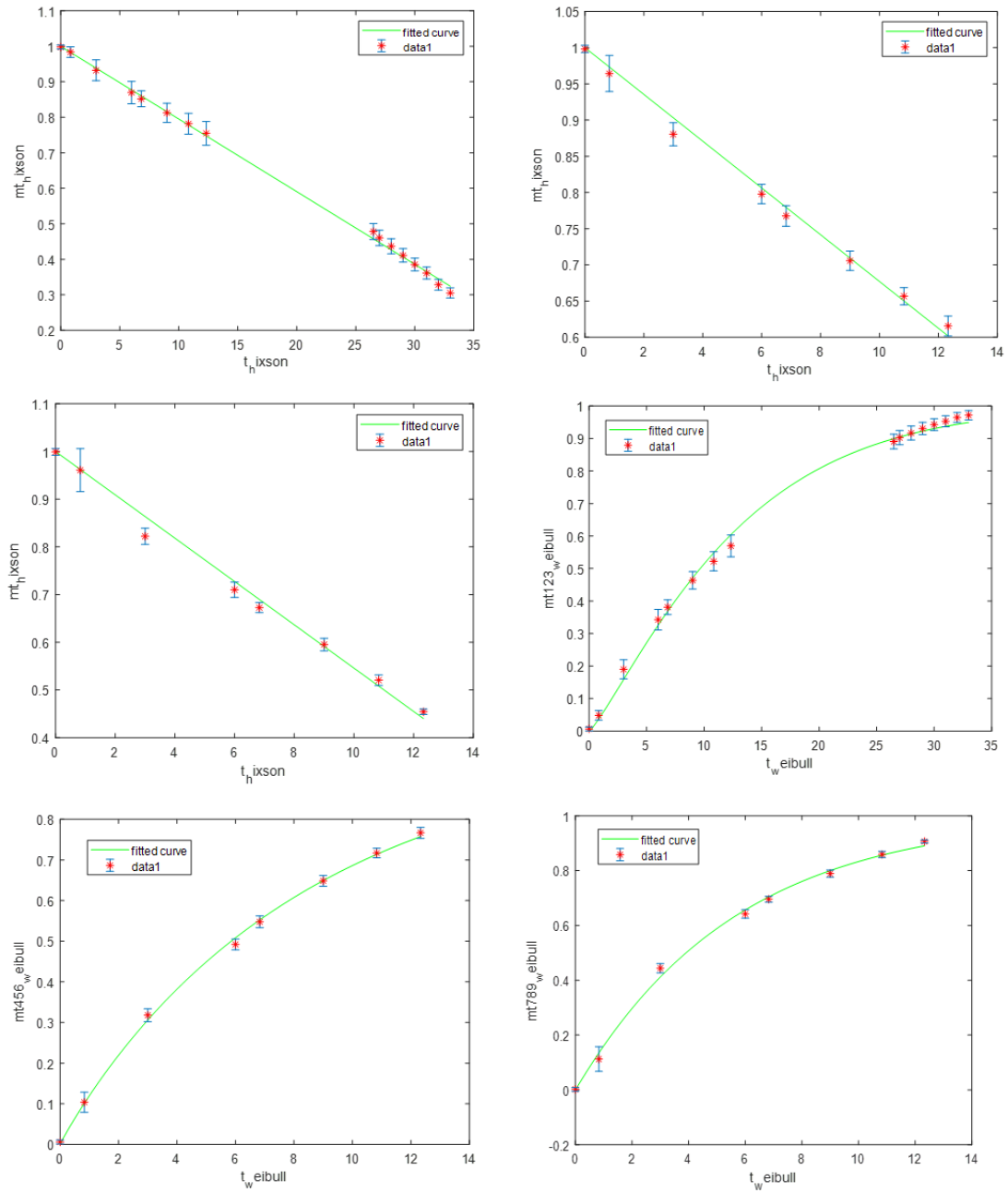
Figure 3-15: Selected best fitted kinetic models for cuboid polymers.

Table 3-5: Release kinetic models fitting for cuboid polymers. The models with their equations, mole ratios of monomers, R², and derived parameters are shown in this table.

Model	Mathematical Equation	PNA:PETMP: EGDT	(R^2)	Estimated Parameters
Zero-order	$C = C_0 - K_0 t$	1:1:0	0.9114	$k_0 =$ -15.53 (-16.76, -14.3)
		1:0.75:0.25	0.9412	$k_0 =$ -32.12 (-35.7, -28.53)
		1:05:0.5	0.8874	$k_0 =$ -38.7 (-44.57, -32.84)
		1:0.25:0.75	0.6547	$k_0 =$ -124.9 (-265.9, 16.07)
First-order	$logC = logC_0 - \dfrac{Kt}{2.303}$	1:1:0	0.9690	$k = 0.09395$ (0.08832, 0.09958)
		1:0.75:0.25	0.9990	$k =$ 0.1163 (0.1144, 0.1181)
		1:05:0.5	0.9936	$k =$ 0.1818 (0.1742, 0.1894)
		1:0.25:0.75	0.9085	$k =$ 0.6756 (0.2746, 1.077)
Higuchi	$\dfrac{C_t}{C_\infty} = K_H t^{\frac{1}{2}}$ $(n = \frac{1}{2})$	1:1:0	0.9803	$K_H =$ 16.81 (16.19, 17.43)
		1:0.75:0.25	0.9782	$K_H =$ 21.06 (19.65, 22.47)
		1:05:0.5	0.9805	$K_H =$ 25.89 (24.28, 27.5)
		1:0.25:0.75	0.8912	$K_H =$ 54.5 (25.18, 83.81)
Korsmeyer-Peppas (Power Law)	$\dfrac{C_t}{C_\infty} = Kt^n$ $log\dfrac{C_t}{C_\infty} = logK + n\,logt$	1:1:0	0.8680	$logk =$ 0.2705 (-0.1763, 0.7174 $n =$ 1.477 (0.9015, 2.052)
		1:0.75:0.25	0.7553	$logk =$ 0.3148 (-0.7788, 1.408) $n =$ 1.89 (-0.08656, 3.867)
		1:05:0.5	0.7067	$logk =$ 0.04847 (-2.358, 2.455) $n =$ 2.762 (-2.652, 8.177)
		1:0.25:0.75	0.8316	$logk =$ 0.1069 (-5.915, 6.129) $n =$ 3.501 (-16.52, 23.52)
Hixson-Crowell	$C_0^{\frac{1}{3}} - C_t^{\frac{1}{3}} = K_{HC} t$	1:1:0	0.9984	$k = 0.02047$ (0.02022, 0.02073)
		1:0.75:0.25	0.9923	$k =$ 0.0323 (0.03092, 0.03368)
		1:05:0.5	0.9902	$k =$ 0.04542 (0.04321, 0.04762)
		1:0.25:0.75	0.7724	$k =$ 0.1758 (0.02395, 0.3277)
Hofenberg	$\dfrac{C_t}{C_\infty} = 1 - \left[1 - \dfrac{K_0 t}{C_l a}\right]^n$ $(n = 1)$	1:1:0	0.9114	$k =$ 3.571 (3.288, 3.854)
		1:0.75:0.25	0.9371	$k =$ 7.452 (6.6, 8.304)
		1:05:0.5	0.8858	$k =$ 8.922 (7.564, 10.28)
		1:0.25:0.75	0.5071	$k =$ 31.88 (-6.816, 70.59)
Weibull	$C = C_0\left[1 - e^{\frac{-(t-T)^b}{a}}\right]$	1:1:0	0.9973	$b =$ 1.188 (1.119, 1.257) $a =$ 21.34 (17.41, 25.27)
		1:0.75:0.25	0.9990	$b =$ 0.9593 (0.8992, 1.019) $a =$ 7.856 (6.872, 8.84)
		1:05:0.5	0.9973	$b =$ 1.009 (0.8991, 1.12) $a =$ 5.712 (4.485, 6.939)
		1:0.25:0.75	0.9796	$b =$ 0.5083 (-3.196, 4.213) $a =$ 0.8737 (-1.289, 3.037)

3.3   References

1.   Burkersroda, F. v. & Goepferich, A. M. An Approach to Classify Degradable Polymers. *MRS Proc.* **550**, 17 (1998).

2.   Tamada, J. A. & Langer, R. Erosion kinetics of hydrolytically degradable polymers. *Proc. Natl. Acad. Sci. U. S. A.* **90**, 552–556 (1993).

3.   Göpferich, A. & Tessmar, J. Polyanhydride degradation and erosion. *Adv. Drug Deliv. Rev.* **54**, 911–31 (2002).

4.   Burkersroda, F. Von, Schedl, L. & Göpferich, A. Why degradable polymers undergo surface erosion or bulk erosion. *Biomaterials* **23**, 4221–4231 (2002).

5.   Poetz, K. L. *et al.* Photopolymerized cross-linked thiol-ene polyanhydrides: Erosion, release, and toxicity studies. *Biomacromolecules* **15**, 2573–2582 (2014).

6.   Kamaly, N., Yameen, B., Wu, J. & Farokhzad, O. C. Degradable controlled-release polymers and polymeric nanoparticles: Mechanisms of controlling drug release. *Chemical Reviews* (2016). doi:10.1021/acs.chemrev.5b00346

7.   Siepmann, J. & Siepmann, F. Modeling of diffusion controlled drug delivery. *Journal of Controlled Release* (2012). doi:10.1016/j.jconrel.2011.10.006

8.   Fu, Y. & Kao, W. J. Drug release kinetics and transport mechanisms of non-degradable and degradable polymeric delivery systems. *Expert Opin. Drug Deliv.* (2010). doi:10.1517/17425241003602259

9.   Mathematical models describing drug release from biopolymeric delivery systems. *Mater. Technol.* (2010). doi:10.1179/175355510X12723642365566

10.   Mathematical models of drug release. in *Strategies to Modify the Drug Release from Pharmaceutical Systems* (2015). doi:10.1016/b978-0-08-100092-2.00005-9

11.   Fallahi-Sambaran, M., Salami-Kalajahi, M., Dehghani, E. & Abbasi, F. Investigation of different core-shell toward Janus morphologies by variation of surfactant and feeding composition: A study on the kinetics of DOX release. *Colloids Surfaces B Biointerfaces* (2018). doi:10.1016/j.colsurfb.2018.06.064

12.   Dash, S., Murthy, P., … L. N.-A. poloniae & 2010, undefined. Kinetic modeling on drug release from controlled drug delivery systems. *ncbi.nlm.nih.gov*

13.   Mulye, N. V. & Turco, S. J. An examination of assumptions underlying the first-order kinetic model for release of water-soluble drugs from dicalcium phosphate dihydrate matrices. *Drug Dev. Ind. Pharm.* (1996). doi:10.3109/03639049609063223

14.   Higuchi, T. Rate of release of medicaments from ointment bases containing drugs in suspension. *J. Pharm. Sci.* (1961). doi:10.1002/jps.2600501018

15.   Higuchi, T. Mechanism of sustained-action medication. Theoretical analysis of rate of release of solid drugs dispersed in solid matrices. *J. Pharm. Sci.* (1963). doi:10.1002/jps.2600521210

16.   Korsmeyer, R. W., Gurny, R., Doelker, E., Buri, P. & Peppas, N. A. Mechanisms

of solute release from porous hydrophilic polymers. *Int. J. Pharm.* (1983). doi:10.1016/0378-5173(83)90064-9

17. Kosmidis, K., Argyrakis, P. & Macheras, P. Fractal kinetics in drug release from finite fractal matrices. *J. Chem. Phys.* (2003). doi:10.1063/1.1603731

18. Hixson, A. W., & Crowell, J. H. Dependence of reaction velocity upon surface and agitation. *Industrial & Engineering Chemistry*. (1931) 23(8), 923-931.

19. Katzhendler, I., Hoffman, A., Goldberger, A. & Friedman, M. Modeling of Drug Release from Erodible Tablets. *J. Pharm. Sci.* (1997). doi:10.1021/js9600538

20. Langenbucher, F. Letters to the Editor: Linearization of dissolution rate curves by the Weibull distribution. *Journal of Pharmacy and Pharmacology* (1972). doi:10.1111/j.2042-7158.1972.tb08930.x

21. Siepmann, J. & Siepmann, F. Mathematical modeling of drug dissolution. *Int. J. Pharm.* **453**, 12–24 (2013).

22. Qiu, S., Wang, K. & Li, M. In vitro dissolution studies of immediate-release and extended-release formulations using flow-through cell apparatus 4. *Dissolution Technol.* (2014). doi:10.14227/DT210214P6

23. Semwal, A., Kakar, S. & Singh, R. Drug release characteristics of dosage forms: a review Aphrodisiac potential of Indian Medicinal plants. View project Chitosan View project Drug release characteristics of dosage forms: a review. *J. Coast. Life Med.* **2**, 332–336 (2014).

24. Rutherglen, B. G., McBath, R. A., Huang, Y. L. & Shipp, D. A. Polyanhydride networks from thiol-ene polymerizations. *Macromolecules* (2010). doi:10.1021/ma102287v

25. Cullity, B. D. & Weymouth, J. W. Elements of X-Ray Diffraction. *Cit. Am. J. Phys.* **25**, 394 (1957).

26. Poetz, K. L., Mohammed, H. S. & Shipp, D. A. Surface eroding, semicrystalline polyanhydrides via thiol-ene 'click' photopolymerization. *Biomacromolecules* (2015). doi:10.1021/acs.biomac.5b00280

27. Kumar, N., Langer, R. S. & Domb, A. J. Polyanhydrides: An overview. *Adv. Drug Deliv. Rev.* **54**, 889–910 (2002).

28. Chickering, D. E., Jacob, J. S. & Mathiowitz, E. Bioadhesive microspheres, II. Characterization and evaluation of bioadhesion involving hard, bioerodible polymers and soft tissue. *React. Polym.* **25**, 189–206 (1995).

29. Shipp, D. A., McQuinn, C. W., Rutherglen, B. G. & McBath, R. A. Elastomeric and degradable polyanhydride network polymers by step-growth thiol-ene photopolymerization. *Chem. Commun.* (2009). doi:10.1039/b911557a

30. Shakesheff, K. M. *et al.* In Situ Atomic Force Microscopy Imaging of Polymer Degradation in an Aqueous Environment. *Langmuir* **10**, 4417–4419 (1994).

31. Zolnik, B. S., Leary, P. E. & Burgess, D. J. Elevated temperature accelerated release testing of PLGA microspheres. *J. Control. Release* **112**, 293–300 (2006).

32. Aso, Y., Yoshioka, S., Li Wan Po, A. & Terao, T. Effect of temperature on mechanisms of drug release and matrix degradation of poly(d,l-lactide) microspheres. *J. Control. Release* **31**, 33–39 (1994).

33. Ho, K.-L. G., Pometto III, A. L. & Hinz, P. N. (No Title). *J. Polym. Environ.* **7**, 83–92 (1999).

34. Akbari, H., D'Emanuele, A. & Attwood, D. Effect of geometry on the erosion characteristics of polyanhydride matrices. *Int. J. Pharm.* (1998). doi:10.1016/S0378-5173(97)00298-6

35. Strickley, R. G. Pediatric Oral Formulations: An Updated Review of Commercially Available Pediatric Oral Formulations Since 2007. *Journal of Pharmaceutical Sciences* **108**, 1335–1365 (2019).

36. Goyanes, A., Robles Martinez, P., Buanz, A., Basit, A. W. & Gaisford, S. Effect of geometry on drug release from 3D printed tablets. *Int. J. Pharm.* **494**, 657–663 (2015).

37. Martinez, P. R., Goyanes, A., Basit, A. W. & Gaisford, S. Influence of Geometry on the Drug Release Profiles of Stereolithographic (SLA) 3D-Printed Tablets. *AAPS PharmSciTech* **19**, 3355–3361 (2018).

38. Reynolds, T. D., Mitchell, S. A. & Balwinski, K. M. Investigation of the effect of tablet surface area/volume on drug release from hydroxypropylmethylcellulose controlled-release matrix tablets. *Drug Dev. Ind. Pharm.* **28**, 457–66 (2002).

39. Makino, K., Ohshima, H. & Kondo, T. Mechanism of hydrolytic degradation of poly(l-lactide) microcapsules: Effects of ph, ionic strength and buffer concentration. *J. Microencapsul.* **3**, 203–212 (1986).

40. Göpferich, A. Mechanisms of polymer degradation and erosion. *Biomaterials* **17**, 103–114 (1996).

41. Khutoryanskiy, V. V. Supramolecular materials: Longer and safer gastric residence. *Nature Materials* (2015). doi:10.1038/nmat4432

42. Shieh, L., J. Tamada, I. Chen, J. Pang, A. Domb, and R. Langer. Erosion of a new family of biodegradable polyanhydrides. *Journal of biomedical materials research* 28, no. 12 (1994): 1465-1475.

43. Rosen, H. B., Chang, J., Wnek, G. E., Linhardt, R. J. & Langer, R. Bioerodible polyanhydrides for controlled drug delivery. *Biomaterials* (1983). doi:10.1016/0142-9612(83)90054-6

44. Durham, O. Z., Poetz, K. L. & Shipp, D. A. Polyanhydride Nanoparticles: Thiol-Ene 'Click' Polymerizations Provide Functionalized and Cross-Linkable Nanoparticles with Tuneable Degradation Times. *Aust. J. Chem.* **70**, 735–742 (2017).

Chapter 4

4   High-throughput Fabrication of Drug-loaded Core-shell Tablets for Personalized Medicine

In this chapter, a high-throughput platform is developed for fabricating drug-loaded tablets. The tablets, achieved using a novel tablet design, have adjustable release rates.

4.1   Materials and Methods

This section details the materials used in this study and describes the methodology used for designing and manufacturing the drug-loaded polymeric tablets with adjustable release profiles.

4.1.1   Materials

4-Pentenoic anhydride (PNA), 2, 2-(Ethylenedioxy)diethanethiol (3,6-Dioxa-1,8-octane-dithiol, EGDT), Pentaerythritol tetrakis(3-mercaptopropionate) (PETMP), 1-Hydroxycyclohexyl phenyl ketone, Trichloro(1H, 1H, 2H, 2H-perfluorooctyl)silane and acid orange 10 (orange G) were purchased from Sigma Aldrich Chemical Co. and were used as received. SU-8 2050 photoresist was purchased from MicroChem Corporation. 3D printer acrylate-based resin (Clear 2005T) was purchased from MiiCraft. Both the Sylgard 184 Silicone Elastomer pre-polymer and the curing agent were purchased from Ellsworth Adhesive Chemical Co., and were used for making PDMS. 3.3 mm poly (methylmethacrylate) sheets (PMMA) were purchased from McMaster-Carr. Tyfon Microbore tubing (ID 0.079 in) was purchased from Cole-Parmer, Inc.

4.1.2   Polymer Synthesis Procedure

1-Hydroxycyclohexyl phenyl ketone (photo-initiator, 0.1wt %) was weighed and placed into a 15 ml Falcon tube. Then, PNA was transferred into the tube, followed by the mixture of EGDT and PETMP. The solution was mixed to obtain a homogenous mixture. The initial mole ratio of PNA to the total amount of monomers containing thiol groups (EGDT and PETMP) was 100:100. In this study, four different initial mole ratios of PNA to PETMP and EGDT were prepared and used including PNA: PETMP: EGDT =

100:100:0, 100:75:25, 100:50:50, and 100:25:75. The homogenous pre-polymer solution was then purged under the inert gas (nitrogen or argon) for 3 minutes and was transferred to PDMS molds. PDMS molds with different designs and geometries were fabricated and used according to the desired final geometry of each polymer (see section 4.1.3 for information on molds fabrication). The pre-polymer solution in molds was exposed to UV-light (CL-1000 UVP Cross-linker) equipped with 365 nm UV lamps (intensity=∼5 mW/cm^2) for 5 minutes. To study the release profiles of dye-loaded tablets, a model compound (acid orange) was added to the pre-polymer solution of some of the tablets. Acid orange 10 (1-3wt %) was weighed and added to the purged solution and mixed using sonication for 25 minutes. Similar to the pre-polymer without the model compound, the dye-loaded solution was transferred to PDMS molds and was synthesized under the same UV light for 5 to 15 minutes. The reaction scheme is presented in Appendix A-1.

4.1.3   Fabrication of 3D Printed Master Molds

3D printer master molds were used to fabricate the PDMS molds in which the pre-polymer solutions were polymerized. The master molds were printed by a commercial DLP 3D printer (PICO2, ASIGA). Desired 3D models were designed by AutoCAD software and were printed layer by layer from a UV-curable resin (Clear 2500T). The layer thickness was set to 250 μm, and the irradiation time for each layer was 5s. The 3D printed objects were treated using sonication in ethanol for 10 min and washed by Deionized (DI) water to remove any uncured polymer.

4.1.4   Tablet Design

The tablet has two main parts: the core and the shell (Figure 4-1A). The core is made of a surface eroding polymer loaded with a drug (shown in orange in Figure 4-1) while the same polymer without any drug is used for the shell (the grey parts in Figure 4-1). The core is enclosed by the shell and is placed closer to the top surface compared to the other faces. When the thickness of the shell is "large enough" for all sides except the top, the release of the drug only from the top surface of the tablet is ensured (Figure 4-1B). This design relies on the surface eroding behavior of the polymer which preserves the tablet structure and integrity during erosion and ensures that the polymer erodes at a similar rate

from all sides. An experiment was conducted that verified the latter (section 4.1.5). Therefore, in this design the water first reaches the drug at the top. As the thickness of the shell is large enough, the drug will be released completely from the top before the water reaches it from the other sides. Accordingly, the release profile of the drug is only governed by the variations in the surface area of the drug-loaded core along with its height (Figure 4-1C). As an example, in Figure 4.1, the surface area of the tablet core from the top is increasing along its height, showing that this tablet is designed for obtaining an increasing release profile (Figure 4-1D).
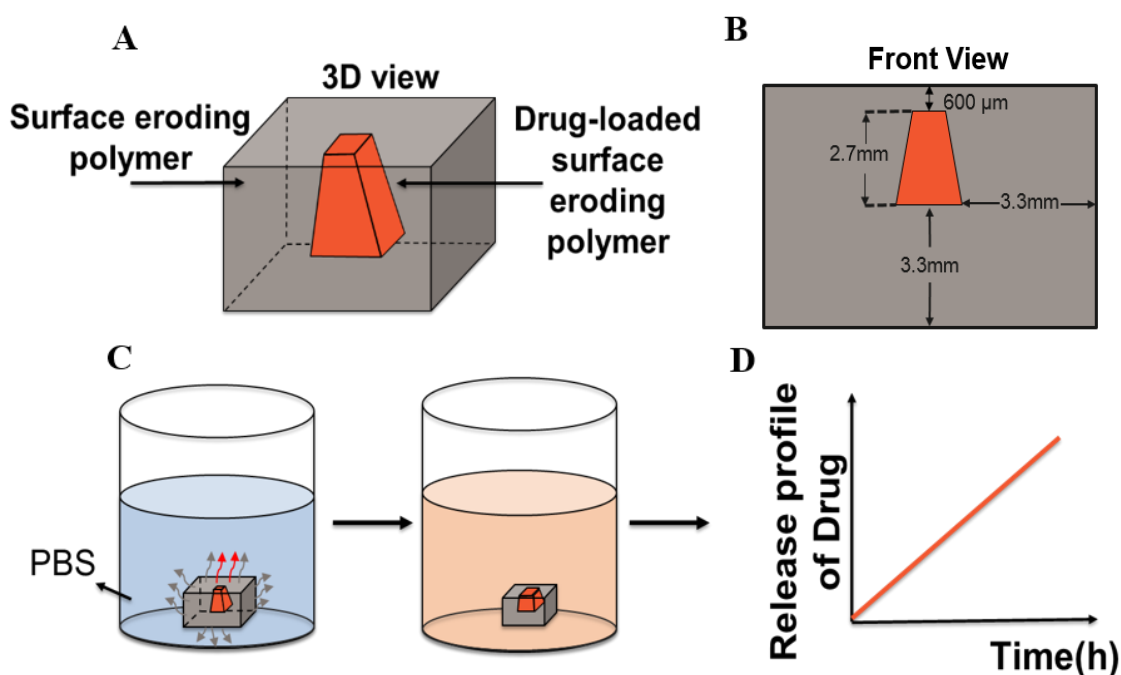
Figure 4-1: Schematic illustrations of core-shell tablet design for an "increasing" release profile. The core is shown in orange, and the shell is the grey part. A) 3D view and B) front view showing that the core is closest to the top surface. The shell is made of the same polymer, with larger thickness than the core's height on the other sides. C) Release of the drug-containing part when the tablet is immersed in PBS. D) The expected release profile of the drug for this tablet design.

4.1.5   Tablet Characterization: Height and Diameter Reduction Rates

To ensure that the polymer erodes at similar rates from all sides, the erosion of cylindrical thiol-ene polyanhydrides was studied. Four thiol-ene polyanhydride cylinders with initial mole ratios of 100:100:0, 100:75:25, 100:50:50, and 100:25:75 were synthesized in cylindrical PDMS molds. The PDMS molds were fabricated using 3D printed master molds with the diameter and height both equal to 8.7mm. The synthesized polymers (cylindrical tablets) were immersed in 10 ml PBS (pH=7.4) in glass vials, before being placed on a shaker (VWR micro-plate shaker). The shaker was set up at room temperature and the shaking rate of 120 rpm. The diameter and height of the tablets were measured frequently (approximately one every hour) during erosion. For each measurement, tablets were removed from the solution and their surfaces were slowly wiped off using disposable wipers. The dried tablets were then put on a printed coloured graph paper, and the photos were taken using a Canon SX201 IS digital camera from four different sides of each tablet, before putting the tablet back in PBS. Images from the top and bottom of the tablet were used to monitor the diameter reduction, while the two images from the sides provided information on variations in the tablet's height. The NIH ImageJ software (version 1.8.0) was used to measure tablet dimensions from photos taken. Experiments were repeated three times for each polymer.

4.1.6   Micro-fabrication of the Tablet Core

A microfluidic network that was fabricated using the conventional standard photo- and soft-lithography techniques[1,2] was utilized to create the dye-loaded polymers used as the core of the tablets. Steps are shown in Figure 4-2 starting from using a silicon wafer as a substrate. The SU-8 photoresist was poured on a four-inch silicon wafer, and a 300 μm-thick layer of photoresist was spin-coated (Laurell Tech Corp.) on the top surface of the silicon substrate. Considering the photo- and soft-lithography procedure for micro-fabrication, a photo-mask that replicated the final desired shape is used. In the design for the core of the tablet, instead of using the shape of a single tablet core for the photo-mask, a high-throughput pattern of tablet cores was designed using AutoCAD software which was then printed as the photo-mask on a high-transparent sheet (Figure 4-2A). The

SU-8 photoresist (with the desired thickness spin-coated on the substrate) was covered by the photo-mask and was exposed to high-intensity UV-light (AB-M Inc.) for 80 seconds. When using a photo-mask, the UV-light only passes through the UV-transparent parts, crosslinking only the desired areas on SU-8. Therefore, the SU-8 photoresist polymer hardened only at the designed pattern and the other parts remained uncross-linked. Lastly, SU-8 developer was used to remove the uncross-linked photoresist from the wafer, yielding the final SU-8 mold (Figure 4-2B).
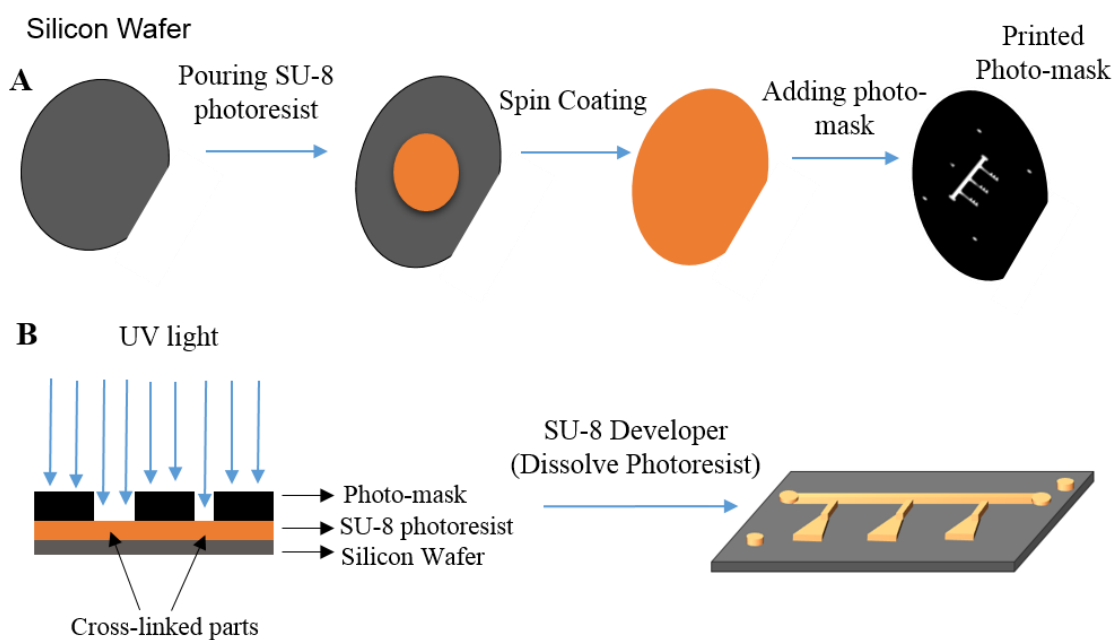
Figure 4-2: Schematic illustrations of the micro-fabrication procedure to create the SU-8 mold. A) Coating the SU-8 photoresist on top of the silicon wafer and putting the printed photo-mask containing the designed patterns on top of the SU-8-coated silicon substrate. B) Exposure of the substrate to the UV light in order to cross-link specific parts and then washing away the uncross-linked parts using the SU-8 developer.

Figure 4-3 shows an example of the design for high-throughput manufacturing of the tablet core for an increasing release profile. First, the SU-8 master molds were fabricated using the above-mentioned steps (Figure 4-3 A, B). To fabricate the microfluidic device, the PDMS polymer mixture containing the 1:10 ratio of the base to curing agent was thoroughly mixed. To eliminate the trapped air bubbles created in the PDMS sample, the

mixture was degassed in a vacuum chamber for 15 minutes. As shown in Figure 4-3C, the negative PDMS mold is developed and peeled off from the SU-8 positive mold. To facilitate the peel-off process, the SU-8 mold was silanized to make the mold's micrometer-sized channels more hydrophobic. The positive SU-8 mold was silanized using (tridecafluoro-1,1,2,2- tetrahydrooctyl) trichloro silane by putting the mold in a sealed petri-dish on a hot plate for 2 hours at 65°C. To make the PDMS replica mold, the mixture was poured on top of the SU-8 mold and were cured in an oven for 2 hours at 80 °C. Finally, the cured PDMS was easily peeled off from the SU-8 master mold, yielding the high-throughput patterns connected through the microfluidic network (Figure 4-3 C).
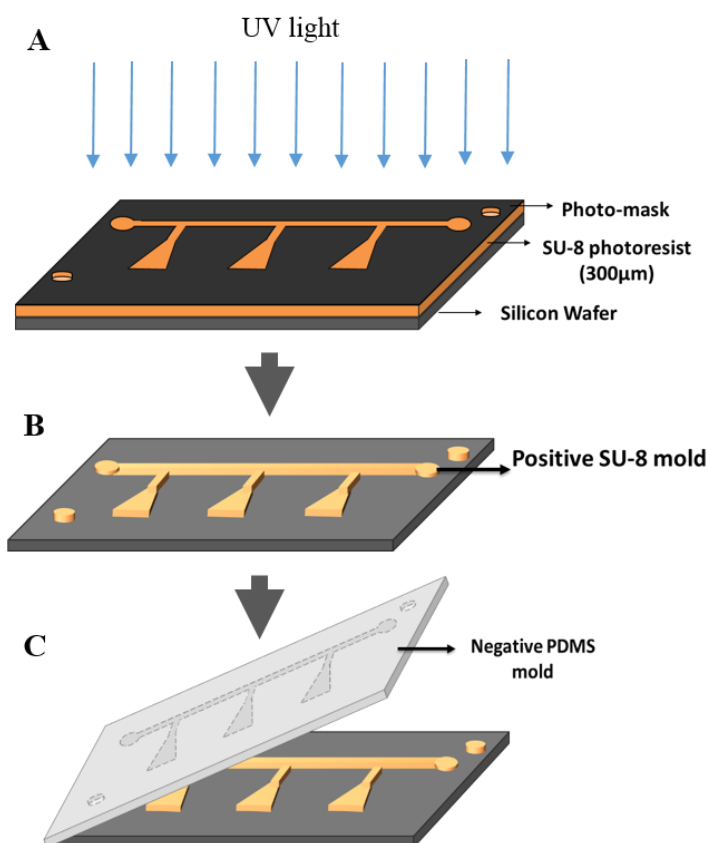
Figure 4-3: Micro-fabrication of a high-throughput design to create the tablet core. A) UV-light exposure to the SU-8 layer covered with the printed photo-mask containing the high-throughput patterns of the tablet core (in this case, the increasing release profile design). B) The positive SU-8 mold containing the embossed features. C) Pouring the PDMS on top of the SU-8 mold and peeling off the final negative PDMS mold once cured in the oven.

A platform for using the fabricated PDMS negative molds to make the polymeric tablet cores was designed (Figure 4-4). Another PDMS negative mold with a pattern mirrored to that of the original was fabricated and placed on top of the original PDMS negative mold, making a microfluidic network with 600 μm in thickness for the channels. The top PDMS negative mold was punched on two sides with a 2 mm biopsy punch (EMS-Core Sampling Tools) to create inlet/outlet ports through which solutions can flow in the channels created by the two PDMS negative molds (Figure 4-4). The two PDMS layers were sandwiched between two rigid PMMA sheets (3.3 mm thickness). Uniformly distributed holes were designed using AutoCAD software and were cut on PMMA sheets using the CO_2 laser (SUNCOO K40 laser cutter). These holes were designed for using screw-nuts through which a uniform force was applied to squeeze two PDMS layers together to prevent any leakage of solutions. At the center of the top PMMA sheet, a pattern was cut using the laser cutter to allow exposure of the solution in the PDMS layers to UV-light (Figure 4-4) for curing the tablet cores.
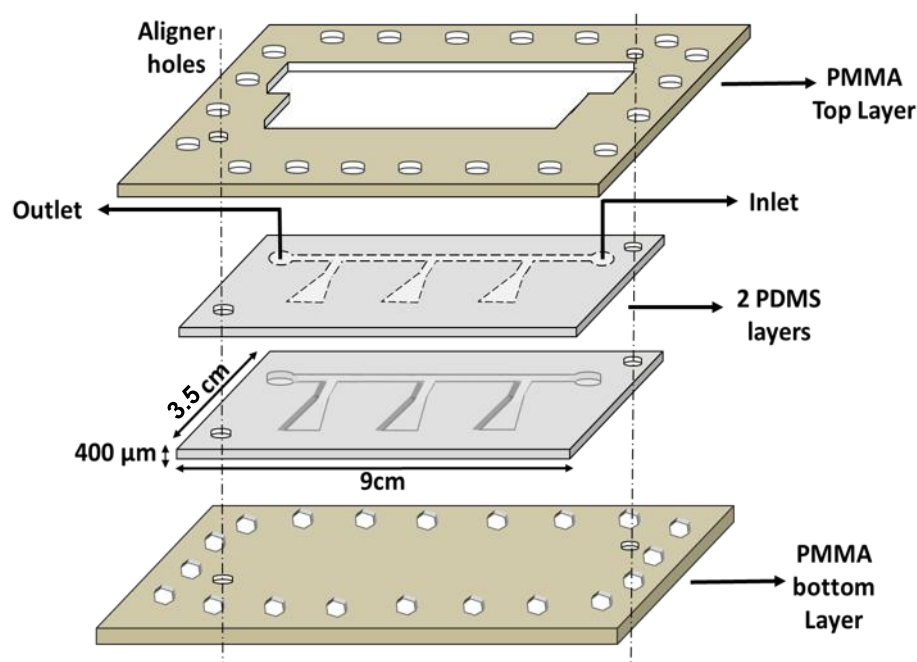
Figure 4-4: Two PDMS layers sandwiched by two rigid PMMA sheets equipped with holes designed to embed screw-nuts for applying uniform forces on PDMS layers. Squeezing two PDMS layers using the uniform forces, eliminates the potential leakage of the solutions through microfluidic channels.

4.1.7   High-throughput Setup for Fabrication of Core-Shell Tablets

Pre-polymer solutions were prepared as described in the polymer synthesis section. In this study, two pre-polymer solutions with initial mole ratios of PNA: PETMP: EGDT = 100:100:0, and 100:75:25 were prepared. Approximately 5 ml of solutions containing 1 wt% of acid orange 10 (orange G) model compound were transferred into a vial. The solution was continuously injected into the microfluidic network from the inlet port using the Tygon Microbore tubing (0.79″ID) (Figure 4-5A). A vacuum pump was connected to the outlet, helping draw the solution to fill the champers. After the solution filled the chambers completely, the features were exposed to UV-light (UVP Crosslinker, intensity = ~5mW/cm^2) for 5 minutes. The screws were then opened and the three connected dye-loaded tablet cores were peeled off by separating the two PDMS layers.

The cured micro-fabricated features (the three connected tablet cores) were then placed in cylindrical PDMS wells (Figure 4-5B) fabricated using master molds printed by commercial DLP 3D printer. The procedures for the fabrication of the 3D printed master molds were the same as the steps described in section 4.1.3. The 3D model of the wells was designed so that when the high-throughput micro-fabricated cores are placed in the wells, each of the cores stay at the center (from the sides, horizontally) and at a pre-determined distance from the bottom and the top of the well (vertical alignment). Particularly, as explained in section 4.1.4, the cores were closest to the top and far enough from all other sides of the wells. After placing the dye-loaded cores in the wells, the empty spaces around the polymers inside the wells were filled using the same pre-polymer solution as the core but without any model compound. Another 5 minutes of UV-exposure was conducted to cure the newly added polymer solution. Finally, three tablets were peeled off from the PDMS wells (Figure 4-5B) and simply were separated using a blade by cutting the connecting part. To allow reusing the PDMS molds, the channels were washed after peeling off the dye-loaded polymer using the mixture of water and ethanol. After washing the channels carefully, they were dried using high-pressure air for 2 minutes that also ensures cleaning the molds from dirt and possible residues.
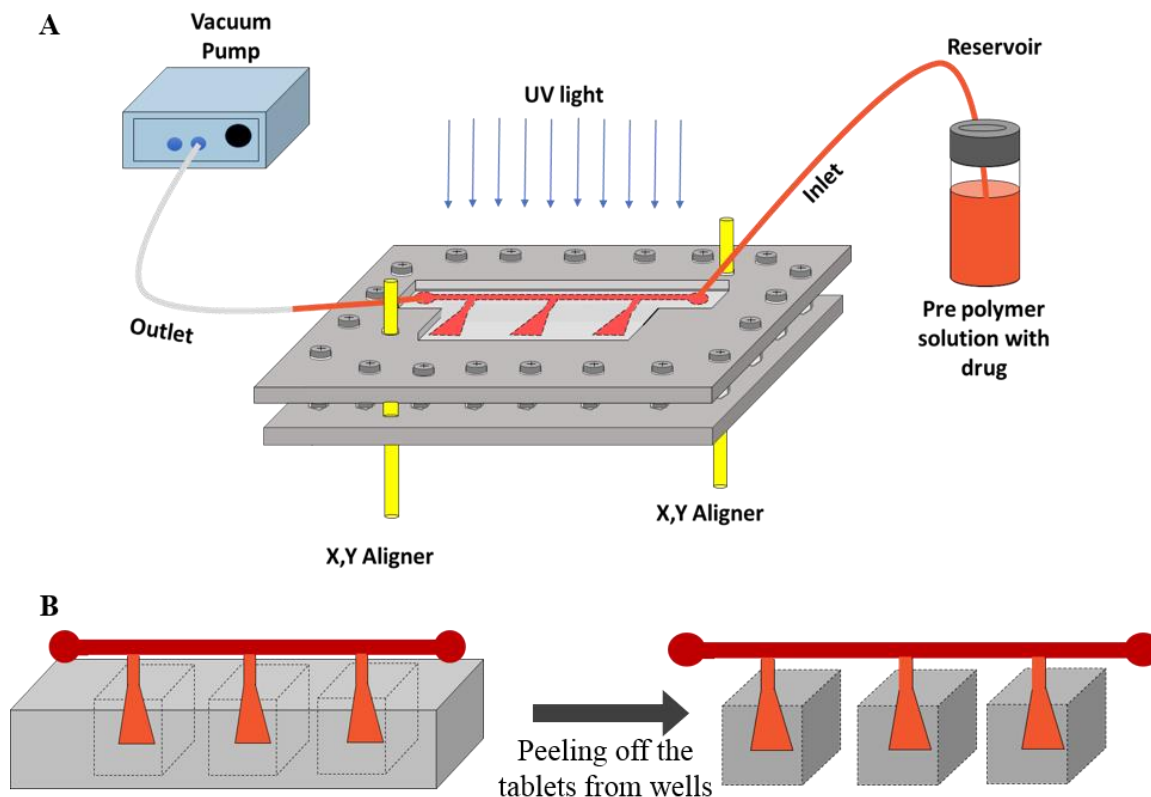
Figure 4-5: Schematic representations for the high-throughput fabrication of the core-shell tablet using A) A high-throughput set up to manufacture the tablet cores. Microfluidic channels were filled by a dye-containing polymer solution that was injected from a reservoir. The vacuum pump helps the solution flow through the network. The first round of the UV-light exposure was used to cure the connected features. B) Micro-fabricated features were placed and aligned in PDMS wells. Empty spaces were filled with the same polymer without any dye. Using the second round of UV-light exposure, the final tablets were fabricated.

4.1.8   Tablets for Achieving Adjustable Release Profiles

The ultimate goal of this study is to achieve different release profiles through a novel tablet design fabricated by a high-throughput fabrication platform. To meet this goal, different tablet geometries were designed using AutoCAD software. Figure 4-6 indicates the design of the high-throughput tablet cores which are connected to each other. These tablet cores were designed for the increasing (Figure 4-6A), and the constant release profiles (Figure 4-6B). The width of the tablet cores design is increasing and uniform from the top along their heights in the increasing and constant tablets, respectively.

Figure 4-6C shows a different design for the core of tablets with constant release profiles that have two, three, or four constant release cores in each connected feature (this design will be described in details in the next section). These designs were printed as photomasks and went through soft-lithography steps for making the PDMS molds containing connected features as a microfluidic network.
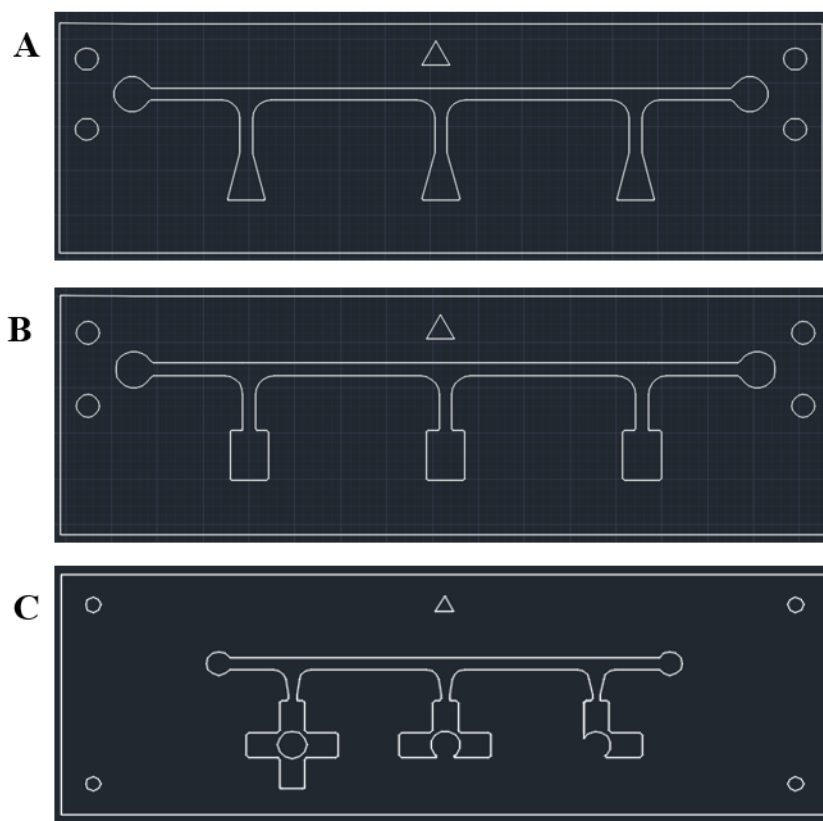
Figure 4-6: High-throughput CAD designs for A) Increasing release profile tablet core. B) Constant release profile tablet core (one-arm design). C) Constant release profile tablet core (two-arm, three-arm, and four –arm designs).

The micro-fabricated cores for the increasing and constant release profiles were placed into PDMS wells where the pre-polymer solution without drug was poured and polymerized under the UV-light. The three tablets for each geometry were placed in 5 mL PBS at pH=7.4 separately before being placed on a shaker which was set at 37°C with shaking rate of 120 rpm. Almost every hour, 750 μl of each PBS solution was withdrawn, transferred into three wells of a 96-well plate (each well contained 250 μl),

and analyzed using a micro-plate reader (Asys UVM 340) instrument. The concentration of the model compound in a 250 µl sample was calculated using the absorbance measured by a micro-plate reader (Asys UVM 340) instrument. The concentrations were calculated using the concentration-absorption calibration curve that was obtained by measuring the absorbance of different known concentration of acid orange 10 in the wavelength with the maximum absorbance of UV light (475 nm) (Appendix D-1). The wavelength in which the model compound (orange G) has the highest absorption of UV-light was identified by finding the maximum absorbance of acid orange 10 in solutions with known concentrations shown in Appendix D-1. For the UV microplate reader device, the absorbance-concentration relation was calculated as shown in Equation 4-1 where A is the absorbance of the UV light by the model compound and C is the concentration of the model compound in the sample. The absorbance is linearly related to the concentration. The slope (α in Equation 4-1) was calculated for the micro-plate reader to be 27.13 by fitting a linear line to absorbance-concentration data.

$$A = \alpha\, C \tag{4-1}$$

The absorbance of each sample was measured using the UV-plate reader, and the concentration of the model compound in the sample was calculated using the Equation4-1. An equivalent amount of the fresh PBS (750 µl) was added after withdrawing the same amount of solution. After collecting the concentration data of the model compound at certain time intervals, the fractional release (Equation 4-2) and the release rates (Equation4-3) of the model compound from each tablet were calculated. In Equation 4-2, M_0 is the initial amount of the dye dispersed in the tablet which is known, C_i is the concentration of the model compound calculated for the i_{th} sample at time t, V_t is the total volume of the sample (e.g., 5mL in this study), and V_i is the withdrawn sample volume (250 µl per well or 750 µl per sample), and $F_i\%$ is the fractional released percentage of the dye.

$$F_i\,\% \;=\; \frac{C_i \times V_t + \sum_1^{i-1} C_j V_i}{M_0} \times 100 \tag{4-2}$$

In Equation 4-3, R_i is the release rate of the model compound at time t for the i_{th} sample, and T_i is the time at which the i_{th} sample was withdrawn.

$$R_i = \frac{(F_i - F_{i-1}) \times M_0}{T_i - T_{i-1}} \tag{4-3}$$

4.1.9 Modified Tablet Designs to Increase the Loading Capacity

The tablet designs were modified to improve the capacity of the tablet for containing higher quantities of therapeutics. One arm, two-arm, and four-arm designs for the core of the tablets were devised to make use of extra spaces in the shell of cylindrical tablets. In the modified designs, instead of using only the axial direction for releasing the dye, the radial directions were used as well by loading the dye in two-arm and four-arm tablet designs. Figure 4-7 A to C shows the schematic illustrations of the one-, two-, and four-arm tablet designs in front view, respectively. Although in the one-arm design, the core is closest to the top of the tablet (same as the tablet designs described so far), in the two and four-arm designs, the core is as close to the right, left, and bottom of the tablet as to the top side. It means the water could access the dye from one, two, and four sides for the tablets shown in Figure 4-7 A, B, and C, respectively.

As was shown in Figure 4-6C, similar to the increasing and constant designs, the modified tablets are designed in a high-throughput connected pattern. The tablet cores were printed as photo-masks and were fabricated using the high-throughput micro-fabrication method previously discussed. Similar to what was described in section 4.1.7, tablets' shells were fabricated with the help of PDMS cylindrical wells. Three separated tablets for each design were immersed in PBS solution for the release test using the same procedure mentioned above. The concentration of the model compound was calculated using the absorbance values measured by the micro-plate reader. The fractional percentage model compound released and the release rates for these three modified designs were calculated using Equation 4-2 and 4-3 and then compared to each other.
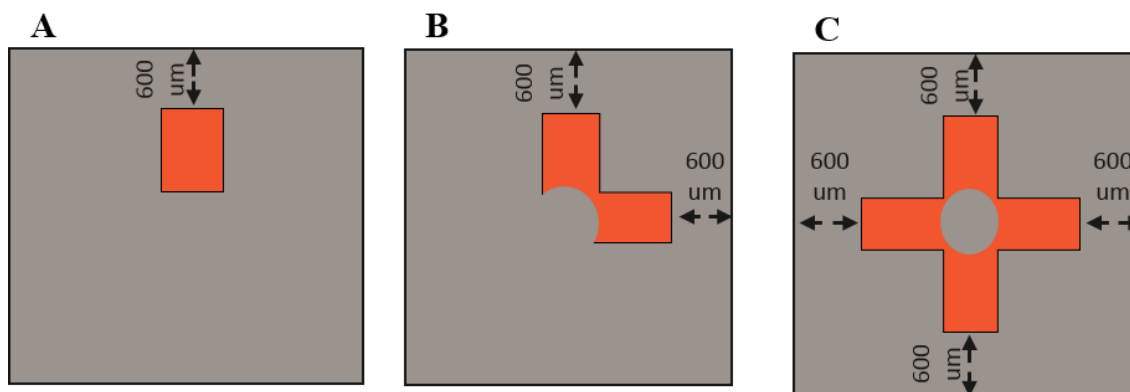
Figure 4-7: Schematic representations of modified tablet design to improve the loading capacity. Front view of A) one-arm tablet design. B) two-arm tablet design. C) four-arm tablet design.

4.1.10   Automated Tablet Designs

After determining the tablet design and choosing the suitable polymers for the tablets, the tablet geometry is usually designed using computer-aided design (CAD) or drawing software. There are several variables that should be considered for designing polymeric tablets. Most of these variables are dependent on the physicochemical properties of the polymers which affect their degradation or erosion kinetics. Polymeric tablets are typically designed by AutoCAD software after solving the complex mathematical equations governing the drug release kinetics. Expert tablet designers use powerful tools and software to calculate the dimensions and design the geometry of the tablet by considering all the essential variables.

Automation of the tablet design process saves a considerable amount of time and money in the manufacturing process of personalized tablets. It also allows physicians to rapidly design a tablet-based on the desired release rate, without the need for an expert designer. A few commercial software programs were recently introduced that helps non-expert individuals design commercially-available tablets in a user-friendly platform. For example, in silico tablet formulations can be developed and tested using the formulation-computer aided design (F-CAD) software platform of CINCAP [3]. Researchers have also

used TabletCAD (Natoli Engineering Company), which is a simple web-based user interface for designing tablets that can be directly linked to the manufacturing process[4].

In the design, using the bio-erodible polymer simplifies the automation of the tablet design. This is due to the decreased calculation complexity required for determining the drug release profiles from these polymers. In this study, a graphical user interface (GUI) was created using the Python programming language for rapid designing of the patient-specific erodible tablets via a user-friendly platform without the need for expert designers. The required dosage (concentration) of the drug during the course of treatment, i.e., the desired release profile of the drug, are determined based on the diagnosis of the physicians (Figure 4-8A). The thickness of the tablet core (which is 600 μm, in this case) and dimensions reduction rates of the polymers, measured in section 4.2.1, were entered as inputs. The weight percentage of the drug dispersed in the polymer was also determined in the visual indicator. The 2D tablet core was automatically designed using the user interface program based on the inputs. (Figure 4-8B). The complete explanation of this developed user interface and an example of automated core design for the pulsatile release tablet is included in Appendix E-1.
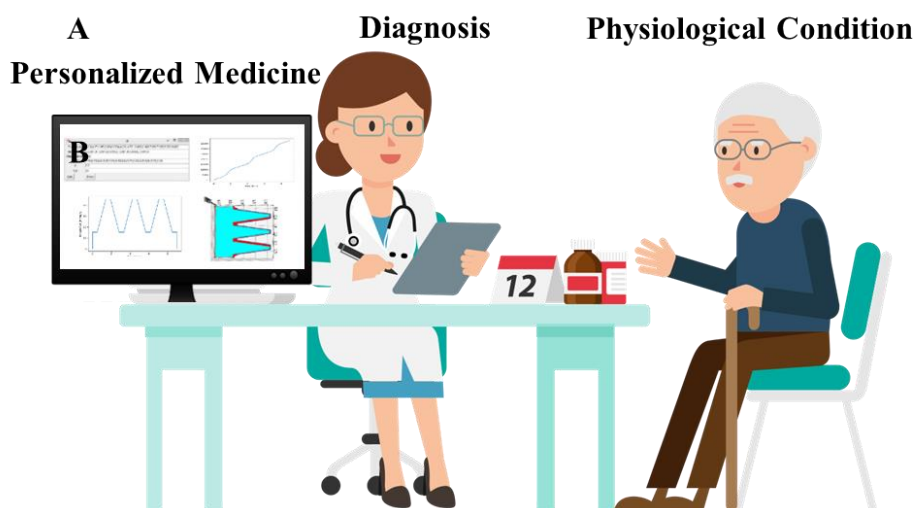
Figure 4-8: Automation of tablet designs. A) The importance of the personalized medicine and automated tablets design based on the patient's physiological condition. "Doctor with Patient Cartoon.svg from Wikimedia Commons by Videoplasty.com, CC-BY-SA 4.0". B) The graphical user interface was created for designing patient-specific tablets with specific release rates.

4.2 Results and Discussion

This section presents and discusses the results of the tablet characterization, high-throughput fabrication of the tablet design, adjustable release profiles obtained from various tablet designs, and modified designs to improve the loading capacity of the proposed controlled-release tablets.

4.2.1 Tablet Characterization: Height and Diameter Reduction Rates

Several studies have shown that polyanhydrides predominantly undergo surface erosion[5,6]. Researchers have connected the surface erosion mechanism to the linear mass loss profile of polyanhydrides that results in a near zero-order drug release from these polymers[7,8]. Most of these studies used polyanhydrides in the form of a slab (a thin layer of polymer). Using the new type of polyanhydrides synthesized by thiol-ene photopolymerization, a rectangular slab ($2 \times 10 \times 10$ mm) made of PNA and PETMP showed a linear mass loss profile. More complicated mass loss profiles were observed for a cube made of the same polymer[9]. In section 3.2.2.8, the mass loss behavior of cylinders and cubes made of the polymers was examined over time. Results showed that the mass loss of these polymers closely followed the cubic and quadratic functions rather than a linear profile. The non-linearity observed in the mass loss profile of the more complex thiol-ene polyanhydride geometries (such as cubes and cylinder), does not contradict the surface eroding behavior of the polymer. Surface erosion behavior is defined as the quality to preserve the tablet structure during the erosion time. This unchanging structure of tablets is attributed to a similar dimension reduction rates in all directions. In this section, the diameter and height variations for each tablet were monitored and calculated from the photos that were taken at specific time intervals (approximately once every hour) after the induction period. The average of the measured diameters and heights from triplicate experiments for each tablet were plotted over time.

Results indicate the linear behavior of the dimension reduction for cylindrical tablets as shown in Figure 4-9A, B. As discussed in section 3.2.2.1, an increased ratio of EGDT to PETMP in the thiol-ene polyanhydrides network results in higher erosion rates. The rates

of the reduction for both diameter and height of all the tablets were calculated by finding the slope of the linear curves fitted to the measured data. Table 4-1 summarizes the results of the reduction rates for diameters and heights of these four tablets. The dimension reduction profiles in Figure 4-8 show that the reduction of diameters and heights for each tablet is linear. In addition, similar diameter and height reduction rates are observed for tablets made of the same polymers. Having the same reduction rate in different dimensions is a very crucial characteristic for a polymer because it increases the polymer's applications in CRSs. The adjustable release rates from the tablet designs rely on similar reduction rates in different dimensions.

The linear behavior of the reduction rates (the calculated correlation coefficients $R^2 \approx 1$) observed in both dimensions (shown in Figure 4-9 A, C), allowed calculating the expected dimension reduction rate of the same polymer for a new cylindrical design. Ideally, this expected reduction rate can be calculated by measuring the dimensions of the tablet at least at two arbitrary time points during erosion and fitting a linear function to dimension vs. time data. The slope of the dimension-time data represents the reduction rate. This linear behavior of the reduction rates showed in this study eliminates the need for monitoring tablet dimensions during the erosion time. For example, by having the initial and final dimensions and the erosion time, the reduction rates can be easily calculated and used in the tablet design for releasing the pre-determined patterns of drugs.
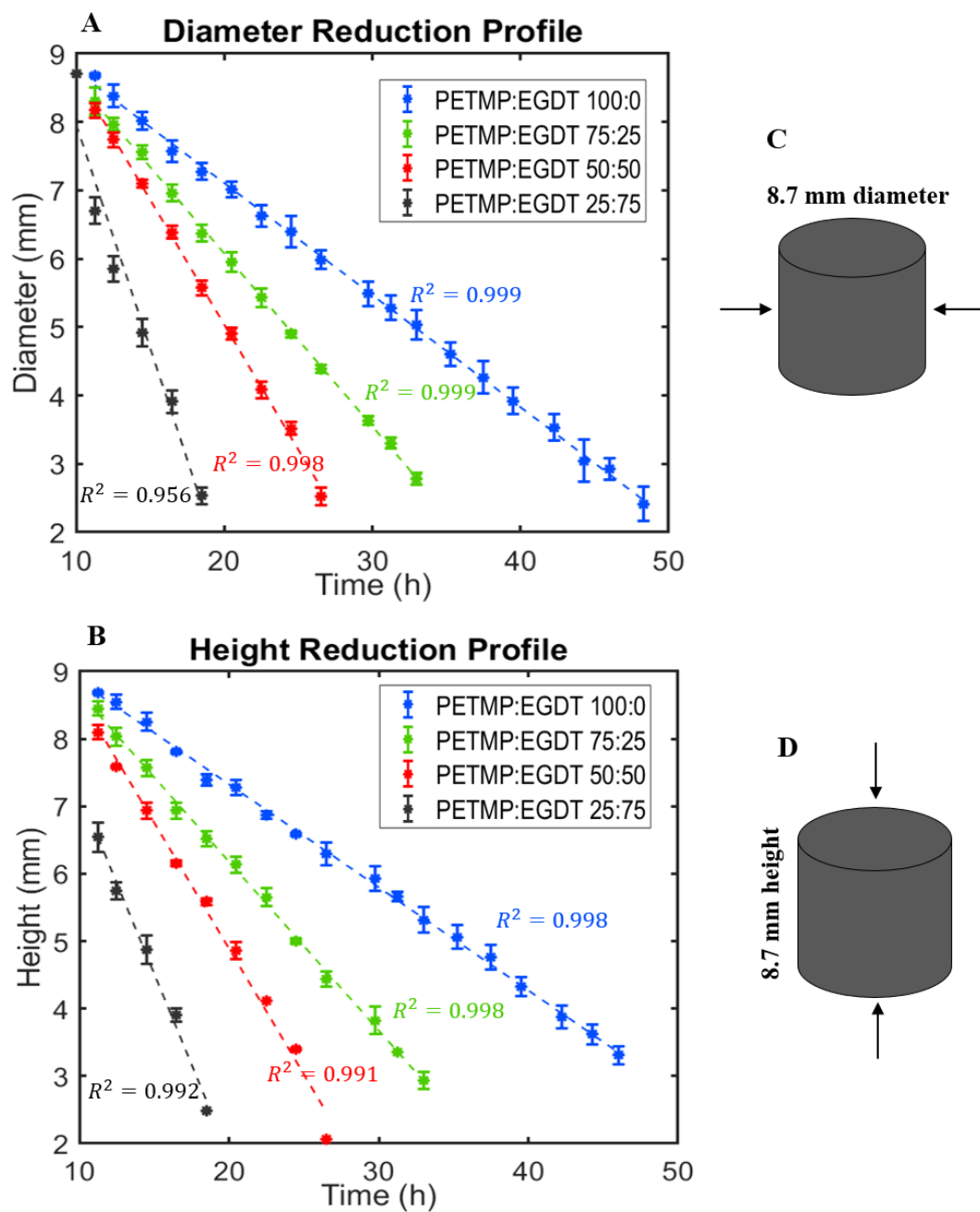
Figure 4-9: Linear reduction profiles of A) Diameters of four cylindrical tablets. B) Heights of four cylindrical tablets. Schematic illustrations of C) horizontal direction of a cylindrical tablet monitored to measure the diameter reduction rates and D) vertical direction of a cylindrical tablet monitored to measure the height reduction rates.

Table 4-1: Diameter and height reduction rates measured for cylindrical tablets.

PETMP:EGDT	Diameter Reduction Rate (mm/h)	Height Reduction Rate (mm/h)
100 : 0	0.16	0.15
75 : 25	0.25	0.25
50 : 50	0.37	0.37
25 : 75	0.65	0.54

4.2.2 Micro-fabrication of Tablet Cores

The designs of tablet cores, previously shown in Figure 4-6, were printed as photo-masks and the SU-8 master molds were fabricated through photolithography steps (Figure 4-10 A). The PDMS molds were successfully fabricated via a standard soft-lithography process using the SU-8 master molds. The depth of the chambers on PDMS negative molds was measured using a microscope (Nikon 334 Eclipse Ti-E). The measured depths ranged from 298 μm to 301 μm for different molds that are very close to the designed value (300 μm), showing the successful fabrication of PDMS negative molds.

The original PDMS layer and the one with the mirrored pattern were put on top of each other to create 600 μm cavities between them (Figure 4-10 B). Typically, two PDMS layers irreversibly bound to each other or a PDMS layer bonds to a glass slide using a standard O_2 plasma activation process to make a microfluidic network[10–12]. However, the pattern can be destroyed by the formation of an irreversible seal between the PDMS mold and a glass slide [13]. Besides, in this study, there was a desire to access the features and remove the dye-loaded polymer solution once it is cured in the network. Therefore, to seal the channels and at the same time prevent the leakage of the fluid, at first, small clamps were used to squeeze the two layers together as shown in Figure 4-10 C. However, leakage of the polymer solution from the microfluidic channels was observed using the clamps. Alternatively, two rigid PMMA sheets were utilized to sandwich the PDMS layers. Screws and nuts were used to apply uniform force and to secure the alignment. This platform was designed and fabricated for creating the tablet cores. The successful injection of the pre-polymer solution containing the model compound via inlet/outlet ports is shown in Figure 4-10 D.
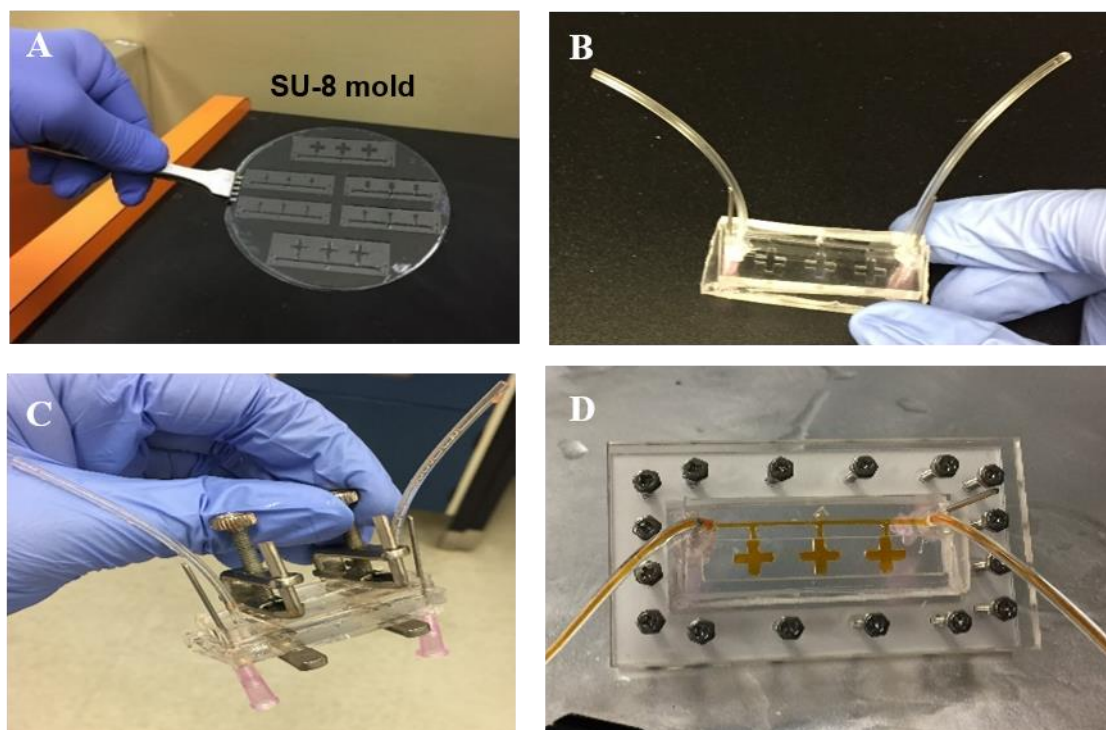
Figure 4-10: Development of the PDMS microfluidic network for creating the tablet core. A) SU-8 master mold fabricated to make PDMS replica molds B) Putting two PDMS layers with the mirror patterns on top of each other to create microfluidic cavities with 600 μm depth in between. C) Using clamps for squeezing two PDMS layers for the elimination of the potential leakage. D) Using two PMMA sheets to apply uniform forces on PDMS layers using uniformly distributed screws.

4.2.3 PDMS Wells for Fabrication of Tablet Shells

To create the tablet shell, PDMS wells were successfully fabricated using 3D printed master molds. Firstly, cubic wells were designed in a way that the distance between every two adjacent cubes was the same as the distance between the two adjacent microfabricated tablet cores. The dye-loaded tablet cores were placed at the center of the wells at a certain height (as explained in section 4.1.7) using external aligners. Two aligners were used to hold the fabricated dye-containing part at the specific XYZ position. Figure 4-11A shows the printed cubic wells, the PDMS negative molds, and the three cubic surface eroding tablets created in the cubic PDMS wells.

Figure 4-11B shows an alternative design for the cubic wells' in AutoCAD in which two aligners were added at both ends of the 3D printed object. Two aligners were designed with certain heights and a notch on them where the micro-fabricated tablet cores hang to ensure the right XYZ position. These two aligners facilitate the correct placement of the fabricated dye-containing part in the right location inside the well, without the need for external aligners. All the tablet shell designs were changed to cylindrical objects (Figure 4-11C) since tablets with cubic shapes have sharp corners that are inconvenient to swallow when used as oral tablets. The final optimized design was the cylindrical wells with two aligners in both sides and two more aligners between every two adjacent wells (Figure 4-11D). Aligners between wells were added to prevent the micro-fabricated part from bending or collapsing due to the gravity.

The resolution of the method used for fabrication of the tablet core is of higher importance than that of the tablet shell. The geometries of the μm-sized tablet cores determine the release profile of the model compound and are also more complex than the geometries of the mm-sized PDMS wells that form the tablet shell. However, this design benefits from a higher resolution technique for producing PDMS wells (DLP 3D printing), that is also capable of printing various geometries with sharp corners or curvatures including cubes, cylinders, and spheres which are the common form of tablets in the pharmaceutical industry. Higher surface quality of the tablet shells also ensures more precise control over the erosion rate of the tablet in the novel design proposed in this study. Lithography-based 3D printers (SLA and DLP) can create objects with more complex designs at a higher speed and higher resolutions compared to the other commercially available 3D printers such as FDM machines. SLA utilizes lasers to cure the photo-curable solution point by point, while DLP uses a digital projector to cast and cure an entire slice of objects[14]. In this study, a DLP 3D printer (PICO2, ASIGA) was used to fabricate the master molds because of its fast and high-resolution manufacturing process compared to the SLA counterparts. The limitation of the lithography-based 3D printers is the limited number of the available UV-curable resins. Clear 2500T resin was used after evaluating its thermal stability in an oven for 2 hours at 80 °C, which is the same thermal condition for curing the PDMS on top of the printed master molds.
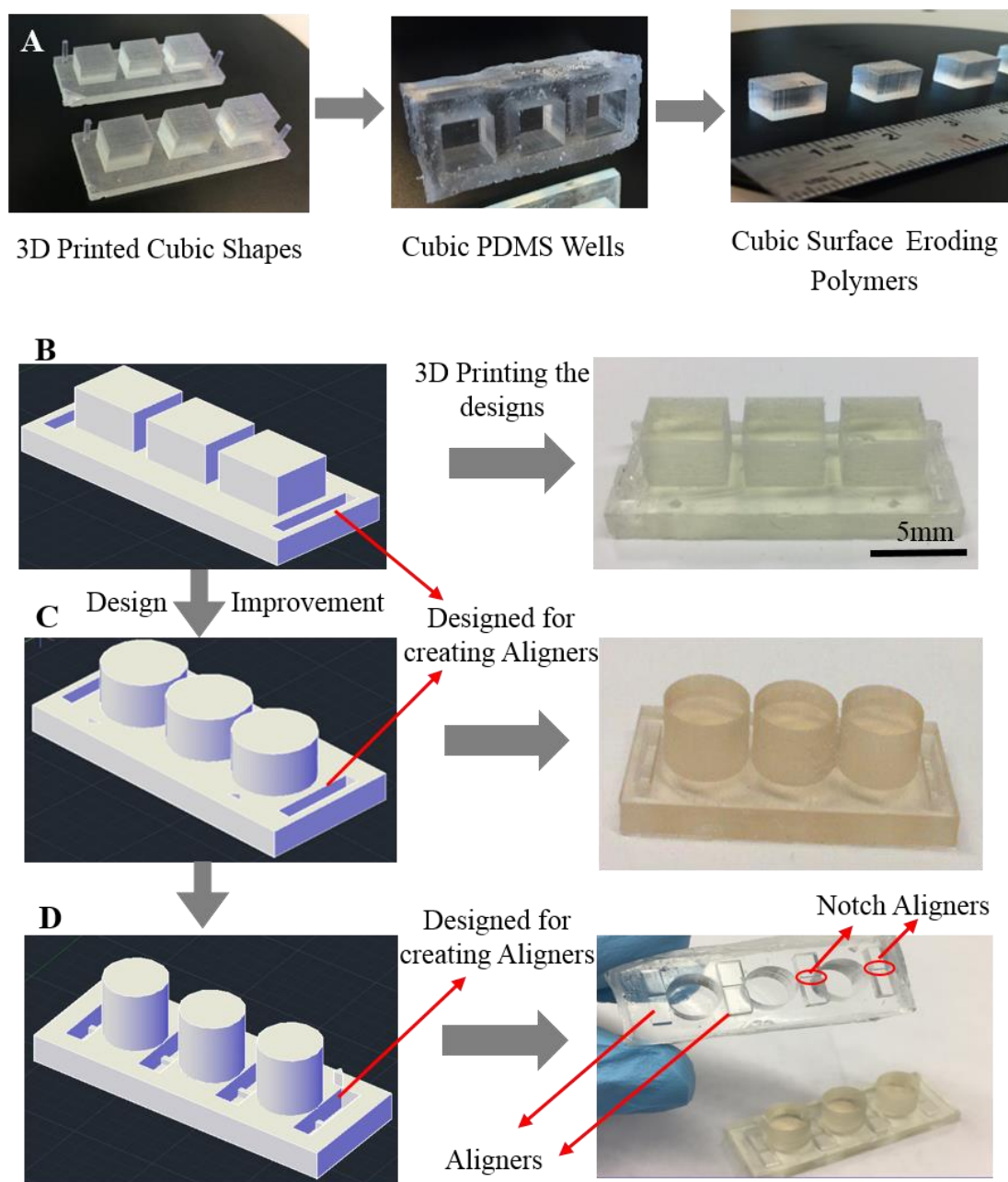
Figure 4-11: Development of PDMS wells fabricated using the 3D printed master molds. A) Cubic 3D printed master mold, PDMS cubic wells created using the master mold, and three surface eroding polymers in a cubic shape fabricated using the PDMS mold. B) The new version of the cubic well design with two aligners in both ends of the mold and the printed master mold. C) Modified cylindrical wells design and the printed object. D) Final optimized cylindrical wells design with four aligners to hold the tablet core.

4.2.4 High-throughput Fabrication of Core-Shell Tablets

The cores and shells of the tablets were fabricated using the developed platform described in section 4.1.74.1.6 for high-throughput manufacturing of the tablets. As an example, the results of the high-throughput fabrication of the increasing release profile tablets are shown in this section. Figure 4-12A shows the final device, developed for fabricating the dye-loaded cores of the tablets. Figure 4-12 shows three tablet cores for the increasing release profile that were fabricated and peeled off from the μm-sized PDMS mold. The cross-linked dye-loaded features were set in place using the notch aligners embedded in the PDMS wells that were created using the 3D printed master molds (Figure 4-12B). Empty spaces in the wells were filled by the same surface eroding polymer without the model compound. All three wells were then exposed to the UV-light, and the final connected tablets were peeled off from the PDMS wells as shown in Figure 4-12C. These connected tablets were simply separated to obtain three individual tablets for the increasing release profile (Figure 4-12D).
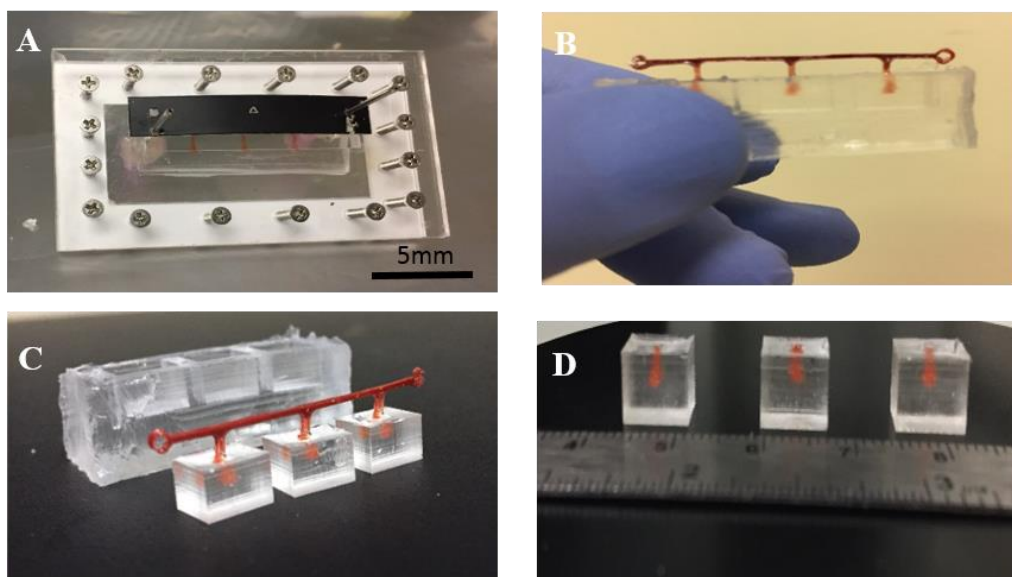
Figure 4-12: High-throughput fabrication of the increasing release profile core-shell tablets. A) High-throughput platform to create the micrometer-sized tablet cores. B) Locating the cured micro-fabricated tablet cores on PDMS wells to create the tablets' shells. C) Three connected core-shell tablets peeled off from the PDMS wells. D) Three separated increasing release profile tablets.

4.2.5   Tablets with Adjustable Release Profiles

The proposed tablet design in this study was tested at first for the constant release profile. The constant release profile tablets were designed such that the surface area of the tablet core from the top along its height was constant (Figure 4-13A). Figure 4-13B shows the constant release profile core-shell tablet in PBS solution after the first half of the core is eroded. The concentration of the model compound in the sample was measured approximately once every hour and the fractional cumulative release of the model compound was calculated and plotted over time (Figure 4-13C). Results show the linear fractional release of the model compound. On the top left on the graph in Figure 4-13C, the release rate of the model compound is plotted. The release rate is not changing over time which agrees with the pre-determined constant release profile intended by the tablet design.

To demonstrate the versatility of the tablet design, a different core-shell tablet was designed and fabricated. The core was fabricated for a decreasing and then increasing release profile of the model compound, as shown in Figure 4-14A. The surface area of the tablet core from the top along its height is decreasing and then increasing. Figure 4-14C shows the fabricated core-shell tablet for decreasing-increasing release profile (Figure 4-14B) in PBS solution after the first half of the erosion period. The fractional cumulative release of the model compound was calculated and plotted (Figure 4-14D) over time. The fractional release of the model compound shows two distinct sections, one during the erosion of the decreasing part and the other happens during the erosion of the increasing part. The data for these two parts were fitted to two quadratic models using MATLAB MathWorks software. On the top left on the graph in Figure 4-14 D, the release rates of the model compound were plotted which show a decreasing and then an increasing release rate over time.
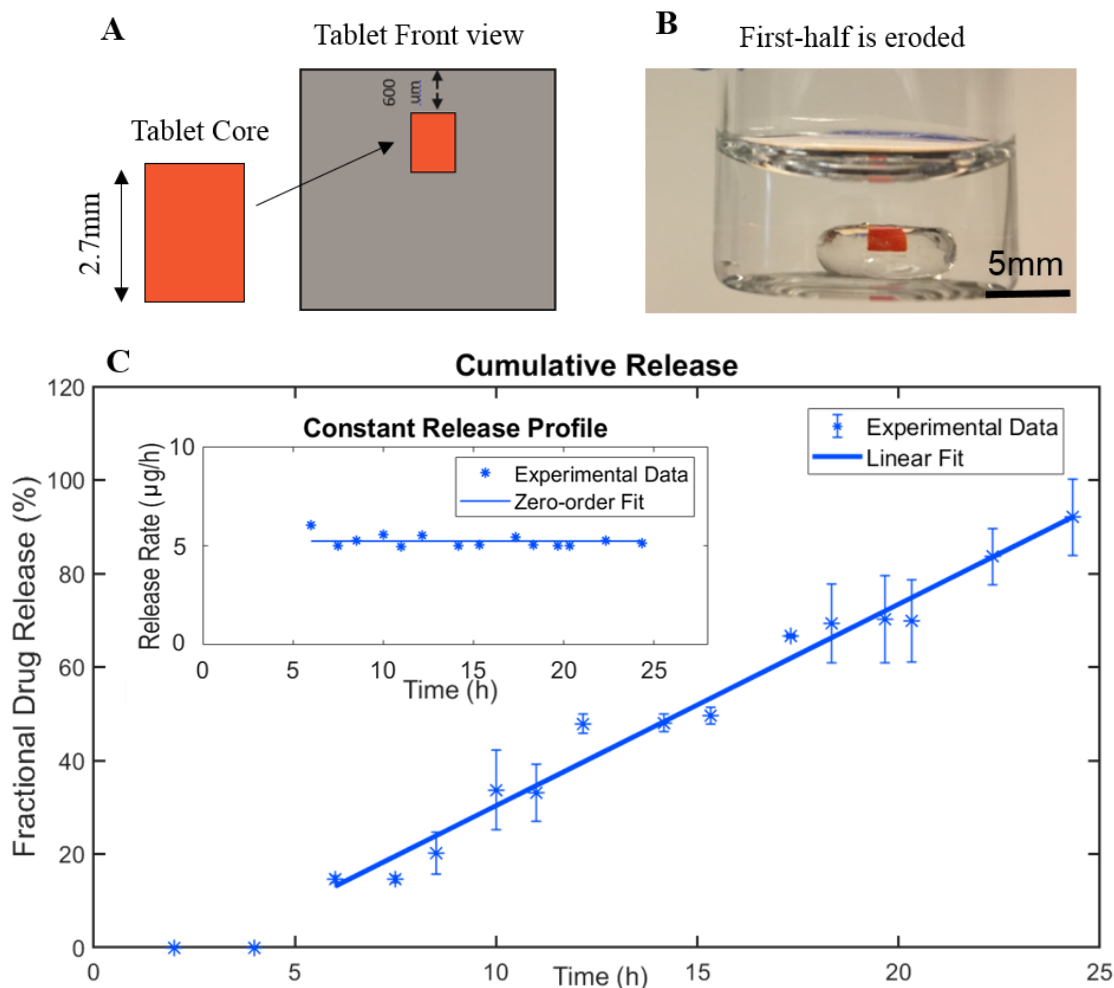
Figure 4-13: Constant release profile of a core-shell tablet. A) The schematic representative of the tablet core with the constant surface area from the top along its height and the position of the tablet core are shown in the tablet front view. B) The fabricated constant release profile core-shell tablet in PBS while it is eroding. C) The linear fractional drug release after the induction period and the constant drug release rate on the top left side.

Release rates calculated for the constant and the decreasing-increasing release profile core-shell tablets showed the feasibility of tuning the release pattern of the model compound from the polymer using the proposed core-shell tablet design. The release profile patterns were only dependent on the tablet's core geometry, particularly the variations in its surface area from the top along its height, as well as the location of the tablet core inside the shell. The linear reduction rates of the erodible tablets' dimensions

(calculated in section 4.2.1), make it possible to estimate the release profiles of the drugs from the tablets. Compared to other studies conducted on obtaining desired release profiles from polymeric tablets[15–17], the presented method is more straightforward and does not require the complex modeling and/or solving of the complicated equations for designing tablets with adjustable release profiles.
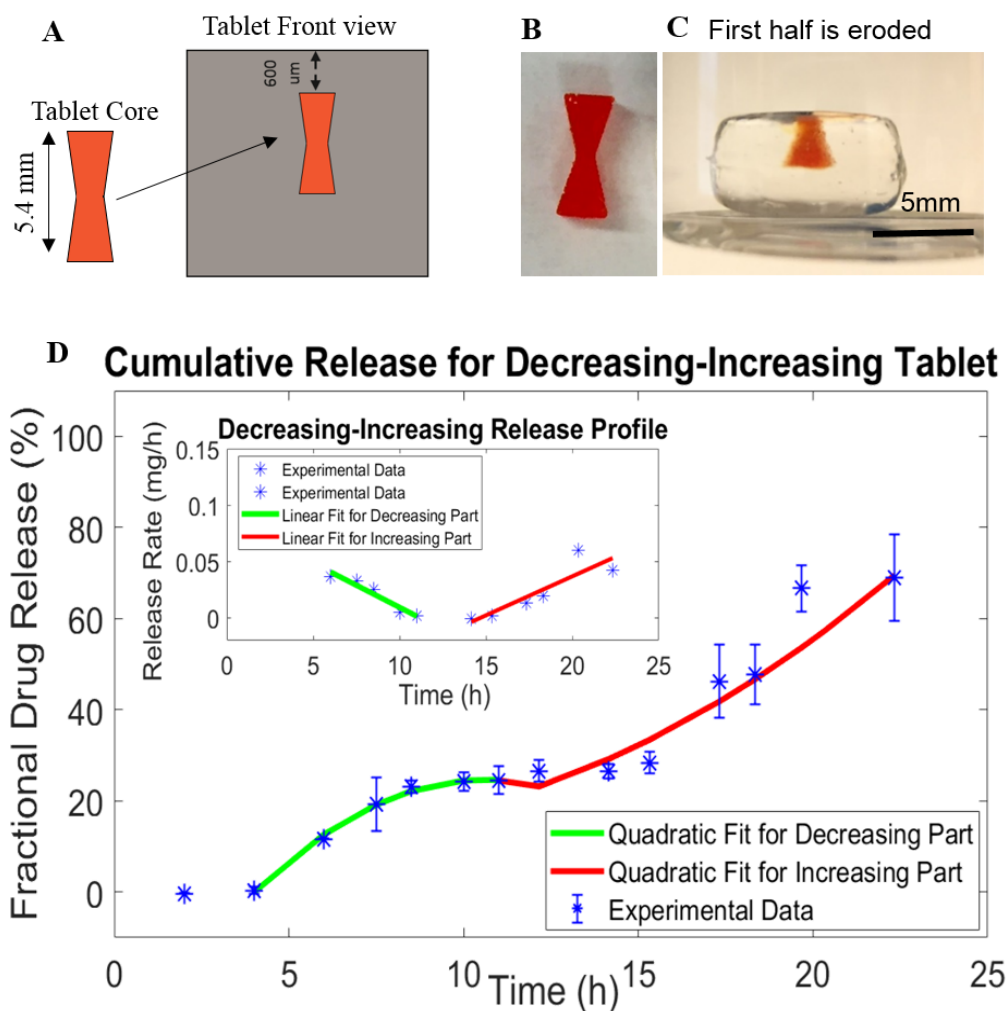
Figure 4-14: The decreasing-increasing release profile core-shell tablet. A) The schematic representative of the tablet core with decreasing and then increasing surface area from the top along its height and the location of the tablet core shown in the front view. B) The fabricated decreasing-increasing tablet core C) The fabricated decreasing-increasing release profile core-shell tablet in PBS while it is eroding. D) The fractional model compound release after the induction period and the decreasing-increasing release rates on the top left side.

4.2.6 Modified Tablet designs towards Increasing the Loading Capacity

The drug-loading capacity of a polymeric delivery system is the total amount of the drug that can be loaded in the system and depends on the polymer, drug, fabrication method, and the design of the DDS. As discussed before in section 3.2.2.6, in the tablet design, a higher intensity UV-light source was required to cross-link the polymers containing higher amounts of the model compound (or any other therapeutics). The high-intensity UV-light transfers very high energy that may damage to therapeutics loaded in the polymer. By modifying the tablet design and utilizing the extra space in the shell of the tablet, higher amounts of the model compound can be loaded into the tablets without increasing the total volumes of the tablets.

The height and the diameter reduction rates for polymers used in this study were measured before in section 4.2.1 and results showed the similarity of the reduction rates. One-arm, two-arm, and four-arm core-shell tablets were fabricated (

Figure 4-15A) using the high-throughput platform. The same weight percentage of the model compound was added to these three tablet designs so that the total initial amount of the dye loaded in the two-arm and four-arm tablets was two and four times higher than the one-arm loaded dye, respectively. The cumulative release of the model compound from all three tablets was calculated and the mean values from triplicate experiments were plotted as shown in Figure 4-15B. Linear curves were fitted to data and slopes were calculated, showing the constant release rates as expected (considering the tablet core designs).

Figure 4-15C, D, and E show the tablets fabricated for constant release profiles while they are eroding in PBS. The cumulative release of the model compound over time was linear for all three fabricated tablets which acted as another indicator of obtaining a constant release profile. Slopes of the linear lines were calculated to show the constant release rates reported in

Figure 4-15B. The release rate of the four-arm tablet was almost four times higher than the release rate of the one-arm tablet and the slope of the linear cumulative release of the

two-arm tablet showed an almost twofold increase when compared to the one-arm tablet. These findings also imply that using the four-arm design, it was possible to load (and release) the same amount of model compound at almost four-times lower weight percentage compared to the one-arm tablet. Consequently, the intensity of the UV-light source required for curing the photocrosslinkable polymeric tablet cores will be reduced which lowers the chances of damages to loaded drugs. Moreover, the results of this experiment showed that more amount of the drug could be released using other sides of the tablet as well as the top side, while preserving the desired release profile.

Researchers have studied the elevation of the loading capacity of controlled DDSs by changing the polymer compositions[18]. Various fabrication techniques such as hot-melt extrusion (HME) and injection molding (IM) were also used to increase the loading capacity of the polymeric tablets[19–21]. In this study, using the modified tablet designs which utilize more dimensions of the tablet for releasing the therapeutics, the loading capacity of the designed tablets was increased by approximately four times.
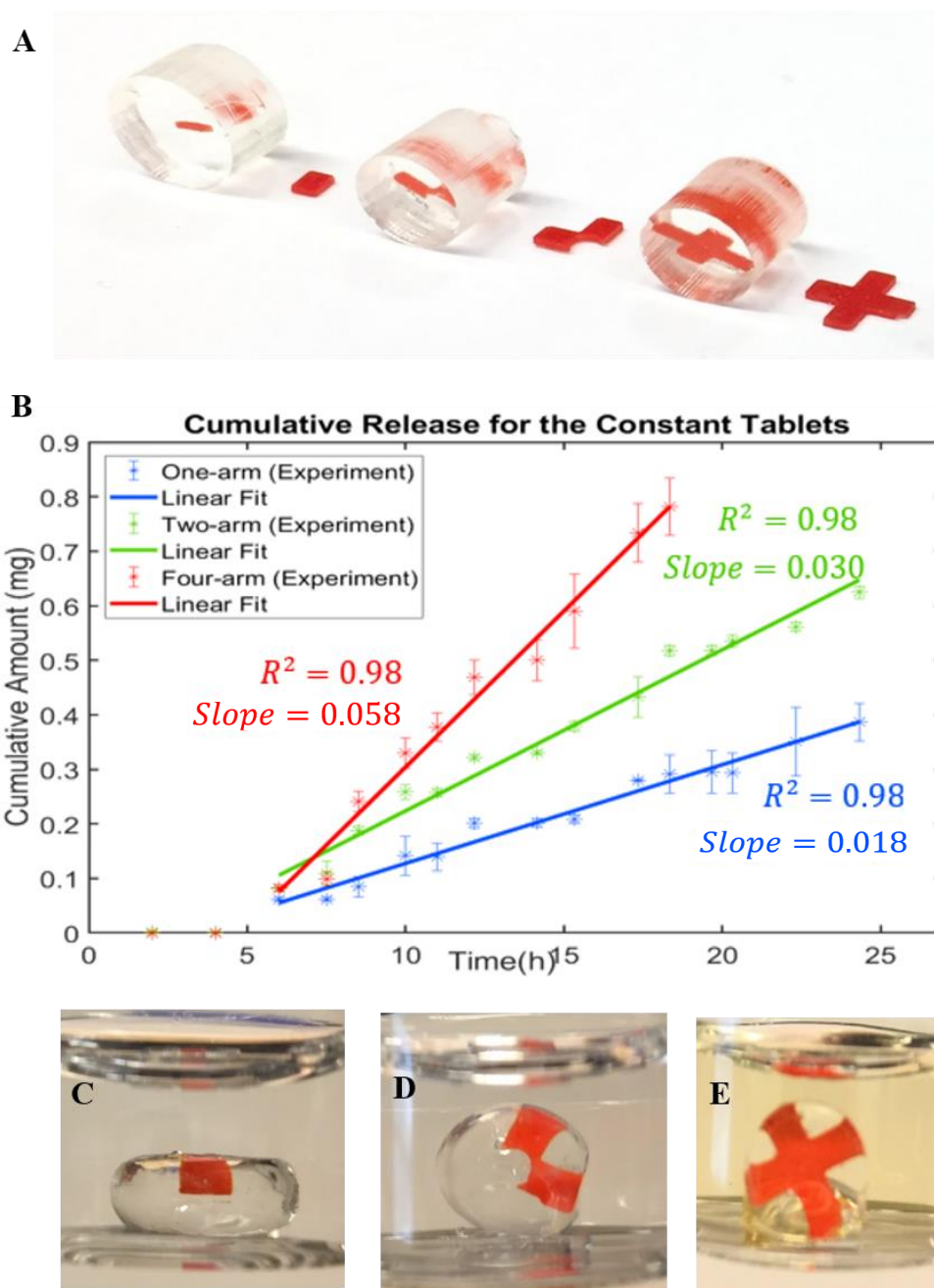
Figure 4-15: Modified core-shell tablet designs to increase the loading capacity of the delivery system. A) Three core-shell tablets, fabricated for constant release profile with one-arm, two-arm, and four-arm cores from left to right, respectively. B) The cumulative amount of the model compound release after the induction period and linear fitted curve to the one-arm (the blue line), two-arm (the green line), and four-arm (the red line) release data. The slopes are showing the constant release rates in mg/hr. The core-shell tablets fabricated for constant release profiles while eroding in PBS for C) one-arm, D) two-arm, E) and four-arm tablets.

References

1. Qin, D., Xia, Y. & Whitesides, G. M. Soft lithography for micro- and nanoscale patterning. *Nat. Protoc.* **5**, 491–502 (2010).

2. McDonald, J. C. *et al.* Prototyping of microfluidic devices in poly(dimethylsiloxane) using solid-object printing. *Anal. Chem.* **74**, 1537–1545 (2002).

3. Leuenberger, H. & Leuenberger, M. N. Impact of the digital revolution on the future of pharmaceutical formulation science. *Eur. J. Pharm. Sci.* **87**, 100–11 (2016).

4. Khatri, P., Katikaneni, P., Desai, D. & Minko, T. Evaluation of Affinisol® HPMC polymers for direct compression process applications. *J. Drug Deliv. Sci. Technol.* **47**, 461–467 (2018).

5. Burkersroda, F. v. & Goepferich, A. M. An Approach to Classify Degradable Polymers. *MRS Proc.* **550**, 17 (1998).

6. Tamada, J. A. & Langer, R. Erosion kinetics of hydrolytically degradable polymers. *Proc. Natl. Acad. Sci. U. S. A.* **90**, 552–556 (1993).

7. Göpferich, A. & Tessmar, J. Polyanhydride degradation and erosion. *Adv. Drug Deliv. Rev.* **54**, 911–31 (2002).

8. Burkersroda, F. Von, Schedl, L. & Göpferich, A. Why degradable polymers undergo surface erosion or bulk erosion. *Biomaterials* **23**, 4221–4231 (2002).

9. Poetz, K. L. *et al.* Photopolymerized cross-linked thiol-ene polyanhydrides: Erosion, release, and toxicity studies. *Biomacromolecules* **15**, 2573–2582 (2014).

10. Jo, B. H., Van Lerberghe, L. M., Motsegood, K. M. & Beebe, D. J. Three-dimensional micro-channel fabrication in polydimethylsiloxane (PDMS) elastomer. *J. Microelectromechanical Syst.* **9**, 76–81 (2000).

11. Duffy, D. C., McDonald, J. C., Schueller, O. J. A. & Whitesides, G. M. Rapid prototyping of microfluidic systems in poly(dimethylsiloxane). *Anal. Chem.* **70**, 4974–4984 (1998).

12. Yoou, M.-S., Cho, S. & Choi, Y. Molecular Docking-assisted Protein Chip Screening of Inhibitors for Bcl-2 Family Protein-protein Interaction to Discover Anticancer Agents by Fragment-based Approach. *BioChip J.* (2019). doi:10.1007/s13206-019-3306-4

13. Khademhosseini, A. *et al.* A soft lithographic approach to fabricate patterned microfluidic channels. *Anal. Chem.* **76**, 3675–3681 (2004).

14. Awad, A., Trenfield, S. J., Goyanes, A., Gaisford, S. & Basit, A. W. Reshaping drug development using 3D printing. *Drug Discovery Today* **23**, 1547–1555 (2018).

15. Siepmann, J., Kranz, H., Peppas, N. A. & Bodmeier, R. Calculation of the required size and shape of hydroxypropyl methylcellulose matrices to achieve desired drug release profiles. *Int. J. Pharm.* **201**, 151–164 (2000).

16. Lin, C. C. & Metters, A. T. Hydrogels in controlled release formulations: Network design and mathematical modeling. *Advanced Drug Delivery Reviews* **58**, 1379–1408 (2006).

17. Siepmann, J., Faisant, N. & Benoit, J. P. A new mathematical model quantifying drug release from bioerodible microparticles using Monte Carlo simulations. *Pharm. Res.* **19**, 1885–1893 (2002).

18. Konar, N. & Kim, C. Water-soluble polycations as oral drug carriers (tablets). *J. Pharm. Sci.* **86**, 1339–44 (1997).

19. Claeys, B. *et al.* Release characteristics of polyurethane tablets containing dicarboxylic acids as release modifiers - a case study with diprophylline. *Int. J. Pharm.* **477**, 244–50 (2014).

20. Claeys, B. *et al.* Thermoplastic polyurethanes for the manufacturing of highly dosed oral sustained release matrices via hot melt extrusion and injection molding. *Eur. J. Pharm. Biopharm.* **90**, 44–52 (2015).

21. Goyanes, A., Robles Martinez, P., Buanz, A., Basit, A. W. & Gaisford, S. Effect of geometry on drug release from 3D printed tablets. *Int. J. Pharm.* **494**, 657–663 (2015).

Chapter 5

5 Conclusions and Future Directions

In this thesis, the mass loss profiles of the thiol-ene polyanhydrides were comprehensively studied, before utilizing them in the fabrication of tablets that were designed to obtain adjustable release profiles. A high-throughput platform for manufacturing the tablets is also presented. This chapter summarizes and highlights the relevance of the thesis and guides future works.

5.1 Conclusions

5.1.1 Chapter 3

The photocrosslinkable thiol-ene polyanhydrides were successfully synthesized as was indicated by the close agreement between the FTIR spectra of the polymers (Appendix A-2) with the previously reported FTIR results for the same polymers. The glass transition temperature values of the synthesized polymers using DSC were in agreement with the values measured by DMA for the same polymers[1].

The impact of the polymer composition on the polymer mass loss profiles (both the induction and the erosion period) was studied by changing the initial mole ratios of the cross-linkers (PETMP to EGDT). Although changing the polymer compositions did not affect the induction period, an increased initial mole ratio of EGDT to PETMP resulted in a shorter total erosion time (Figure 3-3). The reasons behind the changes in the erosion times were investigated. The water contact angles of polymers were decreased for higher EGDT to PETMP ratios. The lower values of the water contact angle indicate the lower relative hydrophobicity of polymers, owing to their less cross-link density[1] (Table 3-2). Results of the PXRD, together with the results of the DSC experiments, illustrated the lack of the crystallinity in the polymer structures (Figure 3-2 and Appendix A-4). The amorphous domains of the polymers ensured that the crystallinity cannot be the reason for the change in the erosion rate. Therefore, the difference in cross-link density, and hence the hydrophobicity of polymers with different EGDT to PETMP ratios was found to be the primary reason for the change in the erosion rates.

The effect of the tablet geometry on mass loss profiles of the polyanhydrides was examined by first comparing the mass loss profiles of small cylindrical tablets with the larger ones made of same polymers. Similar induction periods and erosion patterns were observed for the two tablet geometries (Figure 3-4), indicating that the thiol-ene polyanhydrides maintain their surface erosion behavior even at very small dimensions (e.g., 3mm which is in the range of our tablet cores' size) similar to other types of polyanhydrides[2]. Results show the potential of this type of polyanhydrides to be used in small-size controlled DDSs, in particular for manufacturing mini-tablets for pediatric patients. In another set of experiments, the impact of the surface area, volume, and SA/V ratio on the erosion behavior of the tablets were examined (Figure 3-6 to 3-8). While the induction period was not affected by these parameters, the mass loss percentage for a polymer with a higher surface area and/or a lower volume was shown to be faster. Polymers with the same SA/V ratios showed similar mass loss percentage rates despite their dissimilar volumes and surface areas. The important role of the SA/V ratio in the degradation behavior of tablets made of other biodegradable polymers has been shown before[3,4].

The impact of parameters such as the temperature, pH, and shaking rate of the PBS on the mass loss profile of thiol-ene polyanhydrides was studied. A decrease in the induction period (from 10 hours to 5 hours) was observed in the mass loss profile of the polymers when the temperature was increased (25°C to 37°C). The erosion was considerably faster at higher temperatures (Figure 3 4). The findings are in agreement with other studies showing that the degradation of biodegradable polymers is accelerated at elevated temperatures[5–7]. The induction periods and mass-loss rates were similar for polymers in different pH, except for the one at pH=7.89, which showed a shorter induction period and a faster mass loss rate (Figure 3 9). The increased mass loss rate of the polymer in the alkaline solution is in agreement with results from other studies that showed an acceleration in degradation of biodegradable polymers in more alkaline environments[8,9]. The induction period and mass loss rate of polymers stayed similar at three shaking rates (0, 60, 120 rpm), with a slightly slower erosion rate observed at a static condition (Figure 3-10). These findings indicated the non-significant effect of the shaking rate on mass loss profile of this type of polyanhydrides which is similar to the behavior observed for

another type of polyanhydride with the slightly slower erosion rate in the solution with a lower shaking rate10. Mostly, adding hydrophilic compounds (such as the neutral form of the lidocaine) to the polymers might decrease the cross-link density, which leads to a faster mass loss. Although the dispersion of various amount of lidocaine (1, 2, and 3wt %) in other cross-linked thiol-ene polyanhydrides caused slightly faster mass loss11, dispersion of the 1 wt% model compound (acid orange 10) in the present polyanhydrides did not make a difference in the mass-loss rates of the tablets (Figure 3-11).

The feasibility of eliminating the undesirable induction period (lag time) of thiol-ene polyanhydrides was studied by pre eroding the polymers in PBS. After pre-erosion, i.e. removing the tablets from PBS after the duration of the induction period and keeping them in vacuum for 10 hours, when placed back in PBS polymers started eroding with a similar mass loss rate without any second induction period (Figure 3-12). Elimination of the lag time for a different polyanhydride (PCPM) by pre-erosion process has been reported[12]. The successful elimination of the pre-erosion can be attributed to a decrease in the hydrophobicity of the polymer surface caused by the hydrolysis that occurs when the tablet is in contact with PBS in the pre-erosion period. Overall, temperature was the only parameter that could affect the induction period substantially. The mass-loss rate, however, was influenced by most of the parameters studied, including the polymer composition and geometry as well as the temperature, pH, and shaking rate of the PBS solution during the in vitro experiments.

Chapter 3 also documented data on the mass loss behavior of the cylindrical and cuboid thiol-ene polyanhydrides by fitting their experimental mass loss data to linear, quadratic, and cubic polynomials. Even though a linear mass loss profile is commonly reported for surface eroding polymers[2,13], the mass loss data of the present polymers more closely followed the cubic and quadratic functions (Figure 3-13 and Table 3-3). The geometry of the tablets is the reason behind this non-linear behavior of the mass loss data. Polymers in the form of a slab show a linear mass loss while cubes or cylinders made of the same polymer show more complicated patterns. The release kinetic models fitting was also conducted to further investigate the mass loss profiles of the polymers. With the highest R^2 and the lowest RMSE, the Hopfenberg and Hixson-Crowell models best fitted to the

cylindrical and cubic systems' mass loss data (Table 3-4 and 3-5). These best-fitted models describe the erosion mechanism of the systems rather than the diffusion mechanisms that govern the other kinetic models used for data fitting.

5.1.2   Chapter 4

The surface erosion behavior of the photocrosslinkable polyanhydride was studied in chapter 3 and results demonstrated that it is an appropriate candidate to be used for fabricating drug-loaded tablets. Chapter 4 presented a novel core-shell tablet design in which the core is made of a surface eroding polymer loaded with a drug, while the same polymer without any drug was used for the shell (Figure 4-1). The position of the tablet core inside the shell is such that the core is closest to the top, and far enough from the other sides, ensuring that the release of the drug happens only from the top surface of the tablet. Accordingly, the release profile of the drug is only governed by the variations in the surface area of the drug-loaded core along its height. This design relies on the surface eroding behavior of the polymer to preserve the tablet structure and integrity during the erosion, as well as the similarity of the erosion rate at all sides of the tablet.

The tablet design requires only one type of surface eroding polymer in contrast to other designs that utilized multiple polymers in tablet fabrication. For example, PLA has been used in the form of layers or containers for achieving delayed, sequential, pulsatile, release profiles as well as designs with adjustable release profiles[14–18]. Using multiple polymers for manufacturing the tablets increases the time and complexity of the fabrication process. Besides, the interactions between different polymers used in a DDS can change their properties, and hence their erosion behavior. If not accounted for, this may result in erroneous estimations of the release profile of drug from the DDS. Therefore, in addition to characterizing the erosion behavior of each of the polymers separately before manufacturing the tablet, studies should be conducted on characterizing the erosion behavior of each of the polymers from the multi-polymer DDS after it is manufactured. In addition, some polymers used in the multi-polymer DDSs have slow degradation rates, e.g. PLA that is usually utilized for fabricating containers can take several months to degrade[19,20]. The tablet design developed in this thesis overcomes the aforementioned issues by utilizing only one surface eroding polymer.

The design for achieving adjustable release rates relies on the similarity of the dimension reduction rate of different sides of the tablet, i.e. the independence of the dimension reduction rate from the orientation of the tablet. The diameter and height reduction rates of cylindrical tablets made of thiol-ene polyanhydrides were obtained from mass loss experiments and were found to be linear and very close to each other (Figure 4-9). The linearity of the dimension reduction rates allows for estimating the dimension reduction rate of a new cylindrical design made from the same polymer, without the need for monitoring the tablet dimensions during the entire erosion time.

High-throughput manufacturing is currently a challenge for producing advanced controlled DDSs with adjustable release rates. Most of the studies reported the fabrication of a single tablet in each experiment[18,21–23], reducing the chances of their practical use in clinical settings. Manufacturing each tablet can take a considerable amount of time, and the reproducibility level is low. In this study, a platform for high-throughput manufacturing of the core-shell tablets was developed to provide adjustable release profiles.

Tablet cores were fabricated using a microfluidic network consisting of two PDMS layers manufactured using conventional soft-lithography techniques. To prevent the leakage of the pre-polymer solution from the microfluidic network, two rigid PMMA sheets were used to sandwich the PDMS layers and to apply a uniform force through a screw/nut configuration. The successful injection of the pre-polymer solution via the inlet/outlet ports was achieved (Figure 4-10). To create the tablet shell, PDMS wells were successfully fabricated using 3D printed master molds. Aligners were designed to ensure the right positioning of the micro-fabricated tablet cores in the shell (Figure 4-11). High-resolution tablet shells were fabricated by using DLP 3D printing for producing PDMS wells. DLP was chosen because it can create objects with more complex designs at a higher speed and higher resolutions compared to the other commercially available 3D printers such as FDM machines which are previously used for manufacturing tablets with adjustable release profiles [18,21–23].

Results of the release rates measurements of the tablets designed for constant and the decreasing-increasing release profiles showed the feasibility of achieving tunable patterns of release using the proposed core-shell tablet design (Figure 4-13 and 4-14). Compared to other studies [26–28], the presented method provides a more straightforward translation of the desired release profiles to the tablet design, owing to the linearity of the surface erosion rate observed in these experiments, along with the core-shell tablet design. Unlike other studies [26–28], complex modeling and/or solving of the complicated equations for designing tablets with adjustable release profiles was not required.

By modifying the tablet design and utilizing the extra space in the shell polymer, higher amounts of the model compound was loaded into the tablets without increasing the total volumes of the tablets (

Figure 4-15). The modified design reduces the chances of the UV-induced damage to therapeutics loaded in the tablet. One arm, two-arm, and four-arm designs for the core of the tablets were devised by using the radial directions for erosion. The two- and four-arm tablets preserved the estimated release pattern. The release rate of the four-arm tablet was almost four times higher than the release rate of the one-arm tablet and the slope of the linear cumulative release of the two-arm tablet showed an almost twofold increase when compared to the one-arm tablet. These findings demonstrated that using the four-arm design, it is possible to load (and release) the same amount of the model compound at approximately four-times lower weight percentage compared to the one-arm tablet. This, in turn, decreases the required UV-light energy for cross-linking the tablet cores and hence reducing the chances of the damage to the loaded drugs. Other groups have studied elevation of the loading capacity of controlled DDSs by changing the polymer compositions[29]. Various fabrication techniques such as HME and IM were also used to increase the loading capacity of the polymeric tablets[30–32]. In this study, using the modified tablet designs, the loading capacity of the tablets was increased by approximately four times, in a straightforward fashion.

5.2   Future Directions

To further advance this study, the mass loss measurements can be conducted in PBS solutions with changing pHs over time[33] to mimic the conditions that a solid oral dosage form would experience through the GI tract. In this regard, additional mass loss experiments that are conducted in more physiologically relevant environments can help provide more accurate predictions of the in vitro and ultimately in vivo erosion behavior of these polymers. The release profile studies also need to be conducted for the tablet loaded with an actual drug instead of a model compound.

To reduce the tablet manufacturing time, automation of some steps involved in the fabrication of the tablets is recommended. A graphical user interface was developed that automatically designs the tablets based on the information provided on the desired release pattern (Appendix E-1). Although a pulsatile release profile was shown as a proof of concept, other desired release profiles can be input to this user-friendly platform that outputs the corresponding tablet design. The output of this program can then be utilized for high-throughput fabrication of the tablets with the desired release profiles.

It is noteworthy that the simultaneous fabrication of three tablets (with either constant or decreasing-increasing release profiles) was presented to demonstrate the potential of the proposed method for large-scale production. Testing a design that includes a higher number of simultaneously fabricated tablets is important to further validate the feasibility of the proposed method for mass production. In addition, the design for achieving adjustable release profiles should be used and tested for achieving other clinically relevant and in-demand release profiles. Lastly, to improve the efficiency of the presented delivery system and to further increase the drug loading capacity, other sides of the tablet shell can also be utilized for drug release. A new modified design, together with a modified fabrication technique is required to realize this goal.

References

1. Rutherglen, B. G., McBath, R. A., Huang, Y. L. & Shipp, D. A. Polyanhydride networks from thiol-ene polymerizations. *Macromolecules* (2010). doi:10.1021/ma102287v

2. Burkersroda, F. Von, Schedl, L. & Göpferich, A. Why degradable polymers undergo surface erosion or bulk erosion. *Biomaterials* **23**, 4221–4231 (2002).

3. Martinez, P. R., Goyanes, A., Basit, A. W. & Gaisford, S. Influence of Geometry on the Drug Release Profiles of Stereolithographic (SLA) 3D-Printed Tablets. *AAPS PharmSciTech* **19**, 3355–3361 (2018).

4. Reynolds, T. D., Mitchell, S. A. & Balwinski, K. M. Investigation of the effect of tablet surface area/volume on drug release from hydroxypropylmethylcellulose controlled-release matrix tablets. *Drug Dev. Ind. Pharm.* **28**, 457–66 (2002).

5. Zolnik, B. S., Leary, P. E. & Burgess, D. J. Elevated temperature accelerated release testing of PLGA microspheres. *J. Control. Release* **112**, 293–300 (2006).

6. Aso, Y., Yoshioka, S., Li Wan Po, A. & Terao, T. Effect of temperature on mechanisms of drug release and matrix degradation of poly(d,l-lactide) microspheres. *J. Control. Release* **31**, 33–39 (1994).

7. Ho, K.-L. G., Pometto III, A. L. & Hinz, P. N. (No Title). *J. Polym. Environ.* **7**, 83–92 (1999).

8. Makino, K., Ohshima, H. & Kondo, T. Mechanism of hydrolytic degradation of poly(l-lactide) microcapsules: Effects of ph, ionic strength and buffer concentration. *J. Microencapsul.* **3**, 203–212 (1986).

9. Göpferich, A. Mechanisms of polymer degradation and erosion. *Biomaterials* **17**, 103–114 (1996).

10. Shieh, L., Tamada, J., Chen, I., Pang, J., Domb, A., & Langer, R. Erosion of a new family of biodegradable polyanhydrides. *Journal of biomedical materials research* 28, no. 12 (1994): 1465-1475.

11. Poetz, K. L., Mohammed, H. S. & Shipp, D. A. Surface eroding, semicrystalline polyanhydrides via thiol-ene 'click' photopolymerization. *Biomacromolecules* **16**, 1650–1659 (2015).

12. Rosen, H. B., Chang, J., Wnek, G. E., Linhardt, R. J. & Langer, R. Bioerodible polyanhydrides for controlled drug delivery. *Biomaterials* (1983). doi:10.1016/0142-9612(83)90054-6

13. Göpferich, A. & Tessmar, J. Polyanhydride degradation and erosion. *Adv. Drug Deliv. Rev.* **54**, 911–31 (2002).

14. Abdul, S. & Poddar, S. S. A flexible technology for modified release of drugs: Multi layered tablets. *Journal of Controlled Release* **97**, 393–405 (2004).

15. Stubbe, B. G., De Smedt, S. C. & Demeester, J. 'Programmed polymeric devices' for pulsed drug delivery. *Pharmaceutical Research* **21**, 1732–1740 (2004).

16. Yamakawa, I., Watanab, S., Matsuno, Y., and Kuzuya, M.,. Controlled release of insulin from plasma-irradiated sandwitch device using poly-DL-lactic acid. *Biological and Pharmaceutical Bulletin* 16, no. 2 (1993): 182-187.

17. Efentakis, M., Naseef, H. & Vlachou, M. Two-and three-layer tablet drug delivery systems for oral sustained release of soluble and poorly soluble drugs. *Drug Dev. Ind. Pharm.* **36**, 903–916 (2010).

18. Sun, Y. & Soh, S. Printing Tablets with Fully Customizable Release Profiles for Personalized Medicine. *Adv. Mater.* **27**, 7847–7853 (2015).

19. da Silva, D. *et al.* Biocompatibility, biodegradation and excretion of polylactic acid (PLA) in medical implants and theranostic systems. *Chem. Eng. J.* **340**, 9–14 (2018).

20. Hoüglund, A., Odelius, K. & Albertsson, A. C. Crucial differences in the hydrolytic degradation between industrial polylactide and laboratory-scale poly(L - lactide). *ACS Appl. Mater. Interfaces* **4**, 2788–2793 (2012).

21. Goyanes, A., Robles Martinez, P., Buanz, A., Basit, A. W. & Gaisford, S. Effect of geometry on drug release from 3D printed tablets. *Int. J. Pharm.* **494**, 657–663 (2015).

22. Tagami, T. *et al.* Defined drug release from 3D-printed composite tablets consisting of drug-loaded polyvinylalcohol and a water-soluble or water-insoluble polymer filler. *Int. J. Pharm.* **543**, 361–367 (2018).

23. Chai, X. *et al.* Fused deposition modeling (FDM) 3D printed tablets for intragastric floating delivery of domperidone. *Sci. Rep.* **7**, (2017).

24. Leuenberger, H. & Leuenberger, M. N. Impact of the digital revolution on the future of pharmaceutical formulation science. *Eur. J. Pharm. Sci.* **87**, 100–11 (2016).

25. Khatri, P., Katikaneni, P., Desai, D. & Minko, T. Evaluation of Affinisol® HPMC polymers for direct compression process applications. *J. Drug Deliv. Sci. Technol.* **47**, 461–467 (2018).

26. Siepmann, J., Kranz, H., Peppas, N. A. & Bodmeier, R. Calculation of the required size and shape of hydroxypropyl methylcellulose matrices to achieve desired drug release profiles. *Int. J. Pharm.* **201**, 151–164 (2000).

27. Lin, C. C. & Metters, A. T. Hydrogels in controlled release formulations: Network design and mathematical modeling. *Advanced Drug Delivery Reviews* **58**, 1379–1408 (2006).

28. Siepmann, J., Faisant, N. & Benoit, J. P. A new mathematical model quantifying drug release from bioerodible microparticles using Monte Carlo simulations. *Pharm. Res.* **19**, 1885–1893 (2002).

29. Konar, N. & Kim, C. Water-soluble polycations as oral drug carriers (tablets). *J. Pharm. Sci.* **86**, 1339–44 (1997).

30. Claeys, B. *et al.* Release characteristics of polyurethane tablets containing

dicarboxylic acids as release modifiers - a case study with diprophylline. *Int. J. Pharm.* **477**, 244–50 (2014).

31. Claeys, B. *et al.* Thermoplastic polyurethanes for the manufacturing of highly dosed oral sustained release matrices via hot melt extrusion and injection molding. *Eur. J. Pharm. Biopharm.* **90**, 44–52 (2015).

32. Goyanes, A., Robles Martinez, P., Buanz, A., Basit, A. W. & Gaisford, S. Effect of geometry on drug release from 3D printed tablets. *Int. J. Pharm.* **494**, 657–663 (2015).

33. Fadda, H. M., Merchant, H. A., Arafat, B. T. & Basit, A. W. Physiological bicarbonate buffers: stabilisation and use as dissolution media for modified release systems. *Int. J. Pharm.* **382**, 56–60 (2009).

Appendices

Appendix A: Polymer prepration and characterization.
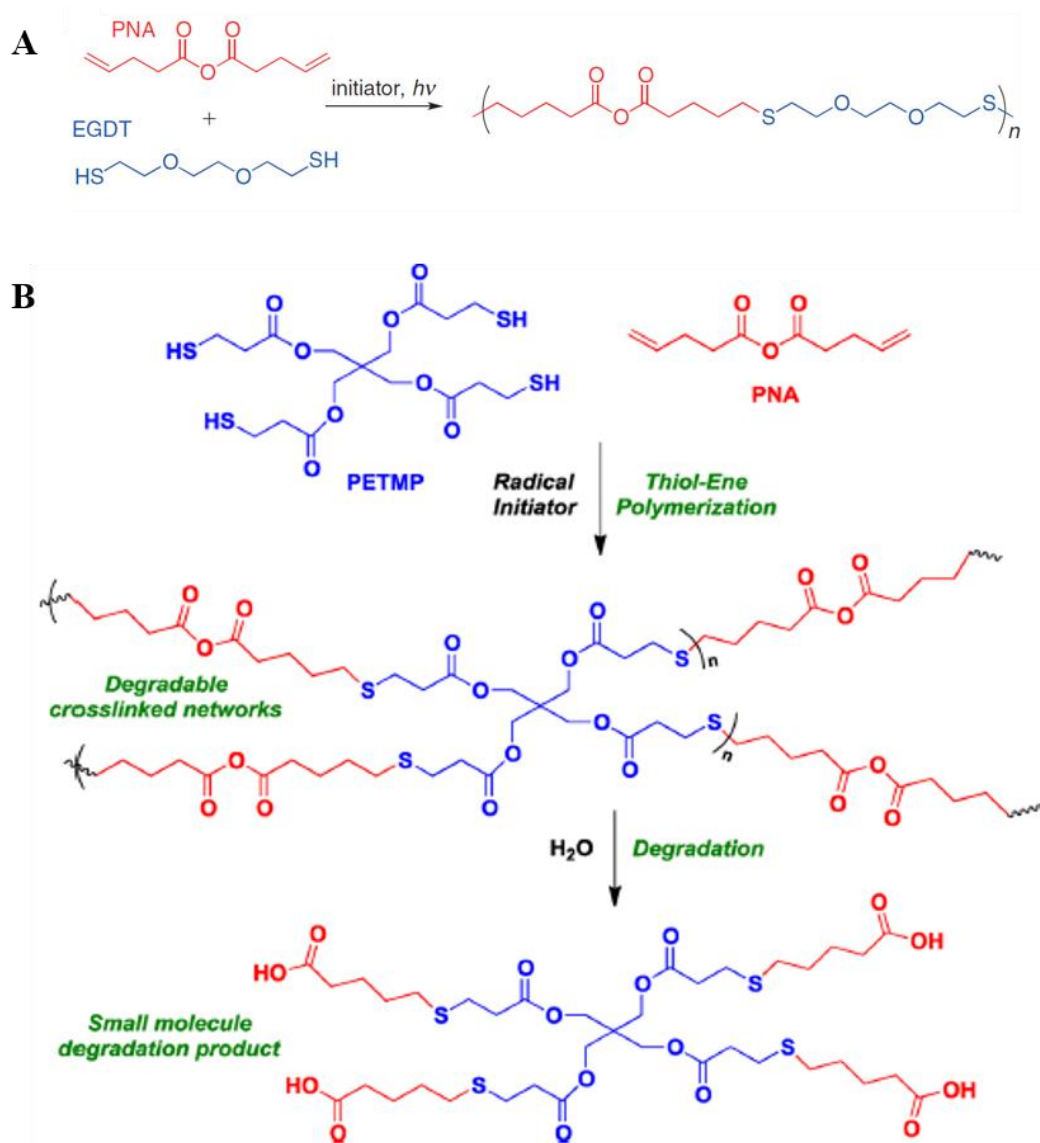
Appendix A-1: Thiol-Ene polymerization process for synthesizing: A) a linear network made of PNA and EGDT. Reproduced from Ref [1] with permission. B) A cross-linked network made of thiol-ene reaction of PNA and PETMP and the following degradation via hydrolysis. One or both of these networks exist in the final polymer structure used in this study. Reproduced from Ref [2] with permission.
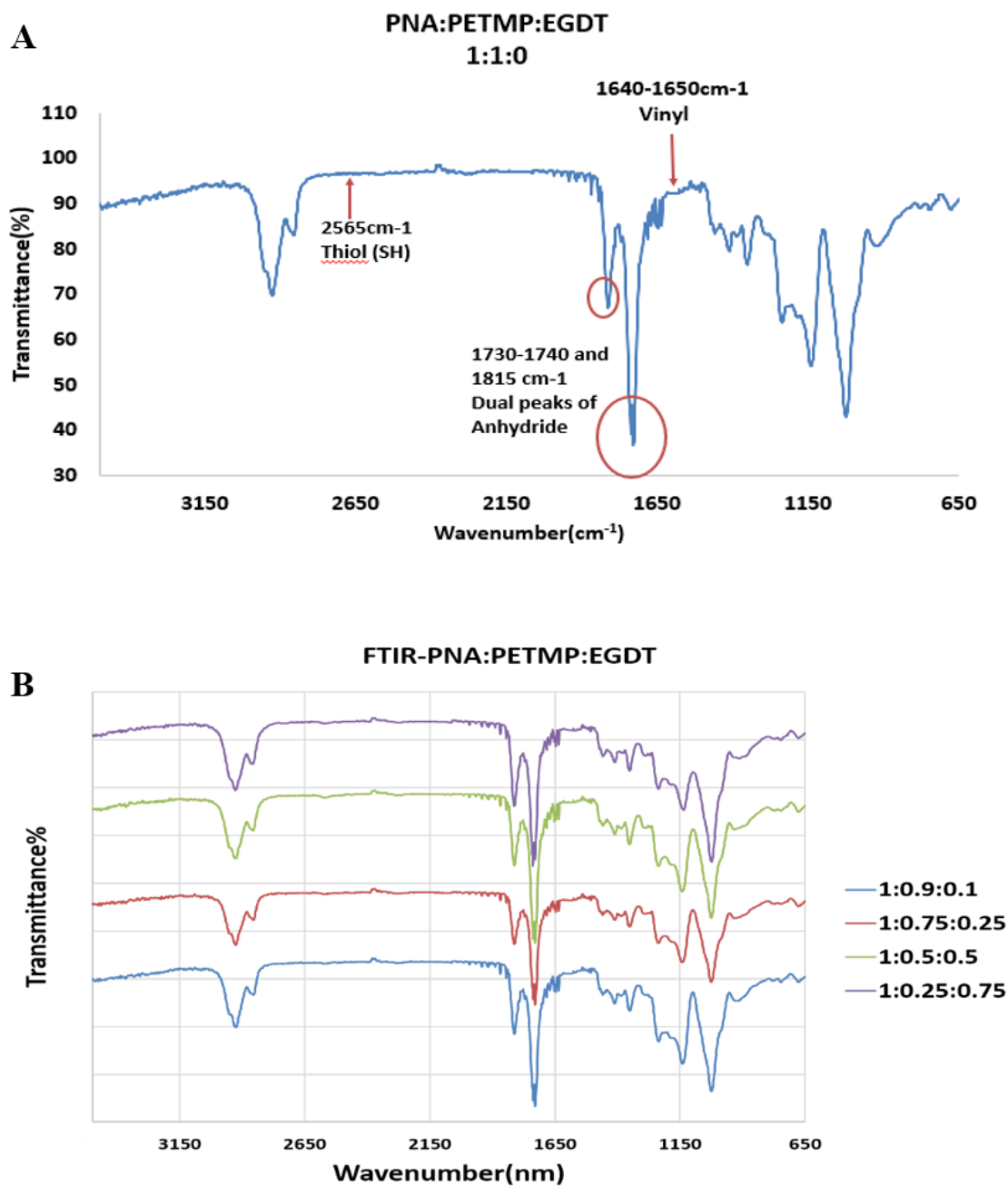
Appendix A-2: ATR-FTIR spectra of A) PNA: PETMP = 1:1 shows the dual peaks of anhydrides and the absence of thiol and vinyl functional groups' peaks similar to Ref [3]. B) The same peaks for other synthesized polyanhydrides with different initial mole ratios of monomers.
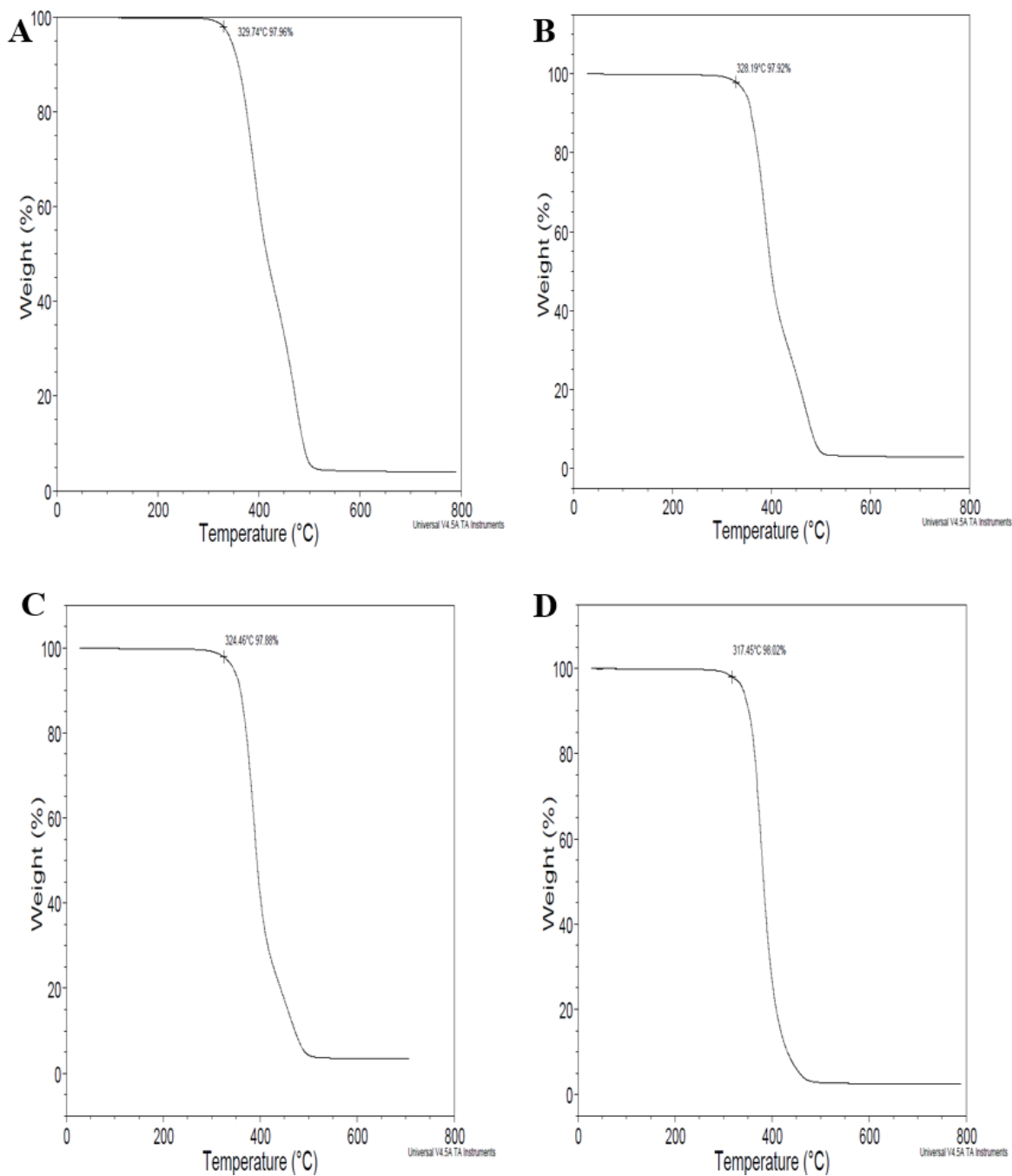
Appendix A-3: TGA traces for four polyanhydrides to check their decomposition temperatures before doing the DSC experiments. Initial mole ratios of monomers used in samples were PNA: PETMP: EGDT= A) 100:100:0. B) 100:75:25. C) 100:50:50. D) and 100:25:75. The decomposition temperatures were seen at 329 °C, 328 °C, 324 °C, and 317 °C respectively.
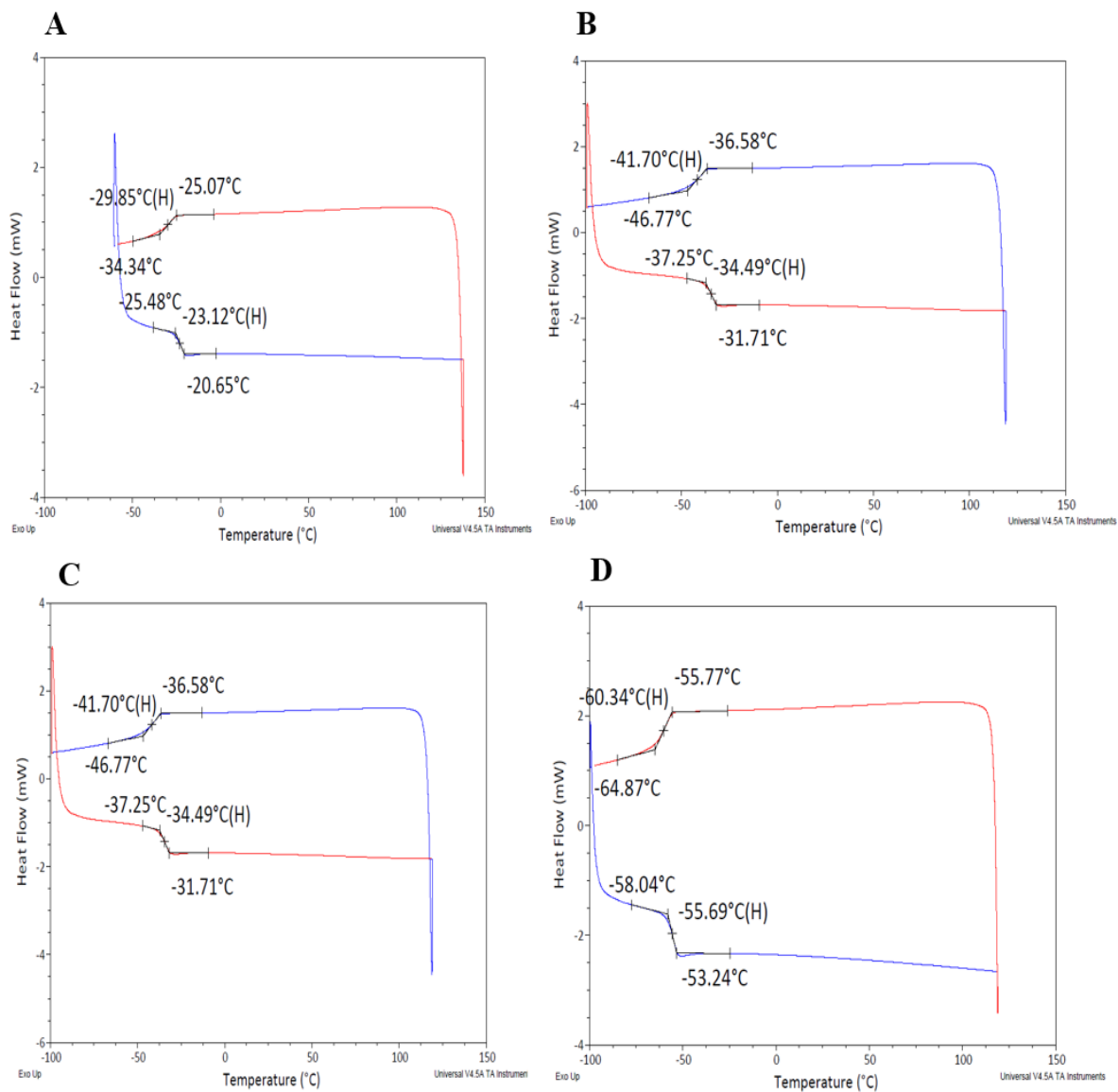
Appendix A-4: DSC of four different polymers with initial mole ratios of PNA: PETMP: EGDT equal to: A) 100:100:0. B) 100:75:25. C) 100:50:50. D) 100:25:75.Tg were specified from the second cycle of heat/cool steps and -25.1°C, -36.6°C, -48.9°C, and -55.8°C respectively.

Appendix B: Mass loss data fitting.
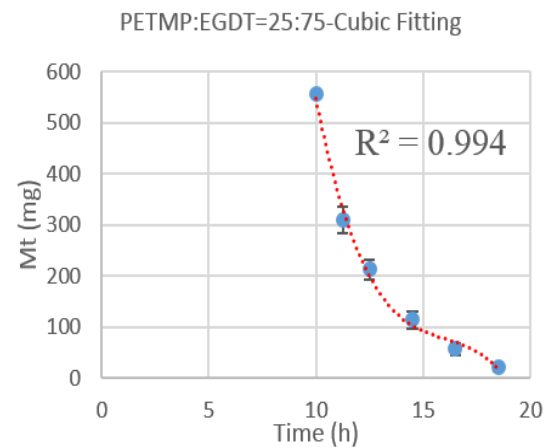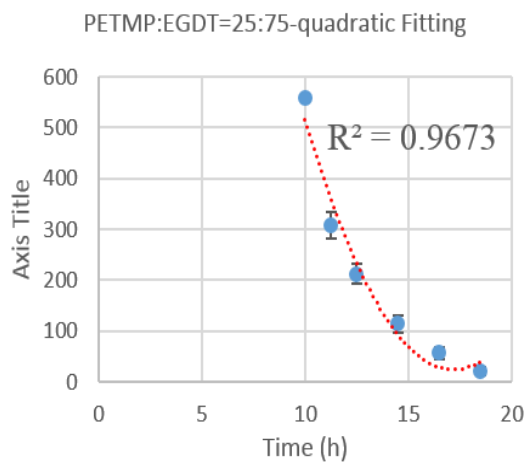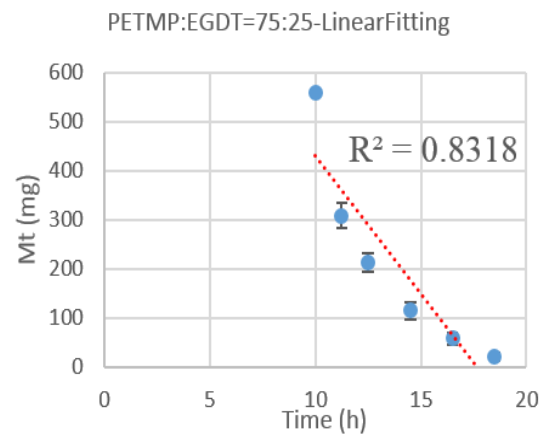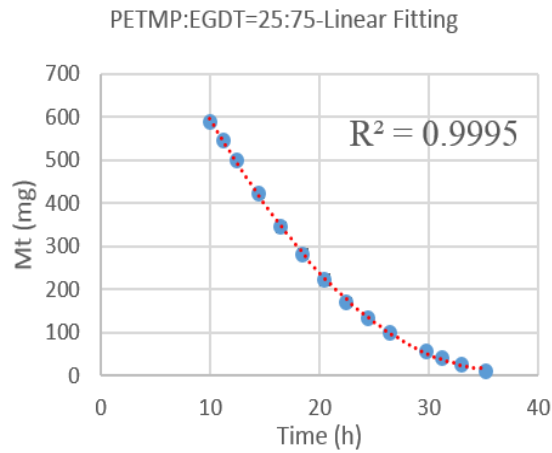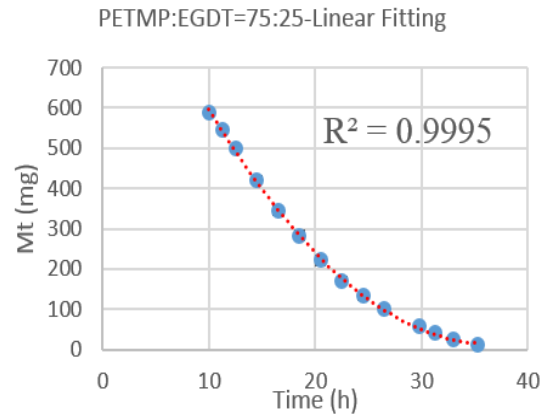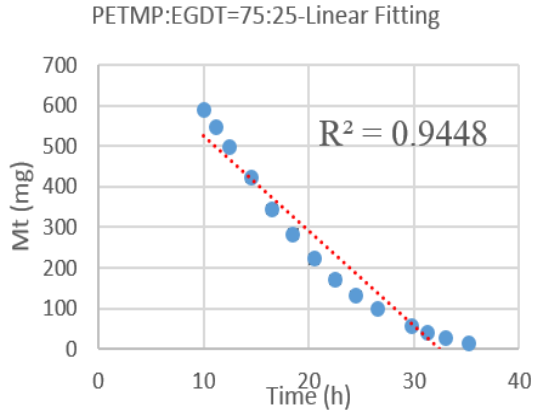
Appendix B-1: Fitting mass loss data for cylindrical polymers. The linear, quadratic, and cubic fitting curves and the R^2 is written in graphs.
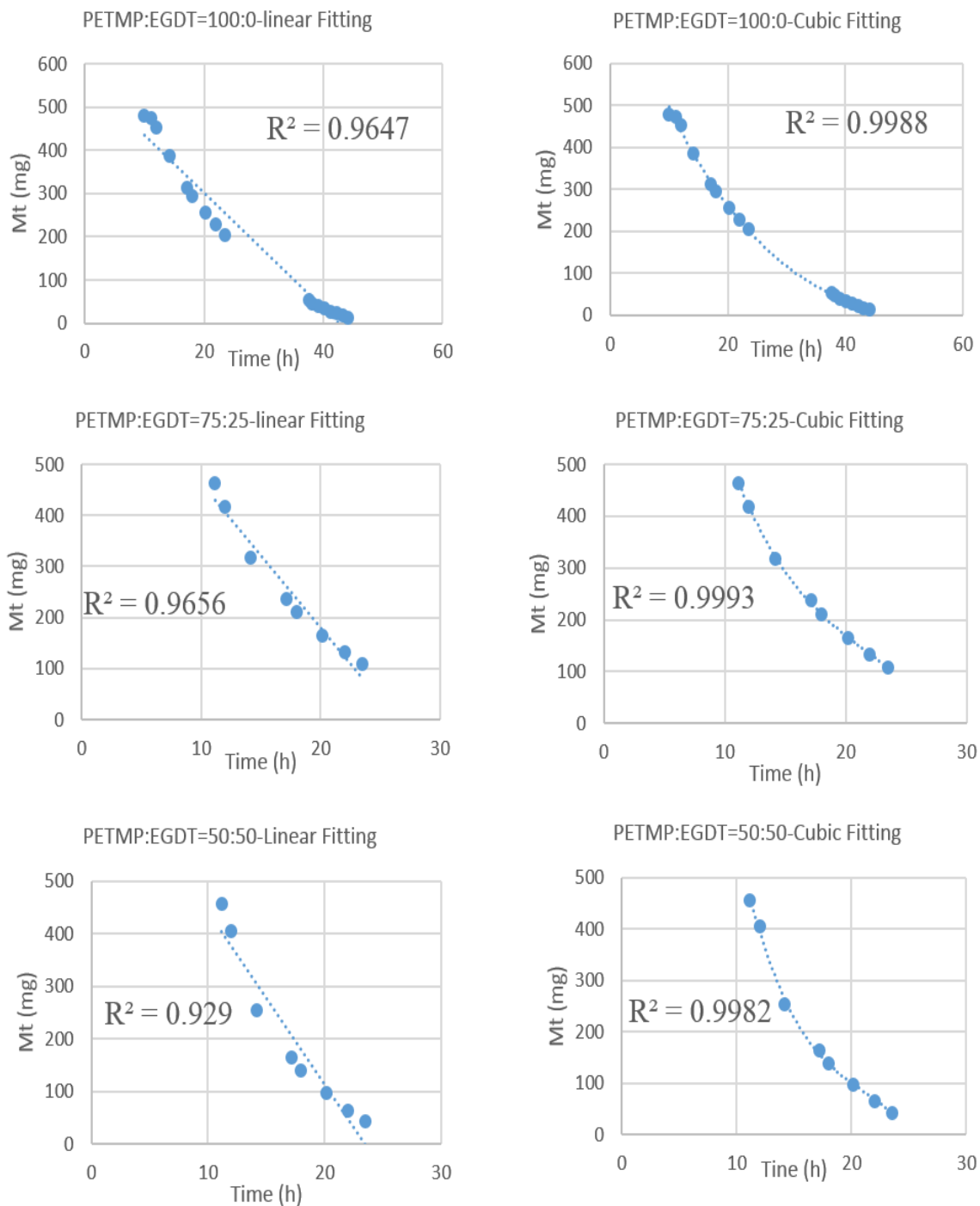
Appendix B-2: Fitting mass loss data for cuboid polymers. The linear, quadratic, and cubic fitting curves and the R^2 is written in graphs.

Appendix C: Release kinetic models fitting.
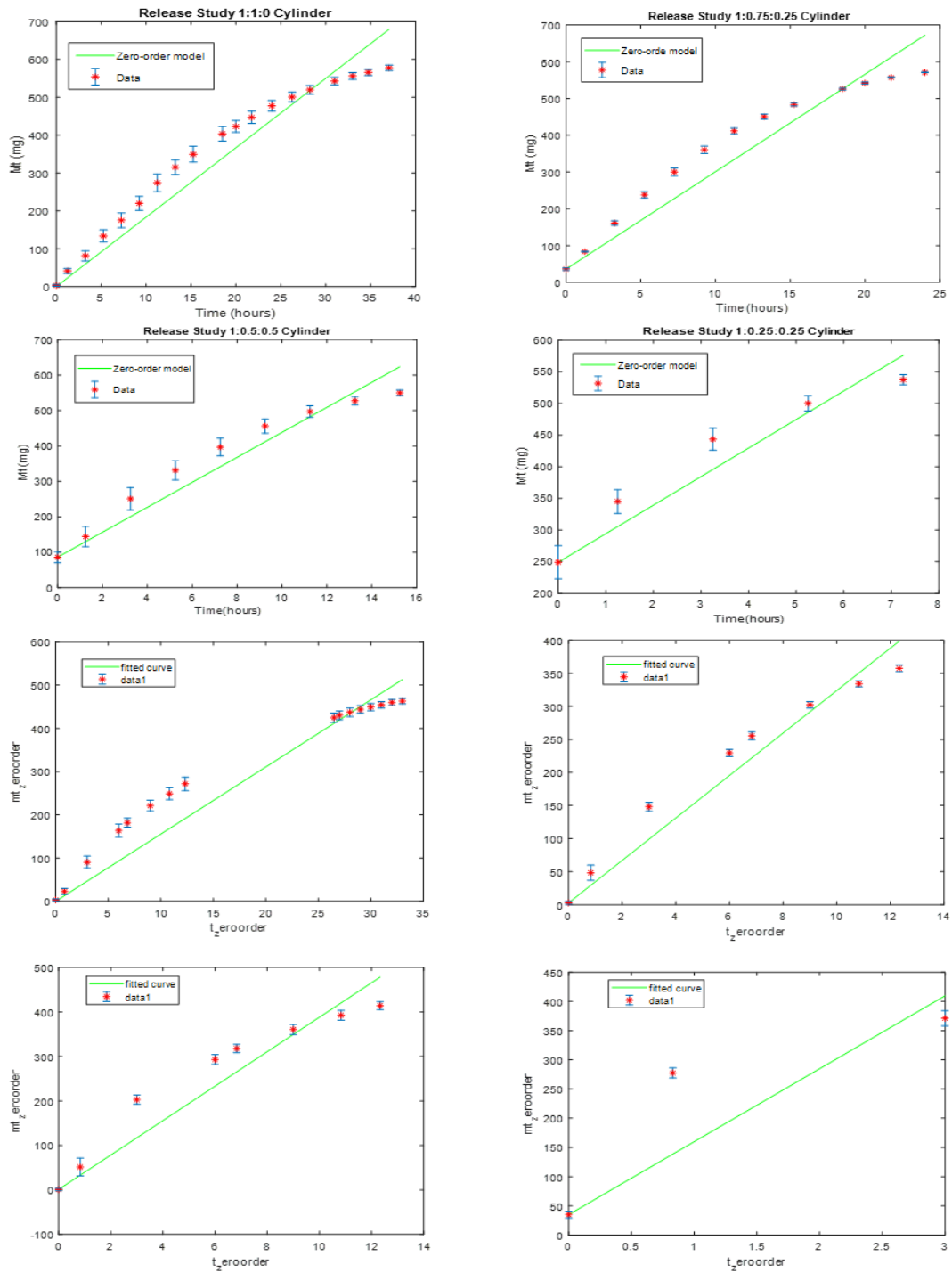
Appendix C-1: Fitting mass loss data to the zero-order kinetic model for cylindrical and cuboid polymers.
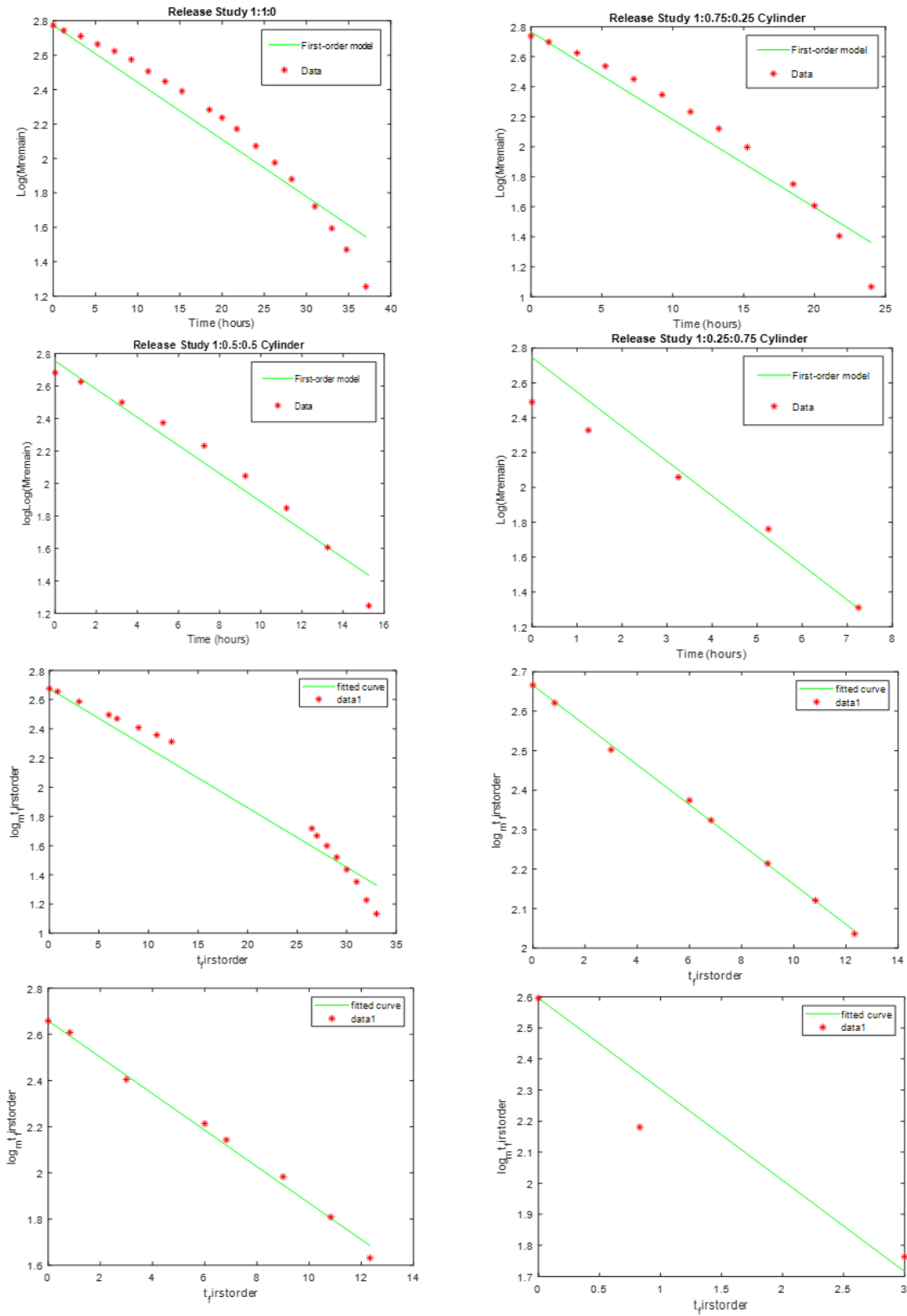
Appendix C-2: Fitting mass loss data to the First-order kinetic model for cylindrical and cuboid polymers.
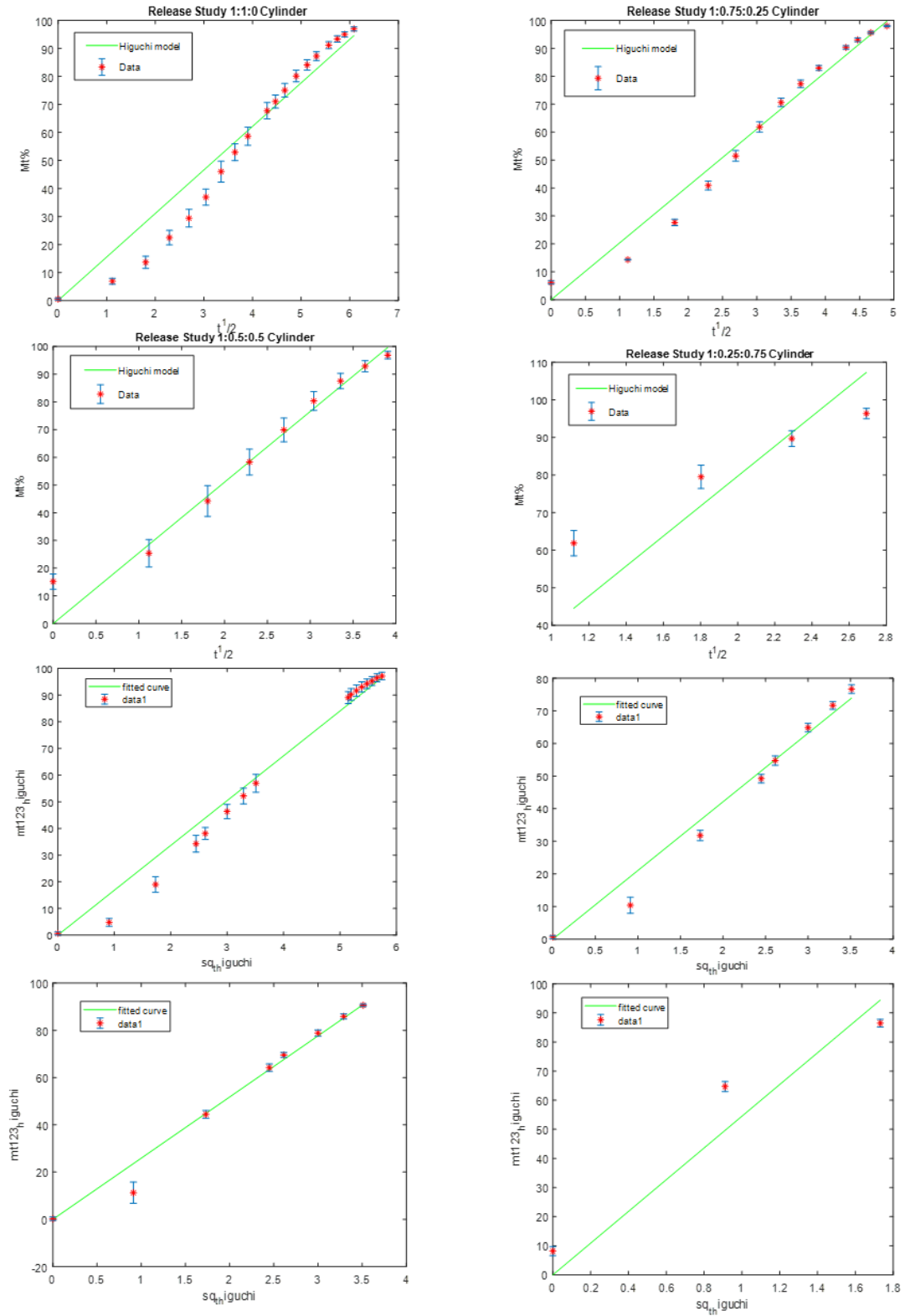
Appendix C-3: Fitting mass loss data to the Higuchi kinetic model for cylindrical and cuboid polymers.
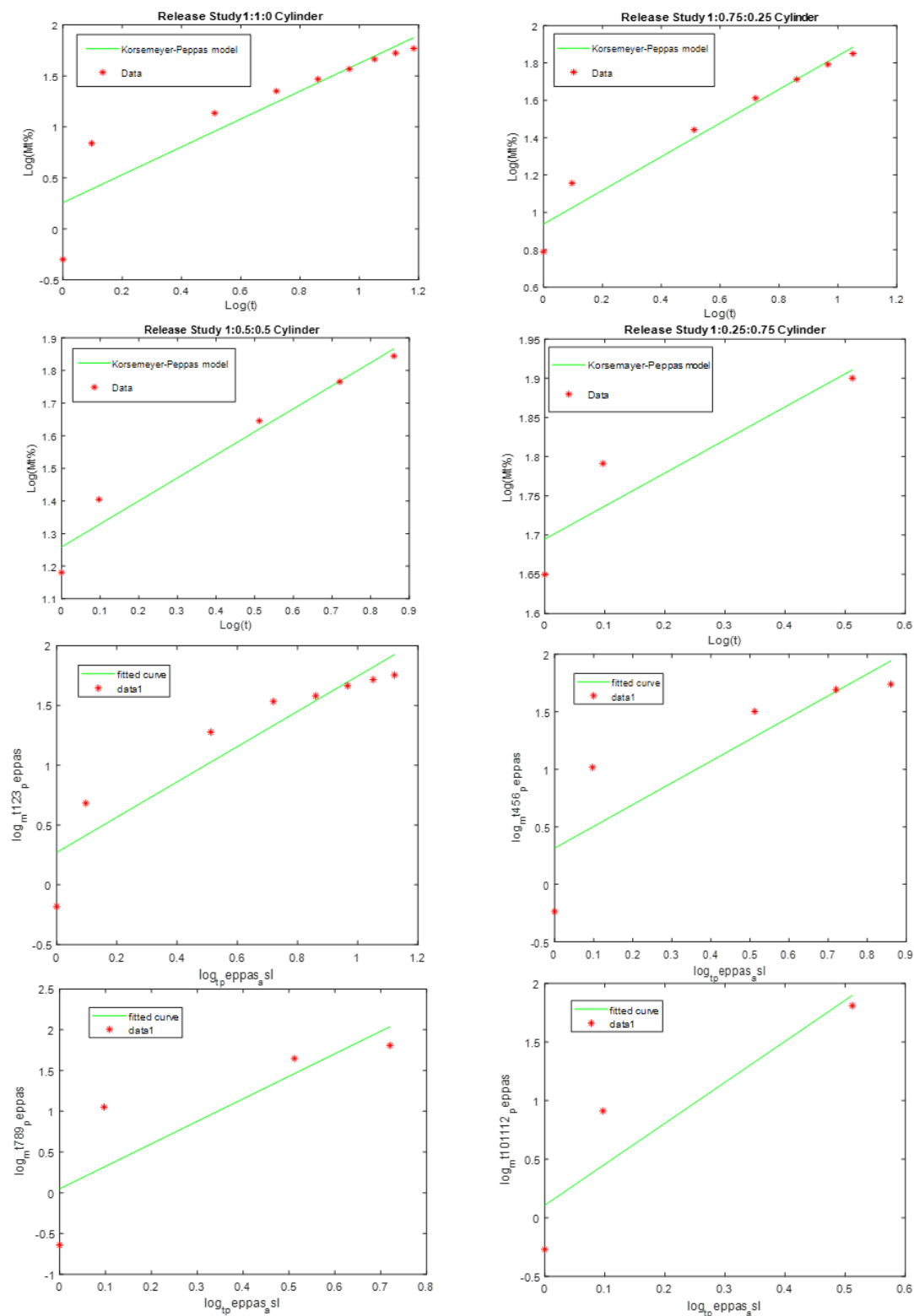
Appendix C-4: Fitting mass loss data to the Korsmeyer-Peppas kinetic model for cylindrical and cuboid polymers**.**
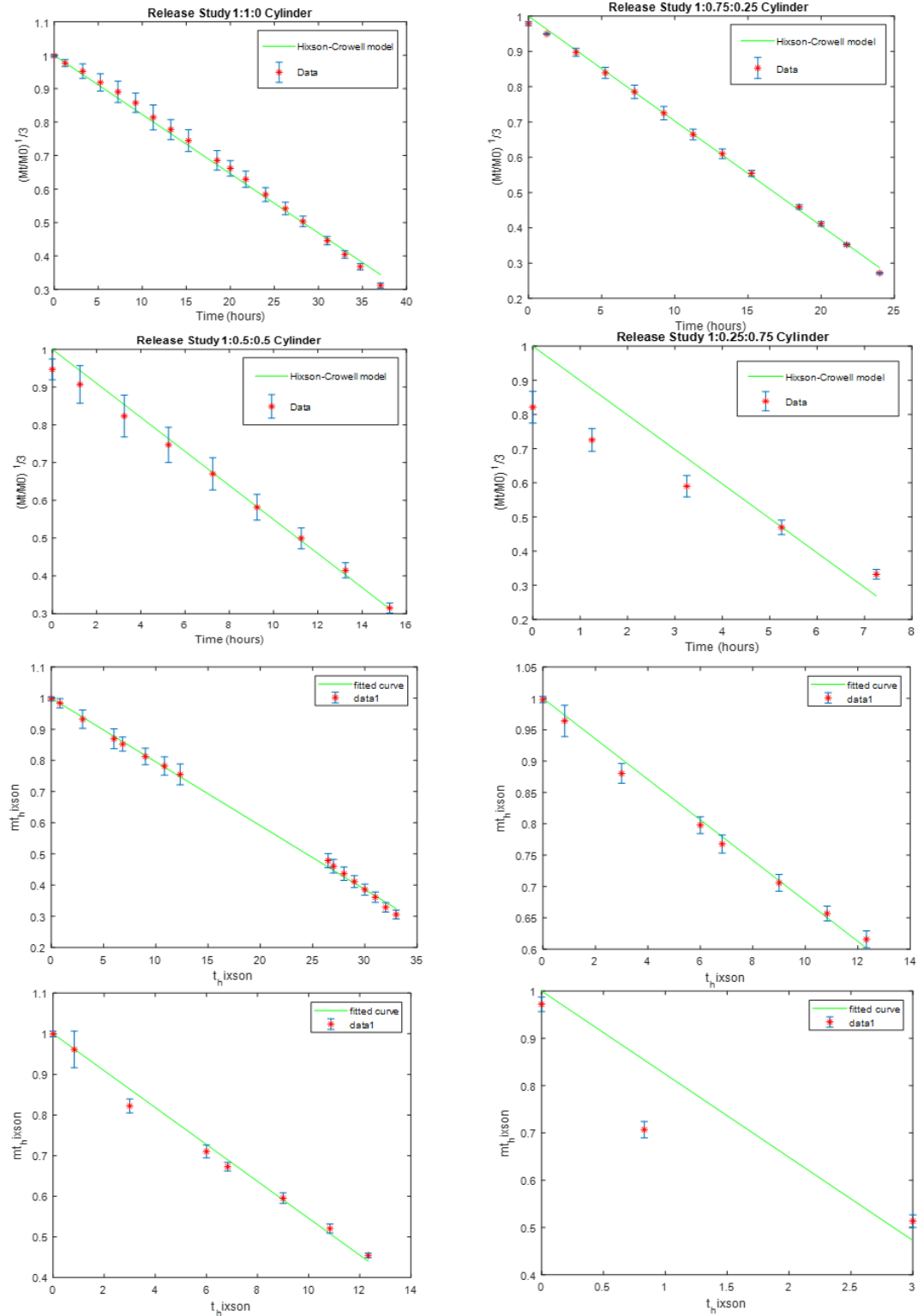
Appendix C-5: Fitting mass loss data to the Hixson-Crowell kinetic model for cylindrical and cuboid polymers.

Appendix D: Model compound (Orange G) absorbance-concentration calibration curve.
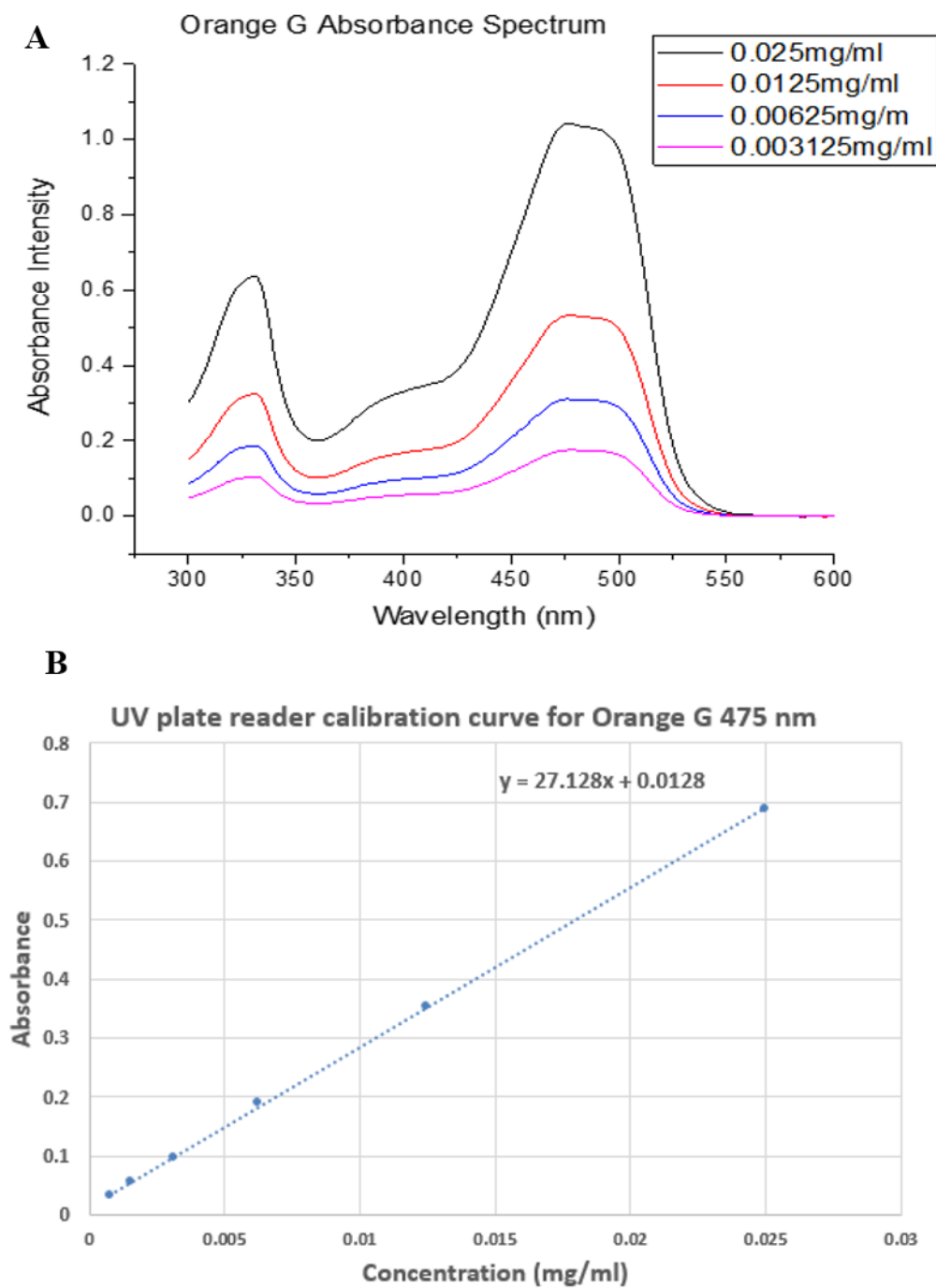
Appendix D-1: Calculation of the model compound (orange G) concentration. A) Finding the wavelength that has the maximum absorbance intensity for OG solutions with known concentrations. B) Concentration-absorbance calibration curve for OG at 475nm (maximum absorbance) for the micro-plate reader.

Appendix E: **Automated Tablet design**

The use of bio-erodible polymers simplifies the automation of the tablet design. This is due to the decreased calculation complexity required for determining the drug release profiles from these polymers. In this study, a graphical user interface (GUI) was created using the Python programming language for automatically designing the patient-specific erodible tablets via a user-friendly platform without the need for an expert designer. The required dosage (concentration) of the drug during the course of treatment, i.e., the desired release profile of drugs, is determined based on the diagnosis of the physicians (Appendix E-1A). The thickness of the tablet core (which is 600 μm, in this case) and reduction rates of the polymers which were measured in section 4.2.1 were entered as inputs. The weight percentage of the drug dispersed in the polymer was also determined in the visual indicator (Appendix E-1B). The 2D design of the tablet core is automatically generated based on the desired release profile that was input to the user interface program. (Appendix E-1D).

For instance, we assume a pulsatile release profile with three peaks over the treatment time is requested by the user (the physician). In the tablet design, the drug release profile is only dependent on the surface area of the tablet core from the top surface along its height. Accordingly, the code calculates the height of the tablet core based on the user-defined inputs such as the total release time, and the polymer- and design-specific variables (e.g. the linear reduction rates of polymers and the amount of drug can be dispersed in the polymer). After plotting the 2D tablet core design, the cumulative drug release is calculated and plotted (Figure 4-9C). Finally, the 3D tablet designs are created in the code by adding the third dimension to the 2D pattern. This thickness is an input to the program (Appendix E-1E).

The 2D tablet core design provided by the user interface program is transferred to the AutoCAD software and is attached to the previously designed connected network (Appendix E-1F, G). The automation process for designing the tablet core was successfully conducted for a pulsatile release profile. The inputs required in this GUI can either be obtained from the previously conducted experiments or from the results of a

modeling study. This automation process eliminates the need for manual calculation and design for each patient.
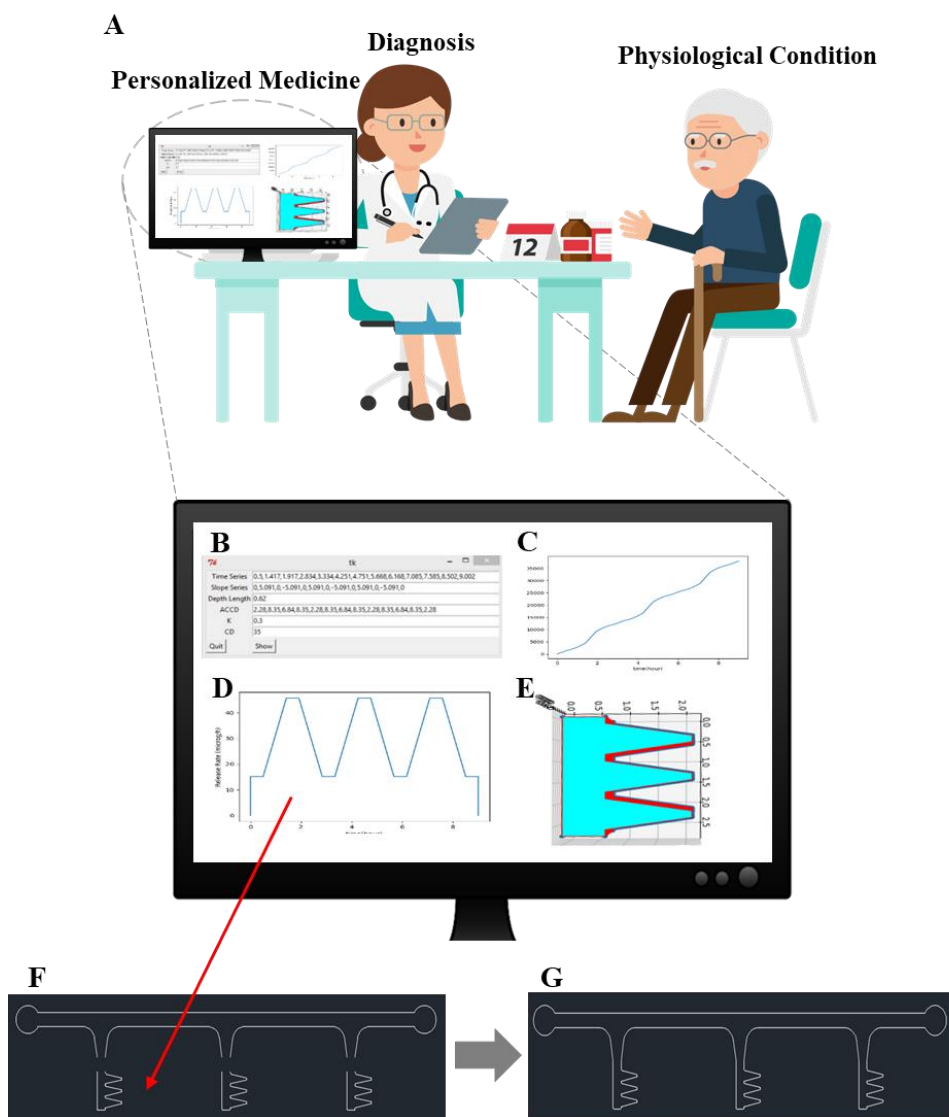
Appendix E-1: Automation of the tablet designs. A) Importance of the personalized medicine and automated designing tablets based on the patient's physiological conditions. "Doctor with Patient Cartoon.svg from Wikimedia Commons by Videoplasty.com, CC-BY-SA 4.0". B) The graphical user interface for designing the patient-specific tablets with specific release rates. C) Cumulative drug release calculated by the program. D) The 2D tablet core designed using the GUI. E) 3D tablet designed using the GUI. F) Transferred 2D tablet core designs to AutoCAD. G) Attachment of the tablet core designs to the connecting network to create the high-throughput tablet core designs.

Appendix F: **Copyright Permissions**

<table>
<tr><td>

ELSEVIER LICENSE
TERMS AND CONDITIONS

Nov 17, 2019

This Agreement between Armin Geraili Nejadfomeshi ("You") and Elsevier ("Elsevier") consists of your license details and the terms and conditions provided by Elsevier and Copyright Clearance Center.

License Number	4707350310823
License date	Nov 13, 2019
Licensed Content Publisher	Elsevier
Licensed Content Publication	Advanced Drug Delivery Reviews
Licensed Content Title	Chronobiology, drug delivery, and chronotherapeutics
Licensed Content Author	Michael H. Smolensky,Nicholas A. Peppas
Licensed Content Date	Aug 31, 2007
Licensed Content Volume	59
Licensed Content Issue	9-10
Licensed Content Pages	24
Start Page	828
End Page	851
Type of Use	reuse in a thesis/dissertation
Portion	figures/tables/illustrations
Number of figures/tables/illustrations	1
Format	both print and electronic
Are you the author of this Elsevier article?	No
Will you be translating?	No
Title	High-throughput Fabrication of Drug-loaded Core-shell Tablets with Adjustable Release Profiles from Surface-erodible and Photocrosslinkable Polyanhydrides
Institution name	Western University
Expected presentation date	Sep 2020
Portions	Fig. 1
	Armin Geraili Nejadfomeshi

</td><td>

SPRINGER NATURE LICENSE
TERMS AND CONDITIONS

Nov 17, 2019

This Agreement between Armin Geraili Nejadfomeshi ("You") and Springer Nature ("Springer Nature") consists of your license details and the terms and conditions provided by Springer Nature and Copyright Clearance Center.

License Number	4707350888176
License date	Nov 13, 2019
Licensed Content Publisher	Springer Nature
Licensed Content Publication	Nature Reviews Microbiology
Licensed Content Title	Microfabrication meets microbiology
Licensed Content Author	Douglas B. Weibel et al
Licensed Content Date	Mar 1, 2007
Type of Use	Thesis/Dissertation
Requestor type	academic/university or research institute
Format	print and electronic
Portion	figures/tables/illustrations
Number of figures/tables/illustrations	1
High-res required	no
Will you be translating?	no
Circulation/distribution	1 - 29
Author of this Springer Nature content	no
Title	High-throughput Fabrication of Drug-loaded Core-shell Tablets with Adjustable Release Profiles from Surface-erodible and Photocrosslinkable Polyanhydrides
Institution name	Western University
Expected presentation date	Sep 2020
Portions	Figure 1
	Armin Geraili Nejadfomeshi

</td></tr>
</table>

ACS Publications
Most Trusted. Most Cited. Most Read.

Photopolymerized Cross-Linked Thiol–Ene Polyanhydrides: Erosion, Release, and Toxicity Studies

Author: Katie L. Poetz, Halimatu S. Mohammed, Brittany L. Snyder, et al
Publication: Biomacromolecules
Publisher: American Chemical Society
Date: Jul 1, 2014

Copyright © 2014, American Chemical Society

PERMISSION/LICENSE IS GRANTED FOR YOUR ORDER AT NO CHARGE

This type of permission/license, instead of the standard Terms & Conditions, is sent to you because no fee is being charged for your order. Please note the following:

- Permission is granted for your request in both print and electronic formats, and translations.
- If figures and/or tables were requested, they may be adapted or used in part.
- Please print this page for your records and send a copy of it to your publisher/graduate school.
- Appropriate credit for the requested material should be given as follows: "Reprinted (adapted) with permission from (COMPLETE REFERENCE CITATION). Copyright (YEAR) American Chemical Society." Insert appropriate information in place of the capitalized words.
- One-time permission is granted only for the use specified in your request. No additional uses are granted (such as derivative works or other editions). For any other uses, please submit a new request. If credit is given to another source for the material you requested, permission must be obtained from that source.

BACK   CLOSE WINDOW

ACS Publications
Most Trusted. Most Cited. Most Read.

Degradable Controlled-Release Polymers and Polymeric Nanoparticles: Mechanisms of Controlling Drug Release

Author: Nazila Kamaly, Basit Yameen, Jun Wu, et al
Publication: Chemical Reviews
Publisher: American Chemical Society
Date: Feb 1, 2016

Copyright © 2016, American Chemical Society

PERMISSION/LICENSE IS GRANTED FOR YOUR ORDER AT NO CHARGE

This type of permission/license, instead of the standard Terms & Conditions, is sent to you because no fee is being charged for your order. Please note the following:

- Permission is granted for your request in both print and electronic formats, and translations.
- If figures and/or tables were requested, they may be adapted or used in part.
- Please print this page for your records and send a copy of it to your publisher/graduate school.
- Appropriate credit for the requested material should be given as follows: "Reprinted (adapted) with permission from (COMPLETE REFERENCE CITATION). Copyright (YEAR) American Chemical Society." Insert appropriate information in place of the capitalized words.
- One-time permission is granted only for the use specified in your request. No additional uses are granted (such as derivative works or other editions). For any other uses, please submit a new request. If credit is given to another source for the material you requested, permission must be obtained from that source.

BACK   CLOSE WINDOW

ELSEVIER LICENSE
TERMS AND CONDITIONS

Nov 17, 2019

This Agreement between Armin Geraili Nejadfomeshi ("You") and Elsevier ("Elsevier") consists of your license details and the terms and conditions provided by Elsevier and Copyright Clearance Center.

License Number	4707360551722
License date	Nov 13, 2019
Licensed Content Publisher	Elsevier
Licensed Content Publication	Journal of Controlled Release
Licensed Content Title	Oral dosage forms fabricated by Three Dimensional Printing™
Licensed Content Author	W.E Katstra,R.D Palazzolo,C.W Rowe,B Giritlioglu,P Teung,M.J Cima
Licensed Content Date	3 May 2000
Licensed Content Volume	66
Licensed Content Issue	1
Licensed Content Pages	9
Start Page	1
End Page	9
Type of Use	reuse in a thesis/dissertation
Portion	figures/tables/illustrations
Number of figures/tables/illustrations	1
Format	both print and electronic
Are you the author of this Elsevier article?	No
Will you be translating?	No
Title	High-throughput Fabrication of Drug-loaded Core-shell Tablets with Adjustable Release Profiles from Surface-erodible and Photocrosslinkable Polyanhydrides
Institution name	Western University
Expected presentation date	Sep 2020
Portions	Fig. 1

Armin Geraili Nejadfomeshi

ELSEVIER LICENSE
TERMS AND CONDITIONS

Nov 17, 2019

This Agreement between Armin Geraili Nejadfomeshi ("You") and Elsevier ("Elsevier") consists of your license details and the terms and conditions provided by Elsevier and Copyright Clearance Center.

License Number	4707360835327
License date	Nov 13, 2019
Licensed Content Publisher	Elsevier
Licensed Content Publication	Journal of Controlled Release
Licensed Content Title	Multimechanism oral dosage forms fabricated by three dimensional printing™
Licensed Content Author	C.W Rowe,W.E Katstra,R.D Palazzolo,B Giritlioglu,P Teung,M.J Cima
Licensed Content Date	3 May 2000
Licensed Content Volume	66
Licensed Content Issue	1
Licensed Content Pages	7
Start Page	11
End Page	17
Type of Use	reuse in a thesis/dissertation
Portion	figures/tables/illustrations
Number of figures/tables/illustrations	4
Format	both print and electronic
Are you the author of this Elsevier article?	No
Will you be translating?	No
Title	High-throughput Fabrication of Drug-loaded Core-shell Tablets with Adjustable Release Profiles from Surface-erodible and Photocrosslinkable Polyanhydrides
Institution name	Western University
Expected presentation date	Sep 2020
Portions	Fig.1, Fig. 2, Fig. 3, Fig. 5

Armin Geraili Nejadfomeshi

ELSEVIER LICENSE
TERMS AND CONDITIONS

Nov 17, 2019

This Agreement between Armin Geraili Nejadfomeshi ("You") and Elsevier ("Elsevier") consists of your license details and the terms and conditions provided by Elsevier and Copyright Clearance Center.

License Number	4707370412359
License date	Nov 13, 2019
Licensed Content Publisher	Elsevier
Licensed Content Publication	International Journal of Pharmaceutics
Licensed Content Title	Stereolithographic (SLA) 3D printing of oral modified-release dosage forms
Licensed Content Author	Jie Wang,Alvaro Goyanes,Simon Gaisford,Abdul W. Basit
Licensed Content Date	Apr 30, 2016
Licensed Content Volume	503
Licensed Content Issue	1-2
Licensed Content Pages	6
Start Page	207
End Page	212
Type of Use	reuse in a thesis/dissertation
Portion	figures/tables/illustrations
Number of figures/tables/illustrations	2
Format	both print and electronic
Are you the author of this Elsevier article?	No
Will you be translating?	No
Title	High-throughput Fabrication of Drug-loaded Core-shell Tablets with Adjustable Release Profiles from Surface-erodible and Photocrosslinkable Polyanhydrides
Institution name	Western University
Expected presentation date	Sep 2020
Portions	Figure 1, Figure 4

Armin Geraili Nejadfomeshi

SPRINGER NATURE LICENSE
TERMS AND CONDITIONS

Nov 17, 2019

This Agreement between Armin Geraili Nejadfomeshi ("You") and Springer Nature ("Springer Nature") consists of your license details and the terms and conditions provided by Springer Nature and Copyright Clearance Center.

License Number	4707750507426
License date	Nov 14, 2019
Licensed Content Publisher	Springer Nature
Licensed Content Publication	Nature Materials
Licensed Content Title	Supramolecular materials: Longer and safer gastric residence
Licensed Content Author	Vitaliy V. Khutoryanskiy
Licensed Content Date	Sep 23, 2015
Licensed Content Volume	14
Licensed Content Issue	10
Type of Use	Thesis/Dissertation
Requestor type	academic/university or research institute
Format	print and electronic
Portion	figures/tables/illustrations
Number of figures/tables/illustrations	1
High-res required	no
Will you be translating?	no
Circulation/distribution	1 - 29
Author of this Springer Nature content	no
Title	High-throughput Fabrication of Drug-loaded Core-shell Tablets with Adjustable Release Profiles from Surface-erodible and Photocrosslinkable Polyanhydrides
Institution name	Western University
Expected presentation date	Sep 2020
Portions	Figure 1

Armin Geraili Nejadfomeshi

References

1.   Durham, O. Z., Poetz, K. L. & Shipp, D. A. Polyanhydride Nanoparticles: Thiol-Ene 'Click' Polymerizations Provide Functionalized and Cross-Linkable Nanoparticles with Tuneable Degradation Times. *Aust. J. Chem.* **70**, 735–742 (2017).

2.   Poetz, K. L. *et al.* Photopolymerized cross-linked thiol-ene polyanhydrides: Erosion, release, and toxicity studies. *Biomacromolecules* **15**, 2573–2582 (2014).

3.   Rutherglen, B. G., McBath, R. A., Huang, Y. L. & Shipp, D. A. Polyanhydride networks from thiol-ene polymerizations. *Macromolecules* (2010). doi:10.1021/ma102287v

Curriculum Vitae

Name:	Armin Geraili Nejadfomeshi
Post-secondary Education and Degrees:	Sharif University of Technology Tehran, Iran 2012-2017 B.Sc. (Chemical Engineering) The University of Western Ontario London, Ontario, Canada 2017-2019 M.Sc. (Biomedical Engineering)
Honours and Awards:	Western Graduate Research Scholarship Western University, London, ON, Canada 2017-2019 Merit & Travel award for best scored abstract at CBS conference Quebec City, Canada Summer 2018 Exceptional Talents Scholarship of Iran Tehran, Iran 2012-2017 Fellowship of National Elite Foundation of Iran Tehran, Iran 2012-2017
Related Work Experience	Teaching Assistant The University of Western Ontario 2017-2019 Intern at BioMEMS and Bioinspired Microfluidic Laboratory University of Calgary Summer 2018 Teaching Assistant Sharif University of Technology 2016-2017 Intern at Institute for Nanoscience and Nanotechnology Sharif University of Technology Summer 2016

Publications:

Geraili, A., Jafari, P., Hassani, M.S., Araghi, B.H., Mohammadi, M.H., Ghafari, A.M., Tamrin, S.H., Modarres, H.P., Kolahchi, A.R., Ahadian, S. and Sanati-Nezhad, A. (2017) "Controlling Differentiation of Stem Cells for Developing Personalized Organ-on-Chip Platforms." *Advanced Healthcare Materials* 5(19) pp. 2459-2480.

Rezaei Kolahchi, A., Khadem Mohtaram, N., Pezeshgi Modarres, H., Mohammadi, M. H., **Geraili, A.**, Jafari, P., Akbari, M. and Sanati-Nezhad, A. (2016) "Microfluidic-Based Multi-Organ Platforms for Drug Discovery." *Micromachines* 7(9), pp. 162-195.

Mohammadi, M. H., Heidary, A.B., Beydaghi, V., **Geraili, A.**, Moradi, F., Jafari, P., Janmaleki, M., Valente, K.P., Akbari, M. and Sanati-Nezhad, A. (2016) "Skin Diseases Modeling using Combined Tissue Engineering and Microfluidic Technologies." *Advanced Healthcare Materials* 5(19), pp.2459-2480.

Oral Presentations:

Geraili, A., Janmaleki, M., Sanati-Nezhad, A., Mequanint, K., (2019) "High-throughput microfabrication of core-shell drug-loaded tablets for personalized medicine". In Canadian Biomaterials Society (CBS) Annual Conference, Quebec City, May 2019.

Geraili, A., Sanati-Nezhad, A., Mequanint, K., (2019) "Core-shell tablets for personalized medicine via high-throughput fabrication". In Tissue Engineering & Regenerative Medicine International Society (TERMIS) AP Chapter and the 7th Asian Biomaterials Congress, Australia, October 2019.